Dottorato di Ricerca in Bioingegneria

XIX Ciclo, Anno Accademico 2005-2006

Sede Amministrativa: Università degli Studi, Bologna

Sede Consorziata: Istituto Universitario di Scienze Motorie, Roma

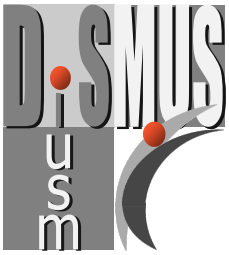

"3-D reconstruction of the human skeleton during motion"

Marco Donati

Supervisore:
Prof. Aurelio Cappozzo
Istituto Universitario di Scienze Motorie, Roma

Prof. Aurelio Cappozzo

Coordinatore:
Prof. Angelo Cappello
Università degli Studi di Bologna

Prof. Angelo Cappello

Contro-relatore:
Prof. Angelo Cappello
Università degli studi di Bologna

a Valentina, per avermi guidato con pazienza e dolcezza a questo traguardo

a Laura che mi è stata sempre accanto

a Mamma, che mi guarda da lassù

a Papà

SOMMARIO

L'analisi del movimento umano ha come obiettivo la descrizione del movimento assoluto e relativo dei segmenti ossei del soggetto e, ove richiesto, dei relativi tessuti molli durante l'esecuzione di esercizi fisici. La bioingegneria mette a disposizione dell'analisi del movimento gli strumenti ed i metodi necessari per una valutazione quantitativa di efficacia, funzione e/o qualità del movimento umano, consentendo al clinico l'analisi di aspetti non individuabili con gli esami tradizionali. Tali valutazioni possono essere di ausilio all'analisi clinica di pazienti e, specialmente con riferimento a problemi ortopedici, richiedono una elevata accuratezza e precisione perché il loro uso sia valido. Il miglioramento della affidabilità dell'analisi del movimento ha quindi un impatto positivo sia sulla metodologia utilizzata, sia sulle ricadute cliniche della stessa.

Per perseguire gli obiettivi scientifici descritti, è necessario effettuare una stima precisa ed accurata della posizione e orientamento nello spazio dei segmenti ossei in esame durante l'esecuzione di un qualsiasi atto motorio. Tale descrizione può essere ottenuta mediante la definizione di un modello della porzione del corpo sotto analisi e la misura di due tipi di informazione: una relativa al movimento ed una alla morfologia. L'obiettivo è quindi .stimare il vettore posizione e la matrice di orientamento necessari a descrivere la collocazione nello spazio virtuale 3D di un osso utilizzando le posizioni di punti, definiti sulla superficie cutanea ottenute attraverso la stereofotogrammetria.

Le traiettorie dei marker, così ottenute, vengono utilizzate per la ricostruzione della posizione e dell'orientamento istantaneo di un sistema di assi solidale con il segmento sotto esame (sistema tecnico) (Cappozzo et al. 2005). Tali traiettorie e conseguentemente i sistemi tecnici, sono affetti da due tipi di errore, uno associato allo strumento di misura e l'altro associato alla presenza di tessuti molli interposti tra osso e cute. La propagazione di quest'ultimo ai risultati finali è molto più distruttiva rispetto a quella dell'errore strumentale che è facilmente minimizzabile attraverso semplici tecniche di filtraggio (Chiari et al. 2005). In letteratura è stato evidenziato che

l'errore dovuto alla deformabilità dei tessuti molli durante l'analisi del movimento umano provoca inaccuratezze tali da mettere a rischio l'utilizzabilità dei risultati. A tal proposito Andriacchi scrive: "attualmente, uno dei fattori critici che rallentano il progresso negli studi del movimento umano è la misura del movimento scheletrico partendo dai marcatori posti sulla cute" (Andriacchi et al. 2000).

Relativamente alla morfologia, essa può essere acquisita, ad esempio, attraverso l'utilizzazione di tecniche per bioimmagini. Queste vengono fornite con riferimento a sistemi di assi locali in generale diversi dai sistemi tecnici. Per integrare i dati relativi al movimento con i dati morfologici occorre determinare l'operatore che consente la trasformazione tra questi due sistemi di assi (matrice di registrazione) e di conseguenza è fondamentale l'individuazione di particolari terne di riferimento, dette terne anatomiche. L'identificazione di queste terne richiede la localizzazione sul segmento osseo di particolari punti notevoli, detti repere anatomici, rispetto ad un sistema di riferimento solidale con l'osso sotto esame. Tale operazione prende il nome di calibrazione anatomica. Nella maggior parte dei laboratori di analisi del movimento viene implementata una calibrazione anatomica a "bassa risoluzione" che prevede la descrizione della morfologia dell'osso a partire dall'informazione relativa alla posizione di alcuni repere corrispondenti a prominenze ossee individuabili tramite palpazione. Attraverso la stereofotogrammetria è quindi possibile registrare la posizione di questi repere rispetto ad un sistema tecnico. Un diverso approccio di calibrazione anatomica può essere realizzato avvalendosi delle tecniche ad "alta risoluzione", ovvero attraverso l'uso di bioimmagini. In questo caso è necessario disporre di una rappresentazione digitale dell'osso in un sistema di riferimento morfologico e localizzare i repere d'interesse attraverso palpazione in ambiente virtuale (Benedetti et al. 1994 ; Van Sint Jan et al. 2002; Van Sint Jan et al. 2003). Un simile approccio è difficilmente applicabile nella maggior parte dei laboratori di analisi del movimento, in quanto normalmente non si dispone della strumentazione necessaria per ottenere le bioimmagini; inoltre è noto che tale strumentazione in alcuni casi può essere invasiva.

Per entrambe le calibrazioni anatomiche rimane da tenere in considerazione che, generalmente, i repere anatomici sono dei punti definiti arbitrariamente all'interno di un'area più vasta e irregolare che i manuali di anatomia definiscono essere il repere anatomico. L'identificazione dei repere attraverso una loro descrizione verbale è quindi povera in precisione e la difficoltà nella loro identificazione tramite palpazione manuale, a causa della presenza dei tessuti molli interposti, genera errori sia in precisione che in accuratezza. Tali errori si propagano alla stima della cinematica e della dinamica articolare (Ramakrishnan et al. 1991; Della Croce et al. 1999). Della Croce (Della Croce et al. 1999) ha inoltre evidenziato che gli errori che influenzano la collocazione nello spazio delle terne anatomiche non dipendono soltanto dalla precisione con cui vengono identificati i repere anatomici, ma anche dalle regole che si utilizzano per definire le terne. E' infine necessario evidenziare che la palpazione manuale richiede tempo e può essere effettuata esclusivamente da personale altamente specializzato, risultando quindi molto onerosa (Simon 2004).

La presente tesi prende lo spunto dai problemi sopra elencati e ha come obiettivo quello di migliorare la qualità delle informazioni necessarie alla ricostruzione della cinematica 3D dei segmenti ossei in esame affrontando i problemi posti dall'artefatto di tessuto molle e le limitazioni intrinseche nelle attuali procedure di calibrazione anatomica. I problemi sono stati affrontati sia mediante procedure di elaborazione dei dati, sia apportando modifiche ai protocolli sperimentali che consentano di conseguire tale obiettivo.

Per quanto riguarda l'artefatto da tessuto molle, si è affrontato l'obiettivo di sviluppare un metodo di stima che fosse specifico per il soggetto e per l'atto motorio in esame e, conseguentemente, di elaborare un metodo che ne consentisse la minimizzazione. Il metodo di stima è non invasivo, non impone restrizione al movimento dei tessuti molli, utilizza la sola misura stereofotogrammetrica ed è basato sul principio della media correlata. Le prestazioni del metodo sono state valutate su dati ottenuti mediante una misura 3D stereofotogrammetrica e fluoroscopica sincrona (Stagni et al. 2005),

(Stagni et al. 2005). La coerenza dei risultati raggiunti attraverso i due differenti metodi permette di considerare ragionevoli le stime dell'artefatto ottenute con il nuovo metodo. Tale metodo fornisce informazioni sull'artefatto di pelle in differenti porzioni della coscia del soggetto e durante diversi compiti motori, può quindi essere utilizzato come base per un piazzamento ottimo dei marcatori. Lo si è quindi utilizzato come punto di partenza per elaborare un metodo di compensazione dell'errore dovuto all'artefatto di pelle che lo modella come combinazione lineare degli angoli articolari di anca e ginocchio. Il metodo di compensazione è stato validato attraverso una procedura di simulazione sviluppata ad-hoc.

Relativamente alla calibrazione anatomica si è ritenuto prioritario affrontare il problema associato all'identificazione dei repere anatomici perseguendo i seguenti obiettivi:

1. migliorare la precisione nell'identificazione dei repere e, di conseguenza, la ripetibilità dell'identificazione delle terne anatomiche e della cinematica articolare,

2. diminuire il tempo richiesto,

3. permettere che la procedura di identificazione possa essere eseguita anche da personale non specializzato.

Il perseguimento di tali obiettivi ha portato alla implementazione dei seguenti metodi:

- Inizialmente è stata sviluppata una procedura di palpazione virtuale automatica. Dato un osso digitale, la procedura identifica automaticamente i punti di repere più significativi, nella maniera più precisa possibile e senza l'ausilio di un operatore esperto, sulla base delle informazioni ricavabili da un osso digitale di riferimento (template), preliminarmente palpato manualmente.
- E' stato poi condotto uno studio volto ad indagare i fattori metodologici che influenzano le prestazioni del metodo funzionale nell'individuazione del centro articolare d'anca, come prerequisito fondamentale per migliorare la procedura di calibrazione anatomica. A tale scopo sono stati confrontati

diversi algoritmi, diversi cluster di marcatori ed è stata valutata la prestazione del metodo in presenza di compensazione dell'artefatto di pelle.

- E'stato infine proposto un metodo alternativo di calibrazione anatomica basato sull'individuazione di un insieme di punti non etichettati, giacenti sulla superficie dell'osso e ricostruiti rispetto ad un TF (UP-CAST). A partire dalla posizione di questi punti, misurati su pelvi coscia e gamba, la morfologia del relativo segmento osseo è stata stimata senza identificare i repere, bensì effettuando un'operazione di matching dei punti misurati con un modello digitale dell'osso in esame. La procedura di individuazione dei punti è stata eseguita da personale non specializzato nell'individuazione dei repere anatomici. Ai soggetti in esame è stato richiesto di effettuare dei cicli di cammino in modo tale da poter indagare gli effetti della nuova procedura di calibrazione anatomica sulla determinazione della cinematica articolare. I risultati ottenuti hanno mostrato, per quel che riguarda la identificazione dei repere, che il metodo proposto migliora sia la precisione inter- che intra-operatore, rispetto alla palpazione convenzionale (Della Croce et al. 1999). E' stato inoltre riscontrato un notevole miglioramento, rispetto ad altri protocolli (Charlton et al. 2004; Schwartz et al. 2004), nella ripetibilità della cinematica 3D di anca e ginocchio. Bisogna inoltre evidenziare che il protocollo è stato applicato da operatori non specializzati nell'identificazione dei repere anatomici. Grazie a questo miglioramento, la presenza di diversi operatori nel laboratorio non genera una riduzione di ripetibilità. Infine, il tempo richiesto per la procedura è drasticamente diminuito. Per una analisi che include la pelvi e i due arti inferiori, ad esempio, l'identificazione dei 16 repere caratteristici usando la calibrazione convenzionale richiede circa 15 minuti, mentre col nuovo metodo tra i 5 e i 10 minuti.

Andriacchi, T. P. and E. J. Alexander (2000). "Studies of human locomotion: past, present and future." J Biomech **33**(10): 1217-24.

Benedetti, M. G., A. Cappozzo, et al. (1994). Anatomical Landmark Definition and Identification.

Cappozzo, A., U. Della Croce, et al. (2005). "Human movement analysis using stereophotogrammetry. Part 1: theoretical background." Gait Posture **21**(2): 186-96.

Charlton, I. W., P. Tate, et al. (2004). "Repeatability of an optimised lower body model." Gait Posture **20**(2): 213-21.

Chiari, L., U. Della Croce, et al. (2005). "Human movement analysis using stereophotogrammetry. Part 2: instrumental errors." Gait Posture **21**(2): 197-211.

Della Croce, U., A. Cappozzo, et al. (1999). "Pelvis and lower limb anatomical landmark calibration precision and its propagation to bone geometry and joint angles." Med Biol Eng Comput **37**(2): 155-61.

Ramakrishnan, H. K. and M. P. Kadaba (1991). "On the estimation of joint kinematics during gait." J Biomech **24**(10): 969-77.

Schwartz, M. H., J. P. Trost, et al. (2004). "Measurement and management of errors in quantitative gait data." Gait and Posture **20**: 196-203.

Simon, S. R. (2004). "Quantification of human motion: gait analysis-benefits and limitations to its application to clinical problems." J Biomech **37**(12): 1869-80.

Stagni, R., S. Fantozzi, et al. (2005). "Quantification of soft tissue artefact in motion analysis by combining 3D fluoroscopy and stereophotogrammetry: a study on two subjects." Clin Biomech (Bristol, Avon) **20**(3): 320-9.

Van Sint Jan, S., V. Feipel, et al. (2002). Lower limb anatomical landmark definition and identification within different experimental contexts.

Van Sint Jan, S., I. Hilal, et al. (2003). "Data representation for joint kinematics simulation of the lower limb within an educational context." Med Eng Phys **25**(3): 213-20.

CHAPTER 1. INTRODUCTION

The observation and analysis of the natural phenomenon "human movement" (human movement analysis, HMA) calls for a prerequisite to be met, which consists in collecting data that allow for the reconstruction, in the 3-D space and in each sampled instant of time, of the subject-specific bones involved in the analysis.

HMA requires the gathering of quantitative information about the relative movement between adjacent bones, the intersegmental loads, and the forces transmitted by individual body tissues such as muscles, tendons, ligaments, etc. These quantities are estimated using mathematical models of the musculo-skeletal system and measures of observable quantities and allow the graphical rendering of the movement of the musculo-skeletal system as a virtual reality 3-D realistic representation.

The anthropomorphic model consists of a kinematic chain of links representing the portion of the locomotor apparatus under analysis. These links are made of soft tissues and a bony part (segment). Whereas the latter is considered non-deformable and, therefore, represented using rigid bodies, soft tissues may or may not be considered deformable; most of the literature chooses the latter option. However, in recent years, some authors have started to advocate for soft tissue deformability to be accounted for in human movement modelling. It has in fact been shown that, by ignoring this deformability, bony segment kinematics reconstructed using non-invasive photogrammetric data of skin-markers is affected by inaccuracies that may hinder the practical usability of the results (Cappello et al. 1997; Lucchetti et al. 1998; Lu et al. 1999; Alexander et al. 2001).

To reconstruct the 3-D kinematics of each body or bony segment during the execution of a motor task, two pieces of information are necessary: bone pose (i.e. position and orientation) and bone morphology (BM). Pose is time-variant while morphology is hypothesized as invariant, that is the bone is considered non-deformable.

The description of the skeletal-system pose involves the definition of a local frame, relative to a global or laboratory frame of reference (GF), rigidly

associated with the bony segment involved, which is referred to as technical frame (TF) (Cappozzo et al. 1995; Cappozzo et al. 1997; Cappozzo et al. 2005)

These quantities are most commonly measured using stereophotogrammetric systems. Positions of target points of either light emitting diodes or retro-reflective cluster of markers, placed on the surface of a body segment, are measured and used to construct instantaneous position vectors relative to a GF.

Relevant results are affected by instrumental errors (Borghese et al. 1990; Morris et al. 1990; DeLuzio et al. 1993; Ehara et al. 1995; Richards 1999; Della Croce et al. 2000; Chiari et al. 2005) and soft tissue artefacts, STA, (Cappozzo et al. 1996; Fuller et al. 1997; Reinschmidt et al. 1997; Tranberg et al. 1998; Manal et al. 2000; Westblad et al. 2000; Leardini et al. 2005). These errors are time variant and affect the reconstructed positions of the markers both in an uncorrelated and correlated manner, thus giving rise to marker cluster deformation and rigid movement relative to the underlying bone, respectively. In the literature, there is ample evidence that the propagation of the photogrammetric errors to the end results of a movement analysis is far less disruptive to the information involved than that of the STA (Cappozzo 1991; Andriacchi et al. 2000) In addition, minimizing the propagation of the uncorrelated error using least squares optimal pose estimators that exploit information redundancy of the reconstructed coordinates of three or more markers is known to be relatively easy (Soderkvist et al. 1993; Cappozzo et al. 1997; Andriacchi et al. 1998). However, the artefact rigid movement of the cluster relative to the bone has not been dealt with satisfactorily (Cappello et al. 1997; Lucchetti et al. 1998; Lu et al. 1999; Alexander et al. 2001). In the movement analysis community, assessment of the STA, as a prerequisite for its minimization and compensation, is one of the highest priorities.

The TF position relative to the bone is not repeatable and, thus, the associated marker cluster technical frame results in an arbitrary pose relative to the bone (Cappozzo et al. 2005). To overcome this problem, the numerical information available relative to bone morphology is used. BM information is obtained by acquiring the position of points, located on the bone external

surface, relative to a morphology technical frame (MF). If the latter frame is different from the CF, then a registration transformation matrix (RTM) that allows to represent BM in this frame must be provided (movement morphology data registration).

In most movement analysis laboratories, a low resolution anatomical calibration is carried out that entails describing BM by using the few external anatomical landmarks (ALs), corresponding to bony prominences identified by manual palpation. After these ALs are identified, their location relative to the relevant CF is determined through photogrammetry, either locating markers on them or pointing the ALs with a pointer fitted with two or more markers (Cappozzo et al. 1995; Cappozzo et al. 1997; Cappozzo et al. 1997). Internal ALs may also be used: a typical example is the centre of the femoral head. Its position can be estimated using the location of superficial ALs and predictive models (Bell et al. 1990; Davis et al. 1991; Seidel et al. 1995; Leardini et al. 1999), or it may be determined as the centre of rotation of the femur relative to the pelvis (functional approach) (Cappozzo 1984; Leardini et al. 1999). When these anatomical calibration procedures are used, the RTM is an identity matrix.

A high resolution anatomical calibration may be carried out using medical imaging. In this case a detailed morphology of the bone is provided relative to a MF that is different from the CF. Relevant ALs can be determined on the 3-D digital model of the bone through a virtual palpation exercise (Van Sint Jan et al. 2003). If the BM information incorporates the technical markers, then the RTM may be estimated. If that is not the case, then the location of selected ALs must be determined also in the CF as illustrated above. The knowledge of the location of the ALs in both frames involved allows for the estimation of the RTM. However, this high resolution calibration is hardly ever possible in movement analysis laboratories, since normally they do not have medical imaging equipments at hand and, in addition, some of these are regarded as invasive.

Anatomical calibration meets the requirements of intra- and inter-subject repeatability since it allows for the definition of anatomical frames (AF), the location of which relative to the underlying bony segment is repeatable, as

opposed to that of the TFs. AFs are determined using selected ALs identified in the most appropriate TF, and a construction rule (Cappozzo et al. 1995; Wu et al. 1995; Cappozzo et al. 1997; Wu et al. 2002). AFs are used to provide the possibility of estimating subject-specific body segment inertia parameters, and muscular-tendineous and ligament geometries. In addition, repeatability of joint kinematics description heavily depends on the repeatability with which the AFs of the adjacent bones are defined (Fioretti et al. 1997). Similar considerations may be carried out with reference to intersegmental loads.

Repeatability of AF definition is affected by the incorrect in vivo location of subcutaneous bony ALs through palpation. This location error has been addressed by several studies (Della Croce et al. 1999; Piazza et al. 2000; Rabuffetti et al. 2002) that highlighted its importance and can be used as guidelines for the choice of the ALs that are most suitable for AF definition. Among the non palpable (internal) ALs, the centre of the femoral head deserves special attention. The precise and accurate estimate is crucial in terms of error propagation to both the kinematic and kinetic variables of both the hip and the knee joints (Kadaba et al. 1990; Stagni et al. 2000; Cereatti et al. 2006). As mentioned above, the centre of the femoral head location can be estimated using either a functional or a prediction approach (Leardini et al. 1999). The former approach gives a more accurate location estimate provided that it is implemented using good practice guidelines. Some aspects of the functional protocol have been investigated and relevant guidelines suggested by Camomilla and Cereatti (Cereatti et al. 2004; Camomilla et al. 2006), however, the effects of STA on the protocol need to be analyzed and the guidelines possibly modified.

The effects of the anatomical calibration errors can be reduced by: improving and standardizing the AL identification procedures; increasing the number of ALs used to define an AF and exploiting the information redundancy; designing rules that construct an AF so that relevant ALs inaccuracy propagations are minimized. This matter has been investigated in a preliminary study and some relevant hints provided (Della Croce et al. 2003).

In summary, the state of the art of knowledge in movement analysis suggests that the minimization of the errors due to the soft tissue artefact

(Andriacchi et al. 2000) and the repeatability with which the anatomical frames can be identified are the critical challenges for the future.

The aim of the present thesis is to contribute to the improvement of human movement analysis to guarantee a repeatable and accurate reconstruction of 3-D joint kinematics. In particular the focus was placed on the following issues:

- a new method was developed to enhance the identification of the anatomical landmarks and consequently of the anatomical frames, based on the determination of the position in the CF of the highest number possible of unlabelled points (UP) distributed over the bone surface and the matching of a template bone, through a scaling and deformation procedure, to the experimentally determined UPs.
- a non invasive method was implemented that allows for a subject- and task-specific estimate of the soft tissue artefact during movement and entails no restriction to skin motion since it uses only stereophotogrammetry.
- a method to minimize the effect of STA was developed on the basis of the previous assessment method.

CHAPTER 2. STATE OF THE ART: HUMAN MOVEMENT ANALYSIS USING PHOTOGRAMMETRY

2.1 Theoretical background

The state of the art was written on the basis of four review articles on human movement analysis, published on Gait and Posture and on the thesis of Valentina Camomilla and Andrea Cereatti. The authors of the reviews, Cappozzo A., Chiari L., Leardini A., della Croce U., and the authors of the thesis are gratefully acknowledged.

2.1.1 Introduction

Human movement analysis aims at gathering quantitative information about the mechanics of the musculo-skeletal system during the execution of a motor task. In particular, information is sought concerning the movement of the whole-body centre of mass; the relative movement between adjacent bones, or joint kinematics; the forces exchanged with the environment; the resultant loads transmitted across sections of body segments or between body segments, or transmitted by individual body tissues such as muscles, tendons, ligaments, bones, etc.; and body segment energy variation and muscular work. The 3-D realistic representation of the movement of the musculo-skeletal system as seen from a point of view of choice (virtual reality) is a further relevant objective. The quantities that provide the above listed information are either measured or estimated using mathematical models of the musculo-skeletal system. In this way, quantitative descriptions of the functions of the locomotor system and their changes (assessment of enhancement or impairment) and/or of the way an individual executes a motor activity (assessment of activity limitation) are obtained.

Normally, the following quantities are measured. Instantaneous positions of markers located on the skin surface are obtained using stereophotogrammetry (motion capture) either based on conventional photography or optoelectronic sensors (Medved 2001). External forces are measured using dynamometers, such as force plates (Berme 1990). Electrical activity of muscles is recorded through electromyography (Basmajian et al. 1985). Metabolic energy is assessed using indirect calorimetry. Anthropometric quantities are acquired either using a scale, a tape measure and callipers, or more sophisticated methods such as 3-D scanners.

Following the work by Braune and Fischer, the anthropomorphic model used to estimate the quantities that are not directly observable consists of a kinematic chain of links. Each link represents a portion of the human body referred to as body segment. These segments are made of a bony part (segments) and by soft tissues. Bony segments are considered non-deformable and, therefore, are represented using rigid bodies, in the Classical Mechanics

sense. So far, no author has disputed this choice or assessed the inaccuracy that it may introduce in the analysis, provided, of course, that the bony segment represents a single bone. Bony segments are connected by joints with 1 to 5 degrees of freedom. The limit cases of 0 and 6 degrees of freedom may be included for the sake of generalisation. The number of bony segments and constraints imposed by the joints contribute to the number of degrees of freedom of the model and its structural faithfulness to reality. Soft tissues around the bony segments may or may not be considered deformable. Most of the literature chooses the latter option, that is the entire body segment is regarded as a rigid body. In principle, under these circumstances, the analysis described above is straightforward: for the most part, Classical Mechanics can solve any related problem and, with the aid of modern computers, can do this without difficulty. However, in recent years some authors have started to advocate for soft tissue deformability to be accounted for in human movement modelling. It has in fact been shown that by ignoring this deformability, both absolute and relative bony segment movements, reconstructed using non-invasive photogrammetric data obtained by using skin-markers, are affected by inaccuracies that may hinder the practical usability of the results (Chèze et al. 1995). Another issue concerns the inertial effects that tissue deformation (wobbling masses) may have on movement kinetics during highly accelerated movements (Hatze 2002). These matters were also debated, at the end of 2001, in the Biomch-L list forum (www.isbweb.org).

In this review of the state of the art the focus is placed on the conceptual and analytical bases that are necessary for the reconstruction and analysis of skeletal system movement by using optoelectronic stereophotogrammetry. In order to pursue this objective, morphological information is also required both for the 3-D realistic reconstruction of the skeletal system and for the numerical description of kinematics. In fact, to the latter purpose, mostly vector quantities are used and their numerical representation depends on the orthogonal set of axes involved. For obvious reasons of repeatability of kinematic description, the latter axes must also be repeatable and the only way to accomplish this is to define them relative to morphology.

No mention is made about the forces involved in the process. In fact, the problems associated with myoskeletal kinetics follow the knowledge of how the system moves (inverse dynamics). However, the perspective of utilizing kinematics for kinetic problem solving will be kept in mind.

2.1.2 Segmental kinematics

The objective of segmental kinematics is the collection of numerical information that allows the reconstruction of a body, considered rigid or not, or bony segment in space in each sampled time instant during the execution of a motor task. For this purpose, two pieces of information are necessary: one relative to morphology and one to movement.

The morphological description of a segment can be obtained by representing it as an ensemble of particles and providing the position vector of each relative to an orthogonal set of axes (local frame, LF):

$$^{l}\mathbf{p} = \left[{}^{l}p_x, {}^{l}p_y, {}^{l}p_z \right] \tag{2.1}$$

It follows logically that the more particles used, the more detailed the description will be (Figure 2-1).

If the body under analysis is considered deformable, then the vector $^{l}\mathbf{p}$ must be given for each particle and each sampled instant of time during the observation interval. However, as is often the case in human movement analysis, if the investigator is not interested in the deformations of the segment involved, but only in its global location in space, then this may be considered non-deformable in an absolute sense and represented as a rigid body. This entails enormous simplification since, under this hypothesis, the above mentioned particle position vectors are invariant with respect to time and/or boundary conditions and can, therefore, be measured only on one occasion and under the most favourable experimental conditions. Similar considerations apply to the inertial parameters (e.g., location of the centre of mass, mass moments of inertia) of the segment involved.

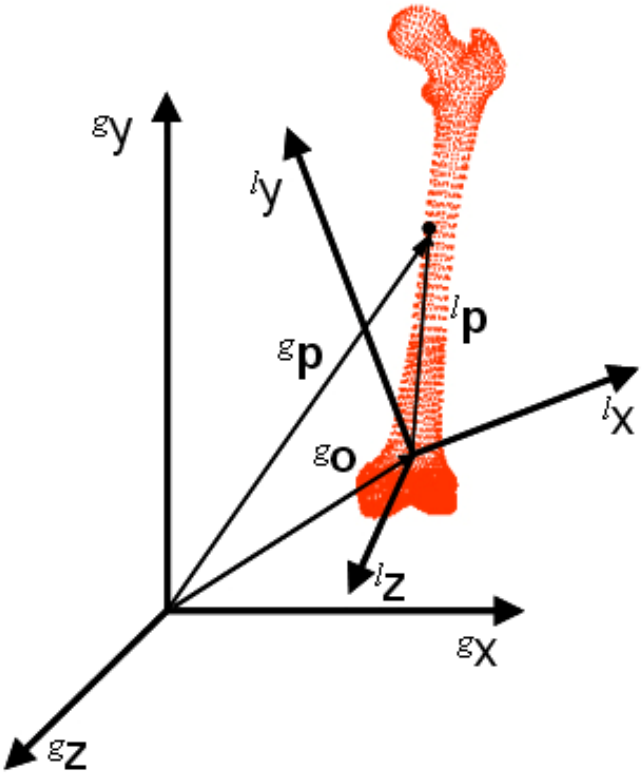

Figure 2-1. The position vector of a particle represented in a global ($^{g}\mathbf{x}, ^{g}\mathbf{y}, ^{g}\mathbf{z}$) and a local ($^{l}\mathbf{x}, ^{l}\mathbf{y}, ^{l}\mathbf{z}$) frame, indicated as $^{g}\mathbf{p}$ and $^{l}\mathbf{p}$, respectively.

The morphology of a segment may be represented with respect to any arbitrary frame, that is, with respect to any observer. Given a LF and another frame, which we refer to as the global frame (GF), it is possible to derive the position vectors of the particles of the segment under analysis defined in the latter frame ($^{g}\mathbf{p}$) provided that those defined in the former ($^{l}\mathbf{p}$) are given (Figure 2-1). This exercise is called vector or coordinate transformation and is obtained through the following equation :

$$^{g}\mathbf{p} = {}^{g}\mathbf{R}_{l}\,{}^{l}\mathbf{p} + {}^{g}\mathbf{o} \tag{2.2}$$

where

$$^{g}\mathbf{R}_{l} = \begin{bmatrix} \cos\theta_{x_g x_l} & \cos\theta_{x_g y_l} & \cos\theta_{x_g z_l} \\ \cos\theta_{y_g x_l} & \cos\theta_{y_g y_l} & \cos\theta_{y_g z_l} \\ \cos\theta_{z_g x_l} & \cos\theta_{z_g y_l} & \cos\theta_{z_g z_l} \end{bmatrix} \tag{2.3}$$

defines the orientation of the LF, relative to the GF frame and is referred to as the orientation matrix, and $^{g}\mathbf{o}$ is the position vector of the origin of the LF relative to the GF, and defines the position of the former relative to the

latter. The column elements of the matrix in (2.3) are the direction cosines, or the unit vector components, defining the orientation of each LF axis relative to the global frame. With reference to these nine matrix elements, it is important to emphasize that they are not independent. In fact, taking into account their definition and the fact that the frame axes they define are mutually orthogonal and that triplets of them represent unit vectors, six scalar equations may be written that reduce the number of independent elements to three. In summary, three scalar independent quantities define the relative orientation, and three the relative position. The ensemble of position and orientation of any one frame relative to another, that is, of a rigid body relative to another, is referred to as pose.

If the problem is representing the segment under analysis in virtual reality, given the invariant position vector of its particles relative to a local frame, then, by providing the computer with the above-mentioned six quantities, it is possible to view the segment from any other global perspective.

The mathematical tool illustrated above may be used to describe segment movement as well. In fact, if the pose of the LF is described in each sampled instant of time during movement relative to a GF by giving the six independent scalar quantities implied in ${}^{g}\mathbf{R}_{l}$ and ${}^{g}\mathbf{o}$, then the segment morphology (${}^{l}\mathbf{p}$) can be reconstructed in its instantaneous location (${}^{g}\mathbf{p}$) through equation 2.2. It is interesting to emphasize that this approach, based on the assumption of rigidity, allows the description of the pose of a body using only six numerical values for each sampled instant of time. To these values, the time invariant local coordinates of the particles used to represent the morphology must be added for virtual reality representation of the movement.

The description of the skeletal-system movement involves the definition of several set of axes that are either global or local.

Global frames

In a movement analysis laboratory, the following inertial, global, frames can be defined (Figure 2-2) (Cappozzo et al. 1995) (Cappozzo et al. 1997)

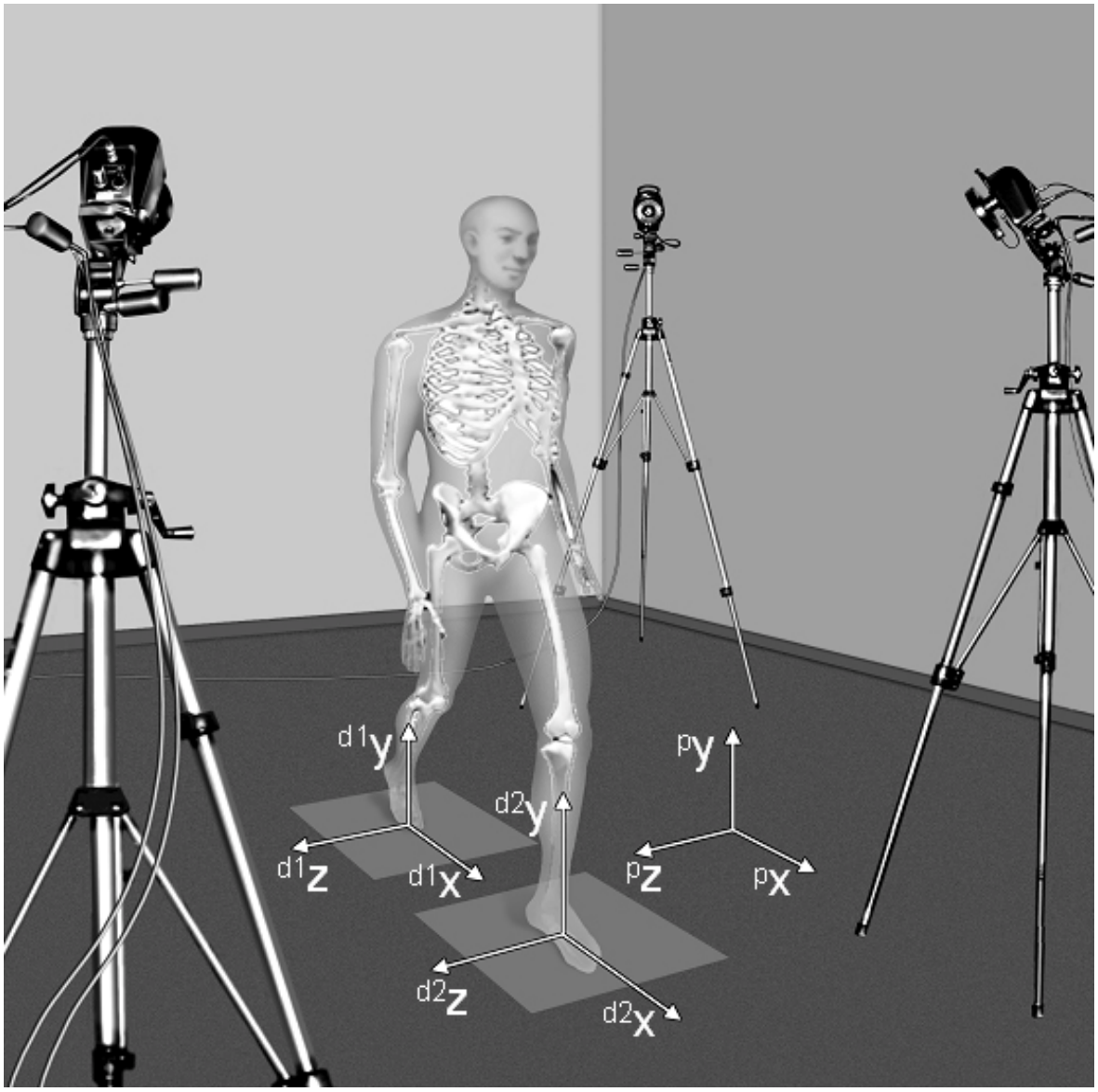

Figure 2-2 The human movement analysis laboratory. Basic measurement instruments are depicted together with their systems of axes (p: photogrammetry; d: dynamometry). If level walking is analysed, the motor task frame may coincide with the frame of one of the two force plates.

Photogrammetric frame: This is the set of axes in which marker position coordinates are provided by the stereophotogrammetric system. These are arbitrarily defined relative to the calibration object or procedure used.

Motor task frame: This frame is consistent with the analysed motor task and sometimes describes its basic features. For instance, when locomotor acts are investigated, one axis of the frame indicates the mean direction of progression, possibly including the orientation of the floor (in case of non-level locomotion). According to the general recommendations from the International Society of Biomechanics (Wu et al. 1995) (Wu et al. 2002), in human movement analysis orthogonal coordinate systems should have the X axis pointing forward in most locomotor tasks coinciding with the direction of progression, Y pointing vertically upwards, and Z pointing to the right.

Dynamometer frame: This is the frame in which force and moment components are given by the instrument and is defined by the relevant calibration matrix.

Plumb Line: This is a single axis and represents the orientation of the gravity line, usually assumed to point downward.

As implicit in the previous section, within the same experiment, different mechanical quantities are measured with respect to different global frames. However, normally, their interpretation, or use as input to the mathematical models that allow for the estimation of non-measurable quantities, requires that all of them be represented in the same frame (primary global frame). The latter role is usually assumed by the motor task frame. Thus, a global frame calibration procedure must be carried out. This consists of the determination of the position vector and the orientation matrix of all secondary global frames involved relative to the primary global frame ($^{pg}\mathbf{R}_{sg}$, $^{pg}\mathbf{o}$). This allows for the transformation of any vector given in the former frames into a vector in the primary frame (see equation 2.2).

From an operative point of view, ad hoc experiments are carried out which allow for the determination of the position vectors of selected fiducial points in both the secondary and primary global frame. By using an adequate number (N) of these points and feeding their position vectors into equations

having the same form of equation (2.2), where the secondary global frame takes the place of the local frame, the unknown orientation matrix and position vector are estimated by the following equation:

$$^{pg}\mathbf{p}_k = {}^{pg}\mathbf{R}_{sg}\,{}^{sg}\mathbf{p}_k + {}^{pg}\mathbf{o},\ k = 1,\ldots,\mathrm{N} \tag{2.4}$$

For the sake of accuracy, this estimation counts on a redundant number of fiducial points and uses a least squares approach (Cappozzo et al. 1997) A typical example is the determination of the pose of the force plate frame relative to the photogrammetric frame by using a set of three or more markers located in known positions in the former frame (Rabuffetti et al. 2003).

Local frames

A generic local frame rigidly associated with a bony segment is referred to as technical frame (TF) (Cappozzo 1984; Cappozzo et al. 1995; Wu et al. 1995; Cappozzo et al. 1997; Cappozzo et al. 1997; Wu et al. 2002). These frames are used to describe the location in space, either stationary or time-varying, of the segment under analysis (Figure 2-3).

Morphology technical frame (MTF): This is the TF used in the course of the experiments that provide the segment morphology. It is defined by the technique and/or measuring equipment used and may be regarded as arbitrary.

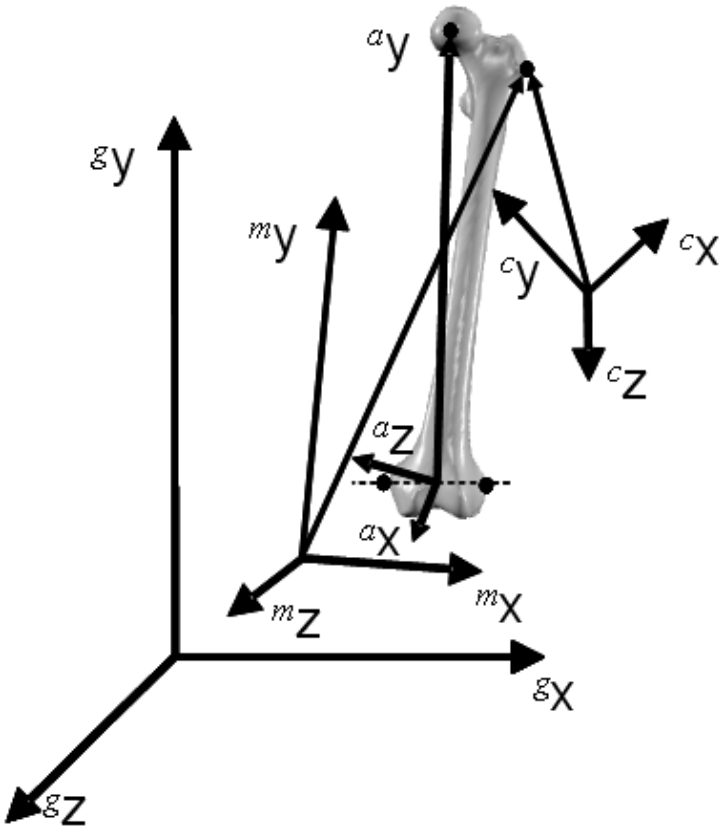

Figure 2-3. Morphological ($^{m}X, ^{m}Y, ^{m}Z$) and marker cluster ($^{c}X, ^{c}Y, ^{c}Z$) technical frames, and anatomical frame ($^{a}X, ^{a}Y, ^{a}Z$). The latter frame is defined as having the y axis joining the midpoint between the lateral and medial femoral epicondyles and with positive direction proximal, the z axis lies in the plane defined by the y axis and the centre of the femoral head and points from left to right, the x axis is orthogonal to the yz plane with its positive direction forward (Cappozzo et al. 1997).

Marker cluster technical frame (CTF): This is the TF used to describe the movement of a segment and is reconstructed using the instantaneous position of at least three non-aligned superficial markers associated with the bony segment and tracked by a photogrammetric system (Figure 2-4 a). These markers, which are named technical markers, are positioned to comply with technical requirements such as visibility to a sufficient number of cameras and to minimize relative movement between them and underlying bone. Normally, their position has no repeatable reference to the morphology of the segment. For this same reason, the CTF has an arbitrary position and orientation with respect to the bone which depend on both the location of the markers and the

analytical procedure used to generate them (Cappozzo et al. 1997) (Cappello et al. 1997). In order to economize the number of markers, some authors construct some CTFs using virtual markers. These are points of a segment for which the location is determined, through some geometric rule, relative to the position of the technical markers in the relevant CTF. If a virtual marker, thus obtained, is supposed to be shared with an adjacent segment, then it may be used to construct the CTF of the latter segment. This is the case, for instance, when the two segments involved are hypothesised to be joined by a spherical hinge and the virtual marker is the centre of rotation (Davis et al. 1991) (Kadaba et al. 1990) (Figure 2-4 b).

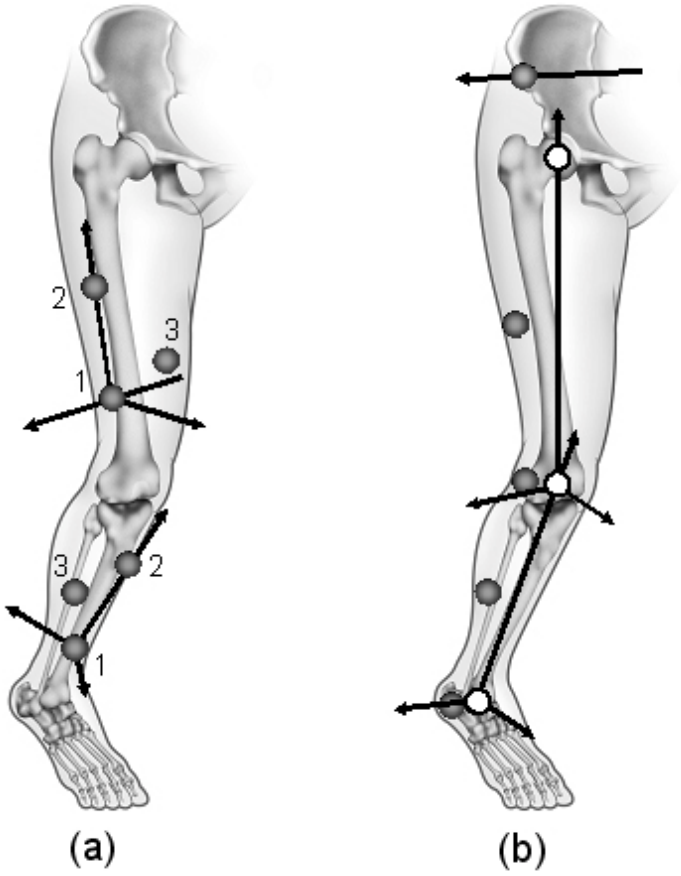

Figure 2-4 Examples of marker set and marker cluster technical frame. a) Three technical markers for each bony segment; the cluster technical frame is constructed using the following rule: $\mathbf{t}_j$ is the position vector of the origin, the z axis is oriented as m1-m2, and the x axis as (m3-m2)x(m1-m2).

Normally, the instrumentation used to record morphology information is different from that used to reconstruct the segment movement, and the two procedures are separate both in time and location. Therefore, the two TFs

referred to above are different (Figure 2-3). This circumstance raises a problem. In order to represent the segment in its instantaneous pose, both movement and morphology data must be given with reference to the same TF. Thus, a transformation of the position vectors given in the MTF into position vectors in the CTF, or viceversa, must be carried out (movement-morphology data registration). For this purpose an anatomical calibration procedure must be carried out (Figure 2-5). Similar to the global frame calibration procedure, the position vectors of a number of selected points belonging to the segment under analysis must be made available in both TFs involved ($^{m}\mathbf{p}$ and $^{c}\mathbf{p}$ in Figure 2-3). These points must coincide with anatomical landmarks (AL) so that they be identifiable in a repeatable fashion (Della Croce et al. 1999). Superficial ALs, usually bony prominences, are used and identified by palpation, and their position in the CTF is determined by locating markers on them (anatomical markers) and using stereophotogrammetry. These markers may be removed prior to tracking the movement under analysis, unless they are also made to play the role of technical markers (Figure 2-4 b). Internal AL positions are normally estimated using the location of superficial ALs and predictive models (Davis et al. 1991). In the case of the centre of the femoral head, the fact that it can be considered to coincide with the centre of rotation of the femur relative to the pelvis allows its location to be determined using movement data (functional approach; (Cappozzo 1984)). The position of the ALs in the MTF is determined using a virtual palpation procedure (Van Sint Jan et al. 2003). A possible alternative to the above-mentioned procedure consists of the determination of the position in the CTF of a highly redundant number of unlabeled points of sufficiently large portions of the bone under analysis (Chen et al. 2001; Glozman et al. 2001; Stindel et al. 2002).

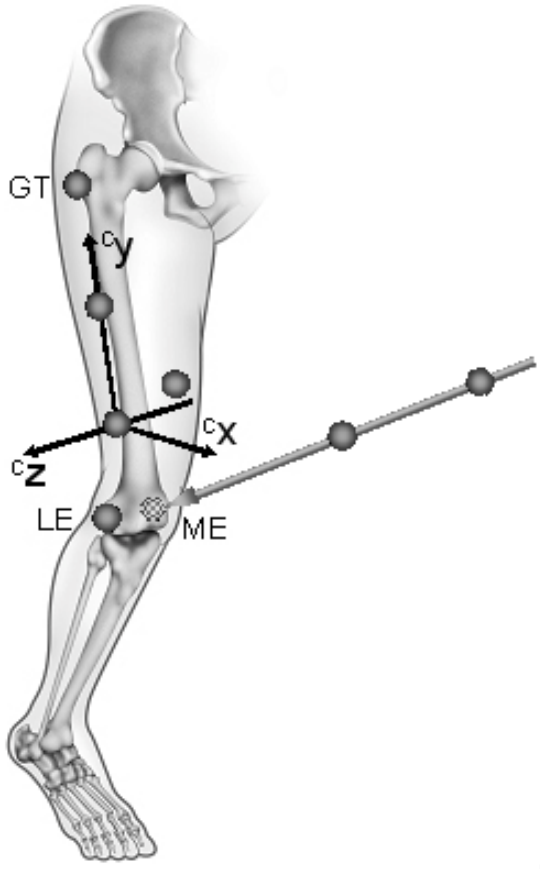

Figure 2-5 Some of them are calibrated using anatomical markers, others using a wand which carries a cluster of markers. Prior to recording, the end point of the wand, the position of which relative to the cluster of markers is accurately known, is made to coincide with the target anatomical landmark.

Anatomical frame: As opposed to the TFs, the location of which, relative to the underlying bony segment, is arbitrary and, as such, non repeatable, anatomical frames (AF) are defined specifically to meet the requirements of intra- and inter-subject repeatability. In addition, their planes normally approximate the frontal, transverse and sagittal anatomical planes. This is achieved by setting a geometric rule that constructs the AF using selected AL's determined in the CTF through the anatomical calibration exercise illustrated above (Figure 2-5) (Kadaba et al. 1990; Wu et al. 1995; Wu et al. 2002). To this end, anatomical markers may also be placed in points that do not denote AL's but lie on anatomical planes as identified by the operator (Kadaba et al. 1990; Della Croce et al. 1999) (Figure 2-4 b). Alternatively, when the bone morphology is available, the AF can be defined using the intrinsic wealth of morphological information and first represented in the MTF and, then, in the

CTF through the registration procedure illustrated above. This topic will be further elaborated upon in a subsequent part of this state of the art.

Following the suggestion made in Cappozzo et al. (Cappozzo et al. 1995), some authors refer to the general approach to human movement reconstruction presented previously as CAST (Calibrated Anatomical System Technique).

2.1.3 Joint kinematics

Joint kinematics is the description of the relative movement between two contiguous bony segments, the proximal (p) and the distal (d). Given the orientation matrices ${}^{g}\mathbf{R}_{d}$ and ${}^{g}\mathbf{R}_{p}$, and the translation vectors ${}^{g}\mathbf{o}_{d}$ and ${}^{g}\mathbf{o}_{p}$ of the local frames associated with the two segments with respect to a selected global frame, the following expressions can be obtained:

$$\mathbf{R}_{\mathrm{j}} = {}^{g}\mathbf{R}'_{p}\,{}^{g}\mathbf{R}_{d}, \qquad \mathbf{t}_{\mathrm{j}} = {}^{g}\mathbf{R}'_{p}({}^{g}\mathbf{o}_{d} - {}^{g}\mathbf{o}_{p}), \tag{2.5}$$

where $\mathbf{R}_{\mathrm{j}}$, referred to as the joint orientation matrix, and $\mathbf{t}_{\mathrm{j}}$ as the joint position vector, carry complete information about orientation and position (pose) of the distal segment relative to the proximal segment and, thus, about joint kinematics. $\mathbf{R}_{\mathrm{j}}$, by its own nature, describes the joint orientation, taking as reference the orientation when the two local frames involved are aligned ($\mathbf{R}_{\mathrm{j}} = \mathbf{I}$; where $\mathbf{I}$ is the identity matrix).

In human movement analysis, the quantities that describe joint kinematics, in order to be effective both in research and application, must be repeatable. In addition, it is desirable that they lend themselves to be interpreted consistently with the language in use in functional anatomy and related disciplines. In fact, it can be said that the objective of biomechanics in this case is to render anatomically valid and reliable measurements.

As far as repeatability is concerned, the following arguments can be made. Given a relative orientation of the two contiguous segments, the value of the scalar quantities that appear in $\mathbf{R}_{\mathrm{j}}$ and $\mathbf{t}_{\mathrm{j}}$ depend on the pose of the two local frames used to derive them relative to the segments. Thus, for each

segment involved, a frame must be used that can be identified in a repeatable fashion. The AFs defined in the previous section comply with this requirement. A possible alternative for the identification of appropriate proximal and distal AFs, is making reference to the so-called joint axes. In fact, some joints have a dominant rotational degree of freedom for which a mean axis of rotation may be defined. Examples in this respect are the knee and the ankle joints. Based on this consideration and when applicable, it is possible to construct the relevant AFs by using this axis in addition to selected anatomical landmarks (Frigo et al. 1998; Ramsey et al. 1999). Whether this functional axis should be subject specific, as the anatomical landmarks are, or estimated using some predictive model is still a matter of discussion.

Therefore, the joint position vector and orientation matrix should be calculated using equation (2.5) and the relevant proximal and distal AFs (Figure 2-6). For the sake of comparison, data sharing, and knowledge building, for each bony segment, a specific AF must be agreed upon by the professional or scientific community involved and standardized (Wu et al. 1995; Wu et al. 2002).

With respect to the interpretability and consistency with the language of functional anatomy, it is desirable that the six independent scalar quantities inherent in $\mathbf{R}_j$ and $\mathbf{t}_j$ be three angles (three rotational degrees of freedom) and three lengths (three translational degrees of freedom) defined relative to given axes. Mechanics provides several methods that permit the extraction of the latter quantities from the joint orientation matrix and position vector. The problem is that this is true from the analytical point of view, but whether the three angles and three lengths thus obtained represent an acceptable answer to the above-mentioned issue, is a matter that needs to be expounded upon.

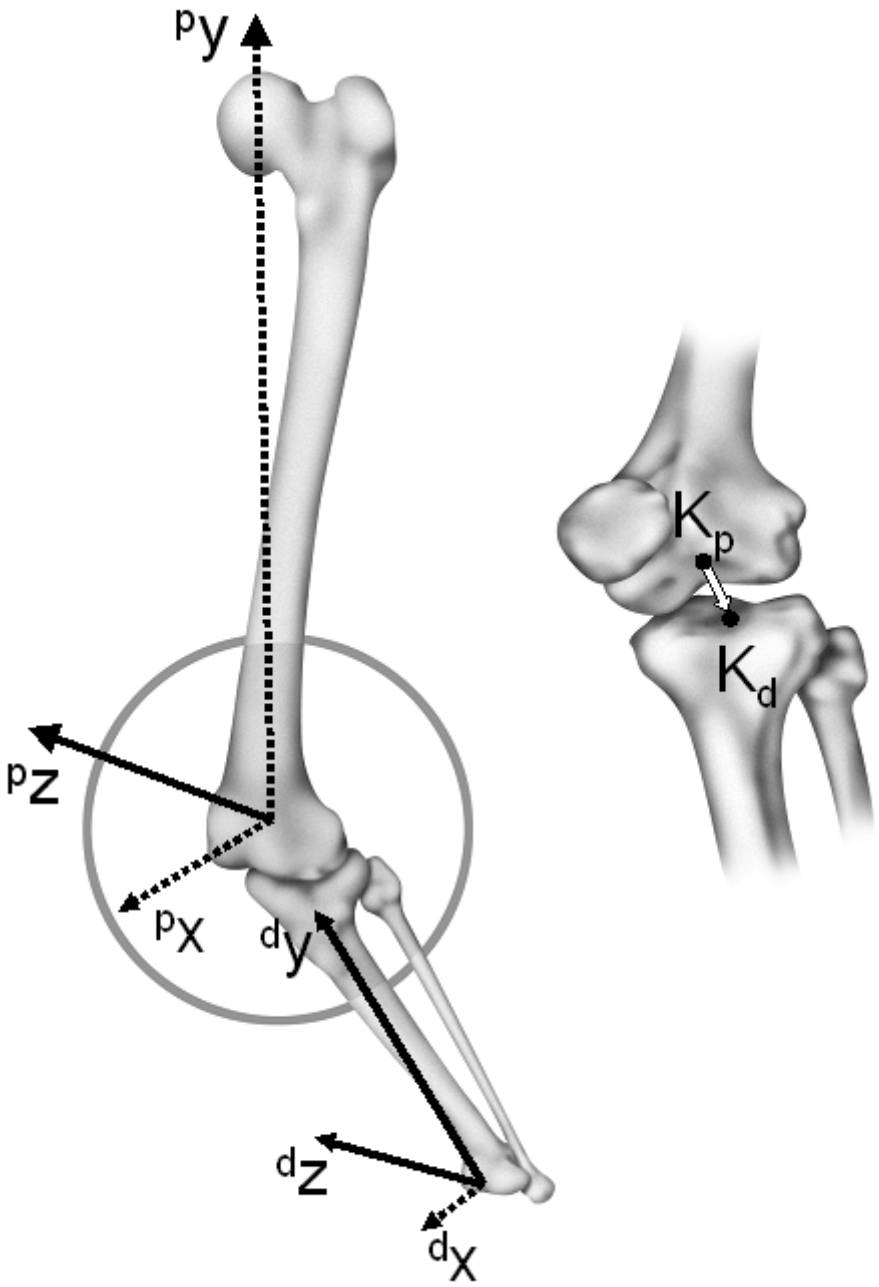

Figure 2-6 Proximal ($^{p}X, ^{p}Y, ^{p}Z$) and distal ($^{d}X, ^{d}Y, ^{d}Z$) anatomical frames used to describe joint kinematics. In the hypothesis of using the Cardan convention, the three rotations used to describe the joint rotational degrees of freedom are thought to occur in sequence about the ^{p}Z (or ^{d}Z) axis (flexion-extension), the ^{d}X axis (adduction-abduction), and the ^{d}Y axis (internal-external rotation). The points defined in the proximal (K_p) and in the distal frames (K_d) used to describe the joint translational degrees of freedom are also indicated.

Translational degrees of freedom

The relative position between two adjacent bones is described by making reference to the vector ($\mathbf{t}_j^*$) joining a point defined in the proximal ($\mathbf{K}_p$) and a point defined in the distal local frames ($\mathbf{K}_d$) (Figure 2-6). If $\mathbf{K}_p$ and $\mathbf{K}_d$ are the origins of the two frames, this vector coincides with $\mathbf{t}_j$ For the sake of the already-mentioned repeatability issue, these reference points should coincide with anatomical landmarks.

The next problem consists of the definition of the anatomical axes with respect to which the scalar components of the above-mentioned vector should most effectively be represented (Ramsey et al. 1999). This is an issue that has not been as yet sufficiently debated in the literature. The reason for this may be that the variations in magnitude of this vector during movement are, normally, too small to be resolved by the presently available experimental and analytical methods.

Rotational degrees of freedom

Assuming that, to start with, the two AF axes are aligned, the distal AF can reach any orientation relative to the proximal AF by undergoing three successive rotations, each time about one of the six axes involved in its current orientation. The three angles thus obtained are used to describe the joint instantaneous orientation.

Calling $\{\mathbf{x}_p\mathbf{y}_p\mathbf{z}_p\}$ the proximal and $\{\mathbf{x}_d\mathbf{y}_d\mathbf{z}_d\}$ the distal system of axes, if $\{\mathbf{x}_d\mathbf{y}_d\mathbf{z}_d\}$ is rotated by an angle α about the $\mathbf{x}_p$ or $\mathbf{x}_d$ axis, then the relevant orientation matrix is:

$$\mathbf{R}_{j\alpha} = \begin{bmatrix} 1 & 0 & 0 \\ 0 & \cos\alpha & -\sin\alpha \\ 0 & \sin\alpha & \cos\alpha \end{bmatrix} \tag{2.6}$$

Similarly, the orientation matrices obtained from rotations about the $\mathbf{y}_p$ or $\mathbf{y}_d$ axis (β) and about the $\mathbf{z}_p$ or $\mathbf{z}_d$ axis (γ) are given respectively by:

$$\mathbf{R}_{j\beta} = \begin{bmatrix} \cos\beta & 0 & \sin\beta \\ 0 & 1 & 0 \\ -\sin\beta & 0 & \cos\beta \end{bmatrix}, \tag{2.7}$$

$$\mathbf{R}_{j\gamma} = \begin{bmatrix} \cos\gamma & -\sin\gamma & 0 \\ \sin\gamma & \cos\gamma & 0 \\ 0 & 0 & 1 \end{bmatrix}. \tag{2.8}$$

These matrices are referred to as basic rotation matrices (Kane et al. 1983; Fu et al. 1988; Fioretti et al. 1997). As mentioned previously, any orientation of the distal frame with respect to the proximal frame can be thought of as the result of three successive and ordered basic rotations. After these basic rotations have occurred, the joint orientation matrix may be obtained using the following rules (Fu et al. 1988):

Initially, both $\{\mathbf{x}_p\mathbf{y}_p\mathbf{z}_p\}$ and $\{\mathbf{x}_d\mathbf{y}_d\mathbf{z}_d\}$ are thought to be coincident, and hence the orientation matrix is a 3×3 identity matrix **I**.

If a rotation occurs about an axis of the proximal frame, then one has to pre-multiply the previous orientation matrix with the appropriate basic rotation matrix.

If a rotation occurs about an axis of the distal frame, then one has to post-multiply the previous orientation matrix with the appropriate basic rotation matrix.

Thus, if, for example, it is hypothesised that the three consecutive rotations occur, first, around the $\mathbf{z}_p$ axis (that coincides with the $\mathbf{z}_d$ axis), second, around the current orientation of the $\mathbf{x}_d$ axis, and, third, around the current orientation of the $\mathbf{y}_d$ axis, then the orientation matrix is:

$$\mathbf{R}_j = \left\{\left[\left(\mathbf{R}_{j\gamma}\cdot\mathbf{I}\right)\cdot\mathbf{R}_{j\alpha}\right]\cdot\mathbf{R}_{j\beta}\right\} \tag{2.9}$$

which can be written as

$$\begin{bmatrix} r_{11} & r_{12} & r_{13} \\ r_{21} & r_{22} & r_{23} \\ r_{31} & r_{32} & r_{33} \end{bmatrix} = \begin{bmatrix} \cos\gamma\cos\beta - \sin\gamma\sin\alpha\sin\beta & -\sin\gamma\cos\alpha & \cos\gamma\sin\beta + \sin\gamma\sin\alpha\cos\beta \\ \sin\gamma\cos\beta + \cos\gamma\sin\alpha\sin\beta & \cos\gamma\cos\alpha & \sin\gamma\sin\beta - \cos\gamma\sin\alpha\cos\beta \\ -\cos\alpha\sin\beta & \sin\alpha & \cos\alpha\cos\beta \end{bmatrix} \tag{2.10}$$

From this system of equations the angles α, β and γ can be obtained as:

$$\begin{aligned}\alpha &= \sin^{-1}(r_{32}) \\ \beta &= \sin^{-1}(-r_{31}/\cos\alpha) \\ \gamma &= \sin^{-1}(-r_{12}/\cos\alpha)\end{aligned} \tag{2.11}$$

Note that a singularity condition occurs when α equals ±π/2 rad (gimbal-lock) and, therefore, large errors may occur when α approaches those values. In addition, the sequence with which the three rotations are made to occur cannot be changed consistent with the fact that matrix multiplication is not commutative (equation 2.9).

If the sequence of rotations involves the three axes of one of either the proximal or distal frames, then the Cardan, or Bryant, convention is used. The specific sequence of basic rotations used in the example, chosen among the several sequences that are possible, is consistent with the so-named Grood and Suntay's convention (Grood et al. 1983). This was first proposed for the description of the angular motion of the lower limb joints since, through a proper selection of the AFs, the above-mentioned singularity condition may be avoided, and they allow the desired consistency with the language of functional anatomy (Chao 1980; Grood et al. 1983; Wu et al. 1995; Fioretti et al. 1997; Wu et al. 2002). If the AFs are chosen so that the x axes are antero-posterior, the y axes are longitudinal, and the z axes are medio-lateral relative to the bony segments involved (Figure 2-6), then the angles α, β and γ may be effectively interpreted as the extent to which the joint is abducted or adducted, internally or externally rotated, and flexed or extended, respectively, relative to the reference aligned orientation.

The three above-mentioned rotations are often described as occurring about three non-orthogonal axes: the $\mathbf{z}_p$ axis, a floating axis (an axis orthogonal to both the $\mathbf{z}_p$ and the $\mathbf{y}_d$ axis), and the $\mathbf{y}_d$ axis (Grood et al. 1983). It is evident that when the second rotation occurs, the floating axis coincides with the $\mathbf{x}_d$ axis. Thus, there is no difference between the two ways of presenting this subject matter.

It is important to remember that the three angles referred to do not describe real rotational movements. Although they may be given a physical

meaning, they simply represent a conventional, univocal way of describing instantaneous relative orientations.

Any given orientation of the distal AF with respect to the proximal AF can also be described by assuming that it is reached, from an initially aligned condition, through a single rotation by an angle, θ around an axis with unit vector $\mathbf{n}$ (Woltring 1994; Fioretti et al. 1997). Thus the joint orientation may be described using the orientation vector $\boldsymbol{\theta}_j = \theta_j \cdot \mathbf{n}_j$. This vector can be derived from the orientation matrix $\mathbf{R}_j$ and vice-versa. The scalar components of this vector may be represented in either AFs, which, apart from a sign inversion, would be identical (Woltring 1994), or in any set of axes of choice, be they orthogonal or not. The specific choice depends, again, on the consistency of the results with the language of functional anatomy.

The components of the orientation vector $\boldsymbol{\theta}_j$ should not be interpreted as actual rotations about the AF axes, but simply as an algebraic method to express a vector in a given coordinate system. Unlike position vectors, and consistent with what has been noted with reference to the Cardan angles, the orientation vectors are not additive. For example, if $\boldsymbol{\theta}_{j1}$ and $\boldsymbol{\theta}_{j2}$ represent the orientation vectors of two different orientations of the $\{\mathbf{x}_d\mathbf{y}_d\mathbf{z}_d\}$ with respect to the $\{\mathbf{x}_p\mathbf{y}_p\mathbf{z}_p\}$ system of axes, the orientation vector that describes the rotation from orientation 1 to orientation 2 is not equal to the difference $\boldsymbol{\theta}_{j2} - \boldsymbol{\theta}_{j1}$. Additivity is valid only under special conditions such as consecutive rotations about parallel axes (planar movements) or infinitesimal rotations. An interesting feature of this convention relates to the fact that it is not prone to gimbal-lock (Woltring 1994).

A third approach, may be proposed for the description of a joint's rotational degrees of freedom. It is based on the projection of axes of an AF onto the planes of the other AF, and in the determination of the angles formed by these projections with suitably selected AF axes (Paul 1992; Cheng et al. 1999). As such, it is referred to as a geometrical convention. For example, in the instance of the knee joint, the following rotation angles can be defined (Paul 1992):

- Flexion-extension angle: the angle formed by the y axis of the tibia and the projection of the y axis of the femur onto the xy plane of the tibia.
- Abduction-adduction angle: the angle formed by the y axis of the tibia and the projection of the y axis of the femur onto the yz plane of the tibia.
- Internal-external rotation angle: the angle formed by the x axis of the tibia and the projection of the x axis of the femur onto the xz plane of the tibia.

This approach is intuitive and close to joint motion representations in functional anatomy. However, these angles are computed following a totally arbitrary definition which has no consistency whatsoever with the sequence of rotations characteristic of the Cardan angles or the orientation vector components (Fioretti et al. 1997).

Comparison among different angular conventions

In the previous sections, it has been shown that a given joint orientation may be thought of as being reached through a specified sequence of three rotations. In order to emphasize the heavy dependence of the three rotation angles on the specific sequence used, the data in Table 2-1 are reported. From them, it appears evident also that the largest angle (γ) is least sensitive to the chosen sequence (Fioretti et al. 1997). $\{\mathbf{x}_d\mathbf{y}_d\mathbf{z}_d\}$

[deg]	$\mathbf{x}_p\mathbf{z}_d\mathbf{y}_d$	$\mathbf{x}_p\mathbf{y}_d\mathbf{z}_d$	$\mathbf{z}_p\mathbf{x}_d\mathbf{y}_d$	$\mathbf{y}_p\mathbf{z}_d\mathbf{x}_d$	$\mathbf{y}_p\mathbf{x}_d\mathbf{y}_d$	$\mathbf{z}_p\mathbf{y}_d\mathbf{x}_d$
α	11.5	6.2	10.0	7.1	6.1	10.0
β	10.7	9.3	5.0	5.7	9.4	4.9
γ	29.5	29.9	30.0	30.7	30.9	30.9

Table 2-1 Angle values obtained using different Cardan sequences (indicated by the sequence of the relevant axes) to describe a given relative orientation between two bony segments. α: rotation about the x_d-axis; β: rotation about y_d-axis; γ: rotation about z_p-axis (see Figure 2-6). The sequence $z_p x_d y_d$ corresponds to that proposed in (Grood et al. 1983).

In order to appreciate the difference between the results yielded by the different conventions illustrated in the previous section, the photogrammetric data, obtained from an adult subject during a level walking trial, have been processed consistently with some of them. In particular, the following angular conventions were used:

a) the Cardan convention suggested by Grood and Suntay ($\{\mathbf{x}_p\mathbf{y}_d\mathbf{z}_d\}$ sequence);

b) joint angles obtained following the geometric approach detailed above (Paul 1992);

c) the orthogonal projections of the orientation vector θ_j onto the proximal (thigh) AF (Woltring 1994);

d) the non-orthogonal projections of the orientation vector θ_j onto the joint axes ($\{\mathbf{z}_p\mathbf{x}_d\mathbf{y}_d\}$) used in (a), taken in their instantaneous orientation.

The femoral and tibial AFs were constructed consistently with the definitions reported in Cappozzo et al.(Cappozzo et al. 1997).

The results reported in Figure 2-7, relative to knee angular kinematics, show that while only minor differences can be observed in the flexion/extension angles, the differences in both abduction/adduction and internal/external rotation angles are substantial. Of course, also the angles assessed while the subject assumed an up-right posture were different (Figure 2-7). These data do not indicate which convention is best, but they do underline the fact that, for the sake of information and data sharing, an agreement within the human movement analyst community on a selected convention seems imperative.

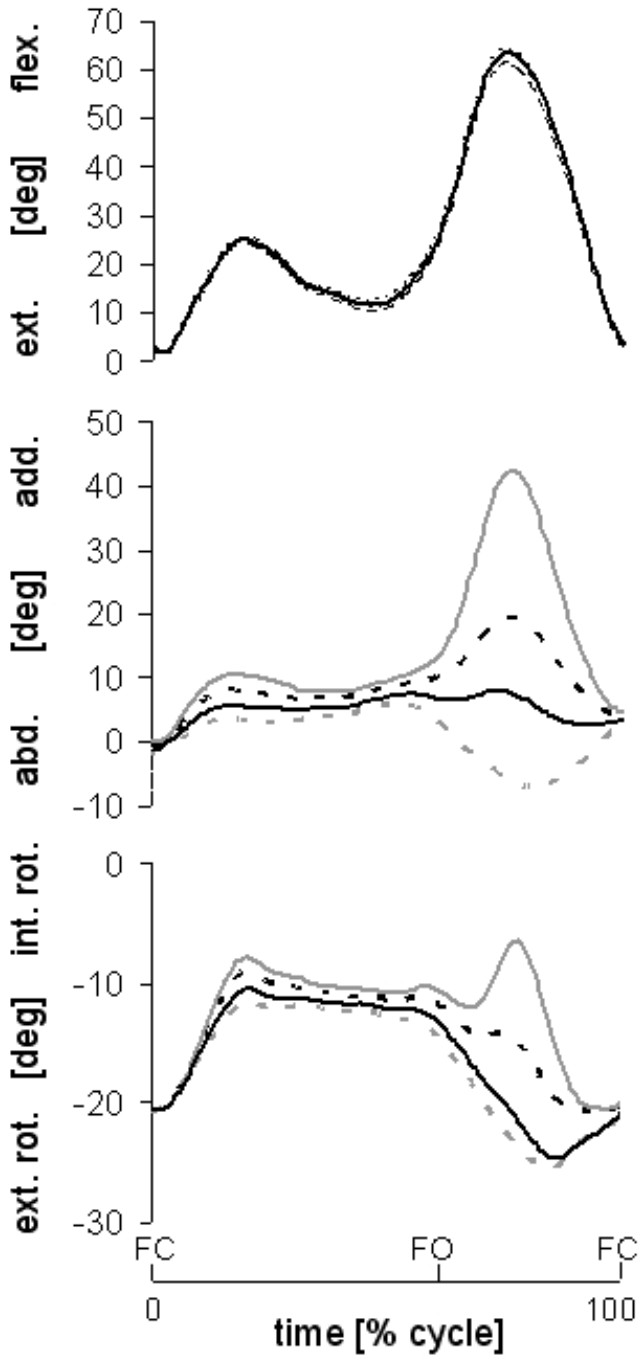

Figure 2-7 Knee joint rotational degrees of freedom, during a gait cycle of a healthy subject, described using four different methods: a) the Cardan convention (Grood and Suntay, 1983); b) the geometric approach (Paul, 1992); c) the orientation vector components as projected onto the axes used for the Cardan rotation sequence (Fioretti et al., 1997), and d) the orientation vector components as projected onto the axes of the proximal (femoral) AF (Woltring, 1994). While the subject assumed an upright posture, for each of the four methods, knee flexion, adduction, and internal rotation had the following values, respectively: a) 7, 6, and -21 degrees; b) 8, 5, -22 degrees; c) 6, 7, -21 degrees; d) 4, 8, -20 degrees. FC: foot contact; FO: foot off

In summary, in order to proceed to the description of segmental kinematics the following information must be acquired:

- the position vector and orientation matrix of a local frame for each musculo-skeletal model segment, relative to a selected global frame, in each sampled instant of time ($^{g}\mathbf{o}_{l}$, and $^{g}\mathbf{R}_{l}$),
- the position vectors of selected particles of the link segments in the relevant local frame.

If required, a registration procedure between movement and morphological data must be implemented.

When the objective is the description of joint kinematics during the execution of a motor task, after having defined an AF for each bone involved in the analysis, the following procedure must be implemented:

- identification of the position vectors of the anatomical landmarks or unit vectors of the functional axes used for defining the AFs in the relevant TFs,
- determination of the position vector and orientation matrix of the AFs relative to a selected global frame ($^{g}\mathbf{o}_{d}$ and $^{g}\mathbf{o}_{p}$, $^{g}\mathbf{R}_{d}$ and $^{g}\mathbf{R}_{p}$),
- and identification of the position vectors of a point ($\mathbf{K}_{p}$) in the proximal AF and of a point ($\mathbf{K}_{d}$) in the distal AF.

In addition the following convention choices must be made:

- the convention to be used to describe the instantaneous joint orientation among the three conventions described above (or others),
- the three axes with respect to which the position vector is represented (normally among the axes of the two AFs involved).

With reference to the joint orientation vector approach, a further convention choice relates to the set of axes with respect to which its scalar components are represented .

All of the above mentioned convention decisions have important effects on the results of the analysis and must, therefore, be stated very clearly when these results are shared.

2.2 Instrumental errors

Nomenclature

2-D	Two-dimensional
3-D	Three-dimensional
AL	Anatomical Landmark
BF	Bone-embedded Frame
CAST	Calibrated Anatomical Systems Technique
DLT	Direct Linear Transformation
DOF	Degrees Of Freedom
HMA	Human Movement Analysis
IRE	Instrumental Random Error
ISE	Instrumental Systematic Error
LF	Laboratory Frame
MAL	Movement Analysis Laboratory
RMS	Root Mean Square
SPS	StereoPhotogrammetric System
SVD	Singular Value Decomposition
WLS	Weighted Least-Squares

2.2.1 Introduction

This section focuses on the experimental procedures which provide such information and on the potential sources of inaccuracy arising from the motion measurement process while the rigid body assumption for body segments is kept valid.

The experimental set-up considered consists of an optoelectronic stereophotogrammetric system (OSS), which allows for a non-invasive estimation of the instantaneous position of points in a 3-D measurement volume. It is worth noting that the lack of invasivity means that physical markers are not rigidly associated with the bones. Moreover even in static conditions reconstructed marker positions are not stationary, due to errors

intrinsic in the measuring system (Della Croce et al. 2000). This circumstance critically affects the accurate estimation of the instantaneous position and orientation) of the musculo-skeletal model segments, relative to the selected global frame. The observed relative movements belong to two classes (Cappozzo et al. 1997):

- apparent movements, due to both the systematic and random errors with which marker coordinates are reconstructed by the OSS in the global frame;
- real movements, due to the interposition of both passive and active soft tissues between markers and the underlying bone.

In this section the focus is placed only on the aspects of assessment and compensation of the apparent movement which originates from the OSS itself, its technology and architecture. For this reason, particular attention is given to the main sources of photogrammetric errors, considered here to include the error with which instantaneous marker positions are reconstructed in the photogrammetric frame and the propagation of this error to the estimated pose of other frames, whether local or global.

2.2.2 Optoelectronic stereophotogrammetry

Measurement technology

Stereophotogrammetric methods, whose applications cover wide-range (as in the earth sciences) and close-range (as in biomechanics) measurements, are used to reconstruct 3-D landmark coordinates from photographs (Greaves 1995), radiographs (Selvik et al. 1983), and video images (Stevens 1997). Photogrammetry has been developed as a photography-oriented science since Muybridge's well-known sequence of a horse in motion dating 1878, and is now under continuous development with the aid of computer vision, pattern recognition and artificial intelligence techniques.

Video images have several potential advantages over the other techniques in terms of time consumption, cost, and potential image distortion of the development process, so that optoelectronic systems are nowadays largely the most popular in movement analysis. More specifically, OSS are used to track, by means of a system of CCD cameras, the 3-D position of a set of fiducial points, constituted from either retro-reflective (passive) or light-emitting (active) markers. Analytical close-range photogrammetry then allows the estimation of 3-D position data from digitized, noisy image data, using the geometrical properties of central projection from multi-camera observations.

Retroreflective passive markers are used together with infrared stroboscopic illumination produced by an array of light-emitting diodes mounted around the lens of each camera. The process of recognizing passive markers in the video frames can be performed either via pattern recognition software (Taylor et al. 1982) or by dedicated hardware circuits (Ferrigno et al. 1990). Conversely, active markers are pulsed sequentially, so the system can detect automatically each marker by virtue of the pulse timing, and marker tracking is more easily performed. The 3-D coordinates of each marker are finally computed based upon the 2-D data from two or more cameras, their known location and internal parameters. For the reconstruction of 3-D coordinates, each marker must be seen simultaneously by at least two

cameras, but in practice more than two are recommended, since markers can become obscured from camera views because of arm swings, walking aids, subject rotation, etc. (Furnée 1997).

Several sources of inaccuracy affect photogrammetric measurements, resulting in an error on marker coordinates. Instrumental errors are of two types: 1) systematic (instrumental systematic error, ISE) and 2) random (instrumental random error, IRE). The former type is in any case associated with a model of the measurement system of limited validity, due either to photogrammetric calibration inaccuracies (bad estimation of model parameters) or to non-linearities that this calibration could not take care of (inadequate model). The magnitude of the systematic errors depends on the size of the measurement field and on the position that the marker assumes within it (Gazzani 1993). Random errors may be due to electronic noise, marker flickering, i.e. the imprecision with which marker images are converted into image points, and the quantization inherent to the digitizing process, which transforms marker image coordinates into their numerical values (Della Croce et al. 2000).

Camera calibration methods

The task of calibration, aims at estimating both the internal and external parameters of each camera. Internal parameters determine how the image coordinates of a point are derived, given the spatial position of the point with respect to the camera. On the other side, external parameters characterize the geometrical relation between the camera and the scene, or between different cameras. Particularly popular is the Direct Linear Transformation (DLT) algorithm, (Abdel-Aziz et al. 1971), where a 3-D calibration object with a grid of control points in known positions throughout the volume of interest is simultaneously recorded by all cameras. Some authors specifically investigated the effect on the system accuracy of changing the number and the 3-D configuration of the control points. It was established that the best accuracy is achieved when the control points are large in number and evenly distributed in the calibration volume (Ji et al. 2001). Recently the attention moved to the development of calibration procedures exploiting the epipolar constraint

between a 3-D point and its 2-D projections on the target of two cameras. This approach, pioneered by Dapena and colleagues, (Dapena et al. 1982), and further developed in the computer vision community (Sabel 1994), allowed to estimate the principal points of the cameras without the use of any additional device and allowed to calibrate on-line the internal and external parameters of an OSS only by surveying a rigid bar in motion inside the working volume. Such procedure closely resembles those implemented by Vicon, Motion Analysis, Qualisys, and Elite.

Compensation for random errors: filtering and smoothing of position data

Human movement data commonly have a low-frequency content, with additive, wide-band noise. Since the late 1970s, a large number of studies has been dedicated to the issue of treating noise in these situations (Cappozzo et al. 1975; Hatze 1981; Woltring et al. 1985; Cerveri et al. 1998; Borghese et al. 2001) The large majority of these studies has investigated the source and the characteristics of the instrumental errors, proposing a wide range of filtering and smoothing techniques. An extensive surveys of these techniques have been provided (Wood 1982). The authors classified the different techniques, both in the time and frequency domain, as graphical methods, finite difference techniques, approximations with least-squares polynomials, spline functions, digital filtering, and Fourier analysis.

Recently, time-frequency analysis has been introduced (Cappello et al. 1996) to estimate kinematic signals incorporating impacts. The accuracy of the second derivative of kinematic signals was assessed by comparing relevant results with accelerometric recordings. A substantial improvement over traditional techniques was obtained.

The estimate of stereophotogrammetric errors

The performance (accuracy and precision) of the system, under the hypothesis of a successful calibration may change upon a large number of factors. These include the adequacy and the quality of the system itself, but also parameters related to the specific laboratory set-up, such as the number

and location of the cameras, the size of the measurement volume, the size and the shape of the calibration object used, and also the care of the user in performing the calibration procedure. Manufacturers quote that the accuracy with which marker positions are reconstructed within a certain field of measurement is generally about 1:3000 of the diagonal of the calibrated volume. The accuracy reported above is largely acceptable in human movement analysis. Nevertheless, the assessment of actual accuracy and precision of marker position measurements deserves an ad hoc investigation in the economy of routine use in the laboratory (Della Croce et al. 2000). Several spot- checks (i.e. tests that the user may perform easily for verification of the preservation of the OSS performance) have been proposed in the literature, based on different target measurements.

Inter-marker distance measurement

This group of tests usually involves very simple devices manually driven by an operator within the measurement volume. A classic method to estimate the instrumental error consists of the static or dynamic recording of a rigid bar of known length carrying at least two markers placed at a known distance. The inter-marker distance is then estimated by the OSS in each sampled instant of time and the systematic and/or random components of its deviation from a gold standard measurement are evaluated (Furnée 1997; Della Croce et al. 2000). Della Croce and Cappozzo with their Movement Analysis Laboratory (MAL) test (Della Croce et al. 2000) pointed out that the magnitude of the errors depends on the markers relative distance and these magnitudes are different for each coordinate. In the static test, the random component of the error is overwhelming. This is mostly represented by high frequency noise superimposed with the so-called flickering effect, which causes sudden shifts of the coordinate value. The dynamic test, in addition to the high frequency noise, exhibits a more evident low frequency error associated with the fact that the markers attached to the rod during the movement assumes different positions in the measurement volume. The latter error component is, therefore, to be associated with the residual measurement volume deformation previously referred to as systematic error. These results confirm the appropriateness of

dividing the photogrammetric error into the additive and uncorrelated components of IRE and ISE.

Specific studies have been devoted to determining the performance of different OSS that are commercially available (Furnée 1997; Richards 1999; Herda et al. 2001). Accuracy and/or precision were reported in a typical gait analysis setting for marker distance estimates. The mean error and accompanying standard deviation ranged from 0.1 mm (SD 0.53 mm) (Muijtjens et al. 1997) to 5.3 mm (SD 4.2 mm) (Furnée et al. 1993). For most systems examined, both mean error and SDs were greater than 1 mm. The absolute error, where reported, ranged from 0.48 mm (Muijtjens et al. 1997) to 11.61 mm (Furnée et al. 1993).

Marker displacement measurement

A number of protocols proposed in the literature investigate marker displacement rather than inter-marker distances. Some tests use only one marker and take advantage of the knowledge of the trajectories that are expected for the moving object to which the marker is fixed to determine the accuracy of the OSS. In this line moves the gravity test formerly proposed in the CAMARC framework (Cappozzo et al. 1993) and the rotating disk test (Cappello et al. 1997). In the latter work, the instantaneous position of a marker firmly attached to the surface of a rotating disk driven by a dc motor was collected and analyzed. The reconstructed trajectories of the marker were found to systematically differ from the expected circular trajectories. This systematic deviation was accounted mainly for by the flickering effect, associated to the fast lightening/darkening of one or more of the camera pixels. The results of the error analysis led to an estimated noise standard deviation between 0.5 and 0.8 mm in the X, Y, and about 2 mm in the Z direction (toward the cameras). It was concluded that OSS could be valuable also in the quantitative clinical analysis of human tremor, mainly characterized by high frequency and very small segment displacement.

Other studies use two or more markers and determine the accuracy of the system by analyzing their relative motion (Everaert et al. 1999). In this way, Everaert and co-workers determined accuracy and precision for an OSS

specifically configured for measuring small and slow displacements within a small measurement volume and proved that motion analysis systems configured for registration within small volumes may allow measurement of minuscule displacements with great accuracy and may therefore be suitable for many applications in rehabilitation research other than gait analysis.

Another study (Richards 1999) adopted a motorized device driving a set of seven markers within the field of measurement, to obtain measurements of the accuracy from several OSSs. This test provides the root mean square (RMS) error of the distance between the markers on the top of a moving bar but also the RMS error of the reconstructed angles formed by three markers mounted on a plate located at one extreme of the bar. Moreover it investigates the ability of the OSS to identify two near markers. Another interesting feature is the ability to perform an analysis on a stationary marker as a function of the minimum distance with an orbiting marker. For most of the OSS assessed, the larger the minimum distance with the rotating marker the better the results.

2.2.3 From marker to segment kinematics

In the light of the results reported so far, it is evident that, due to stereophotogrammetric error on each marker position data, the position vector and orientation matrix of an arbitrary local frame, relative to a selected global frame, suffer from a certain degree of inaccuracy. In the present section, we will provide a survey of experimental and analytical methods aimed at minimizing the propagation of instrumental errors from the kinematics of markers to the kinematics of segmental frames.

Positioning of the external markers

Markers located on the body surface are tracked by the OSS with the ultimate aim of obtaining a reliable estimate of the instantaneous pose of an anatomical frame. Most protocols so far developed for clinical gait and movement analysis (Kadaba et al. 1990; Davis et al. 1991; Frigo et al. 1998) define the AF axes from the location of subcutaneous and/or internal ALs. A set of these frames for lower limb segments has been defined and proposed for standardization (Cappozzo et al. 1995). The most common subcutaneous ALs

are relatively easy to identify if located by palpation using specific instructions (Cappozzo et al. 1995). Within these protocols, such ALs become the suggested location of the set of markers. Of course, the more points on the bone can be located, the more reliable the definition of the AF will be.

Conversely, there is emerging evidence from the literature that, in order to obtain a reliable stereophotogrammetric measurement of human movement, different requirements need to be met by the local frame that give some limitations to the AF-based strategy for marker positioning (Cappozzo et al. 1996). Few general rules, valid for all protocols, dictated only by experimental requirements and which can facilitate bone pose reconstruction have been provided (Cappozzo et al. 1995) and are listed as follows:

a) each marker should be within the field of view of at least two cameras at any given time;

b) markers attached to the same segment should be adequately distributed to minimize position error propagation to bone orientation;

c) movement between markers and underlying bones should be minimal;

d) it should always be possible to place markers even in the presence of external appliances such as orthoses, prostheses or external fracture fixators;

e) marker disturbance to the subject under analysis should be minimal;

f) marker mounting on the subject should be overall a fast, easy and safe procedure.

It was observed that when the cluster of markers is mounted on rigid or semi-rigid fixtures a faster and easier fixation and a better visibility could be obtained and a reduction of soft tissue artefacts using these fixtures might be expected (Holden et al. 2003).

It is well evident that ALs often do not satisfactorily comply with the above-mentioned experimental requirements and therefore may not represent ideal locations for marker placement unless using additional fixtures. Hence a different positioning for the markers is recommended, thus working, at a first instance, with TF rather than AF. Consequently, a registration procedure should be provided for the instantaneous reconstruction of the AF pose from that of the estimated TF pose. To this purpose an anatomical calibration procedure must be carried out. This can be achieved, e.g., as proposed in the

CAST protocol, that gives no strict rules on the exact placement of markers (Cappozzo et al. 1995). Here the sequence of suggested operations is the following:

i) place the marker on the subjects only according to the general guidelines mentioned above;

ii) define a TF from marker coordinates;

iii) by means of a specific static calibration procedure identify the position vectors of selected ALs in the TF;

iv) estimate the time-varying pose of the TF in a global frame during movement; and, finally,

v) reconstruct the AF pose from the TF pose with simple vector transformations.

The estimation of a segment pose from marker position data

Both non-optimal (NOPE) and optimal (OPE) estimators have been used to calculate the pose of a segment from the coordinates of markers (Andriacchi et al. 1980; Spoor et al. 1980; Cappozzo 1984; Arun et al. 1987; Veldpaus et al. 1988; Kadaba et al. 1990; Riley et al. 1990; Davis et al. 1991; Soderkvist et al. 1993; Challis 1995; Cappello et al. 1996). In the NOPE the TF is constructed using simple geometric rules and it is assumed that the position of the markers is error-free.

OPE methods are generally based on least-squares minimization and allow to optimally determine segment pose, even in the presence of noise.

Marker cluster design

A further critical aspect of TF pose estimation is the optimal design of the marker clusters, very limitedly addressed in the literature (Cappozzo et al. 1997; Carman et al. 2005). The performance of a cluster geometrical configuration was shown to depend on the number of markers (n), their relative geometry, and the position and orientation of the cluster with respect to the target anatomical landmarks (Cappozzo et al. 1997). The error propagation to TF pose (here $\boldsymbol{\theta}$ defines the orientation vector of the TF and t the position vector) was quantified by the following expressions:

$$rms\|\Delta\mathbf{t}\| = \sigma\sqrt{\frac{3}{n}} \qquad rms\|\Delta\boldsymbol{\theta}\| = \frac{\sigma}{r}\sqrt{\frac{\mu}{n}}$$

where $\mu = 4.5$ for a 3-D isotropic marker distribution, $\mu = 5$ for a 2-D isotropic marker distribution, σ is the standard deviation of the noise superimposed to the marker coordinates, and r is a size index calculated as the RMS distance of the markers from their mean position. Interestingly, the study advised that

a) a number of markers equal to four seems to be a good compromise between accuracy and practicality,

b) the mean radius of the cluster should be greater than ten times the assessed standard deviation of the experimental error,

c) the three-dimensionality of the cluster is not a critical factor,

d) in quasi-planar clusters, the 2-D isotropic index should be higher than 0.5,

e) the longest principal axis of the cluster should be oriented toward the relevant AL.

2.3 Soft tissue artifact assessment and compensation

2.3.1 Introduction

The fundamental role of human movement analysis in the advancement of the comprehension of musculo-skeletal system physiopathology is well established, and its utilization continues to flourish. However, full maturity in this field is impeded by limited awareness of the methodological fundamentals and experimental inaccuracies associated with the instrumentation and with the fact that it is dealing with a biological system. In Fact, routine in-vivo movement analysis experiments must deal with deformable tissues. This circumstance introduces methodological problems that are recognized to be the primary limitation to further advancements of human movement analysis (Andriacchi et al. 2000).

Two different sources of error originate at the interface between the stereophotogrammetric system and the bony segment under analysis: anatomical landmark mislocation and soft tissue artefact (STA). In this section the latter source of error is addressed, the nature of which resides in the relative movement between the markers which are by necessity stuck on the external surface of the segment, and the underlying bone. This is associated with the specific marker set and experimental protocol adopted. Inertial effects, skin deformation and sliding, which occur mainly in areas closer to the joints (Cappozzo et al. 1996), and deformation caused by muscle contractions, contribute independently to STA. Because of its nature, the artefact has a frequency content similar to the actual bone movement and it is therefore very difficult to distinguish between the two by means of any filtering technique.

A comprehensive review of the studies aimed at assessing STA and at devising methods for the minimization of its effects on the description of the musculo-skeletal function is presented first. Proposed techniques designed to

minimize these effects are also reported, as divided into those analyzing skin surface motion and deformation and those including joint motion constraints.

2.3.2 Soft tissue artefact assessment

A 'soft tissue shifting' effect of body surface markers, very critical particularly when precise analyses of joint motion are needed, was already presumed a long time ago (Hoschek et al. 1984). Since then, a remarkable number of studies that describe patterns and magnitudes of STA have been reported. The most relevant works are reported here, organized according to the technique used, namely intracortical pins, external fixators, percutaneous skeletal trackers and Roentgen photogrammetry.

Techniques based on intracortical pins

A few pioneering studies (Levens et al. 1948; Lafortune 1984) were conducted using intracortical pins to analyze skeletal motion during walking. In 1991, Lafortune and Lake (Lafortune et al. 1991) used intracortical pins inserted into the tibia to quantify STA magnitude at heel strike during running. The magnitude of the relative movement between markers fixed with the bone and attached to the skin reached 10 mm, and was also dependent also upon the type of impact. A later study by the same authors (Lafortune et al. 1992) reported actual tibio-femoral 3D kinematics during walking using target clusters fixed directly into the bones, but no information was provided for describing patterns of STA.

Another study used external marker devices each consisting of a instrumented with three reflective spherical markers (Karlsson et al. 1994). Two of these devices were anchored on the distal femur and on the proximal tibia. Three skin markers were also stuck on the distal thigh and on the proximal shank. Two volunteers were asked to perform hip internal-external rotation with the knee in extension while standing. Internal-external rotation of the knee when measured with the former cluster of markers revealed a range of about 20 degrees, which was observed to be about 50 degrees when measured with the latter skin cluster. The skin displacement tracked by shank markers was found to be smaller than that by thigh markers.

Reinschmidt and colleagues, (Reinschmidt et al. 1997), assessed STA contribution both in knee (tibiofemoral) and ankle complex (tibiocalcaneal) motion during walking. It was confirmed that most of knee rotation errors are due to STA at the thigh. It was concluded that skin markers can only be used to reliably determine flexion/extension (Fl/Ex) at the tibiofemoral joint, whereas for the knee abduction/adduction (Ab/Ad) and internal/external rotations (In/Ex), the error introduced by the STA can almost be as high in magnitude as the real joint motion.

The same authors (Reinschmidt et al. 1997), used a similar technique to also determine the effect of STA on 3D joint rotations in the stance phase of five running trials. A recent study assessed the difference in ankle complex (tibia- talus-calcaneus) motion during the stance phase of walking as measured by skin- and bone-anchored markers (Westblad et al. 2000). The results showed that the mean maximal differences between the skin- and bone- based joint rotations were smaller than 5 degrees. The smallest absolute difference was found for plantar/dorsiflexion.

Very recently, Benoit and colleagues, (Benoit et al. 2005), studied the effects of STA on the reporting of knee joint kinematics during gait and cut movement. The kinematics derived from the bone pin markers was compared with that of the skin markers. Rotational errors of up to 4.4 and 13.3 degrees and translation errors of up to 13 and 16 mm were noted for the walk and cut respectively.

Techniques based on external fixators

Angeloni and colleagues, (Angeloni et al. 1992), first made use of patients wearing external devices for fracture fixation at either the femur or the tibia to analyze STA. These devices allowed, through adequate marker mounting, the definition of a set of axes rigidly associated with the underlying bone. Markers were placed on the skin surface over four ALs: greater trochanter (GT), lateral epicondyle (LE), head of the fibula (HF), lateral malleolus (LM). Additional markers were placed on rigid plates strapped to the proximal half of the thigh and the shank using large elastic bands and Velcro fasteners. It was shown that skin mounted markers are subjected to larger STA than the markers

mounted on the rigid plates. More detailed results were reported in a later paper by the same authors (Cappozzo et al. 1996) using the same technique. AFs associated with skin- and fixator CTFs were defined using calibrated ALs. Markers were also located above the bony prominences typically used in gait analysis: GT, LE, HF, LM. Several motor tasks were analyzed: level walking at a natural speed, cycling on an exercise bike, flexion of the lower limb while standing, repetitive isometric muscular contraction, and hip external rotation while standing with the knee in hyperextension. Typical local trajectories of the GT, LE, HF and LM skin markers in the relevant fixator-based AF during a walking stride are reported in Figure 2-8. The marker position errors associated with STA showed remarkable magnitudes (up to 40 mm), as much as an order of magnitude larger than stereophotogrammetric errors. In general, the value of the STA associated with the GT, LE, HF and LM markers was found to be related to the relevant joint angle, irrespective of the motor task performed. STA caused a peak-to-peak error in bone orientation between 6 and 20 degrees in the femur, and between 4 and 10 degrees in the tibia. It was concluded that the estimation of knee joint kinematics might be affected by inaccuracies that for Fl/Ex, Ab/Ad, and In/Ex can be respectively as large as 10%, 20%, and 100% of the relevant expected range of motion.

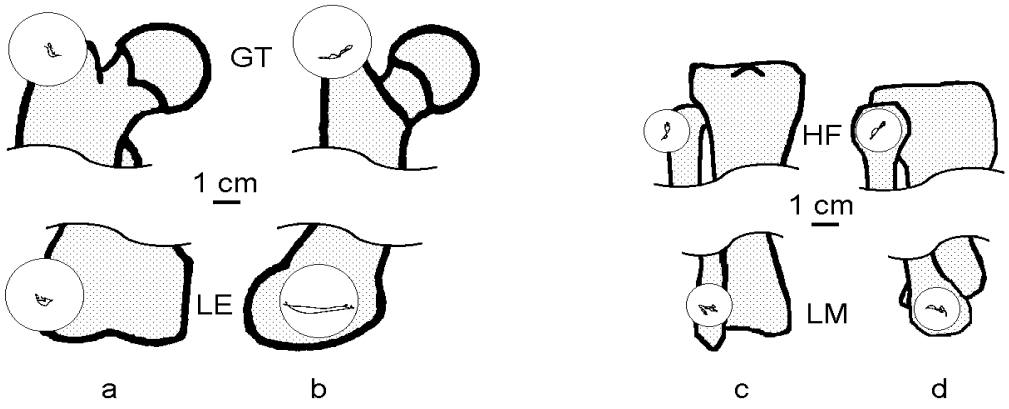

Figure 2-8 local trajectories of GT, LE, ME and LM markers (from Cappozzo et al., 1996).

Techniques based on percutaneous trackers

Another set of studies has been performed recently using percutaneous skeletal trackers. These were metal devices rigidly attached to bony segments

by using a number of halo pins inserted into the periosteum on opposite sides, instrumented with a rigid array of four retroreflective markers. Using this technique, the motion of the shank during self selected speed walking was tracked (Holden et al. 1997). The relative 3D difference between the skeletal- and the surface-based AFs was calculated and considered as a measure of the STA. The first internal rotation error peak, at 8% of gait cycle, had a mean value of 4 degrees over the three subjects analyzed. Additional rotation errors occurred during the terminal stance and most of the swing phase, with a magnitude that reached 8 degrees in one subject. The largest relative rotations about the AP and ML axes were less than 3 degrees. Maximum absolute displacements of the skin-based AF reached 10.5 mm superiorly.

Another study (Manal et al. 2000) used a single tracker clamped to the two malleoli. Three subjects performed several walking trials for different configurations of markers stuck on the shank. Larger errors were observed during the first and last thirds of the stance phase, probably associated respectively to inertial effects at heel-strike, and to muscle contraction for ankle push-off. Rotational errors about the AP and ML axes were similar in magnitude (1-2 degrees). The maximum rotational errors were observed about the SI axis (7-8 degrees).

Techniques based on Roentgen photogrammetry

2D Roentgen photogrammetry was used to investigate STA at the foot and ankle during rear foot inversion/eversion manoeuvres (Maslen et al. 1994). Small steel markers were stuck over the two malleoli, the navicular tuberosity, the sustentaculum tali and the base of the fifth metatarsal. Lateral view radiographs from ten volunteers were collected and analyzed. Mean displacement between the skin markers and the silhouette of underlying bones varied from 2.7 to 14.9 mm, with the two malleoli markers showing the largest artefact.

Sati and colleagues, (Sati et al. 1996), first performed a study to assess quantitatively the relative movement between skin and underlying bone at the knee using standard fluoroscopy. Small metallic markers were individually taped on the medial and lateral aspects of the distal thigh. Fluoroscopic

images were collected during approximately 65° of active knee flexion from upright posture in three male subjects. Root mean square (RMS) values of marker movements varied from 2.1 to 17.1 mm, with a 42.5 and 39.2 mm maximum peak-to-peak respectively along the AP and SI directions. This skin-to-bone movement varied considerably with marker location, the largest skin displacement was observed for markers located closest to the joint line. These results provide valuable information for marker placement in routine movement analysis.

Characterization of the STA was also recently obtained by means of a technique combining stereophotogrammetry and 3D fluoroscopy performed on a total knee replacement patient (Stagni et al. 2005). Sit-to-stand and stair climbing motor tasks were analyzed. The 3D pose of the prosthesis components was reconstructed from each 2D fluoroscopic projection from the knowledge of corresponding CAD models. The skin marker trajectories from the stereophotogrammetric system were reported in the relevant prosthesis component reference frames. Markers on the thigh, particularly those located more postero-proximally, exhibited the largest STA. The maximum amount of this STA was 40, 51, and 55 mm along the AP, ML and SI directions, respectively. The Ab/Ad and In/Ex rotations were the most affected by STA propagation with RMS errors up to 192% and 117% of the corresponding range respectively. Very recently, Sangeux and colleagues (Sangeux et al. 2006), studied the magnitude and the effect of the STA on the knee joint kinematics during flexion of the knee. The results shown that the marker movement differs from the bone movement at their maxima 22 mm in translation and 15° in rotation.

The studies reported provide a large quantity of data for describing the amount and the effects of STA at the lower extremities. The discrepancies between the values reported by different authors may be justified by the different techniques used, by the large variability in the subjects analyzed and in the tasks performed, but mainly by the different locations of the skin-mounted markers.

However, the following general conclusions can be drawn:

a) errors introduced by the STA are much larger than stereophotogrammetric errors;

b) the pattern of the artefact is task dependent;

c) STA is reproducible within, but not among, subjects;

d) the STA associated with the thigh is larger than any other lower limb segment.

Skin markers can therefore be used to determine reliably joint Fl/Ex, whereas Ab/Ad and In/Ex rotations should be regarded much more sceptically.

Analyses based on external fixator devices and percutaneous skeletal trackers arise drawbacks associated with the status of the soft tissues in these patients and to the likely non-physiological pattern of locomotion caused by the wearing of the device. Moreover, assessment of STA in patients with external fixators and in volunteers with percutaneous pins is limited by the skin sliding restrictions imposed by the pins, typically mounted in traditional skin marker locations (epicondyles and malleoli).

Roentgen photogrammetric techniques, based on single X-ray radiograms are invasive as well and provide only 2D information. The techniques based on fluoroscopy are minimally invasive, provide a complete 3D measurement of the STA, and enable analyses of a larger number of skin markers, although this is limited to a single joint at time and extensive image data processing is necessary.

2.3.3 Soft tissue artefact minimization and compensation

STA strongly affects AL trajectories and, consequently, relevant segment AFs and finally joint kinematics and kinetics. Techniques for minimizing its contribution and compensating for the relevant effects are certainly fundamental in human movement analysis. Several methods have been proposed and they are described in the present section.

Before reporting on the analytical methods, a brief mention of the clusters of markers which are usually employed is necessary. There is still a

debate on the optimal non-invasive marker set for tracking motion of human body segments (Manal et al. 2000). Skin marker clusters, during the movement due to STA, undergo both to a deformation and a rigid displacement relative to the underlying bone. The displacement of the cluster with respect to the bone can thus be interpreted as the summation of an internal deformation plus a rigid displacement. The internal deformation may be reduced by the use of rigid supports (Holden et al. 1997; Leardini et al. 1999; Leardini et al. 1999; Manal et al. 2000). These devices, however, do not guarantee a more rigid linkage to the bone and they may even introduce systematic rigid artefacts associated with their own inertial effects.

"Solidification" procedure

A so-called "solidification" procedure was proposed (Chèze et al. 1995) to address only the cluster deformation effect. This was aimed at defining marker trajectories consistent with the rigid body assumption.

To validate this method, nominal trajectories of markers rigidly assembled in two clusters associated with the shank and thigh respectively were generated using experimental data obtained during the swing phase of gait. Artificial noise representing typical artefacts during gait was introduced to obtain perturbed marker trajectories. The ability of the method to recover nominal knee kinematics was evaluated. Results revealed that the proposed procedure works just as well as the least-squares method in reducing kinematic errors. The authors explicitly claimed that the only advantages of the proposed technique are its ability to identify erroneous frames and the use of unambiguous rigid body theory while maintaining the kinematic accuracy of the least-squares method.

Double anatomical landmark calibration

An enhancement of CAST technique was proposed later to compensate for the skin sliding associated with joint flexion during the execution of the target motor task (Cappello et al. 1997; Cappello et al. 2005). The proposed method is based on the flexion-extension angle interpolation of two anatomical landmark calibrations taken at the extremes of motion. The procedure was validated on a

knee kinematics data set obtained by the synchronous combination of traditional stereophotogrammetry and 3-D fluoroscopy during the execution of different motor tasks. With respect to the original single-calibration procedure, the RMS error on Ab/Ad and In/Ex rotation angles decreased from 3.7° and 3.7° to 1.4° and 1.6°. The knee translations calculated from stereophotogrammetric data using the proposed compensation method were found to be reliable with respect to the fluoroscopy-based gold standard. The residual mean values of the root mean square error were 2.0, 2.8, and 2.1 mm for anterior/posterior, vertical, and medio/lateral translations, respectively.

A limitation of compensation methods based on multiple AL calibrations is that they should be designed specifically for the motor task under analysis, according to the expected range of joint rotations.

Dynamic calibration

Another combined experimental and analytical procedure to be included in routine movement analysis was proposed for subject- and task- specific assessment of STA and for its compensation by means of a dynamic model of the CTF-to-AL relationship (Lucchetti et al. 1998). Cluster of markers were affixed to the pelvis using a rigid plate and directly on the skin of the thigh and of the shank. Marker position data were collected in upright posture and during level walking at natural cadence.

Then further tasks were performed with the knee locked in hyperextension with voluntary muscle contraction: a) a hip Fl/Ex followed by Ab/Ad, b) a lower limb pendulum swing, and c) hip and pelvis 3D rotation simulating as much as possible the swing phase of walking. A model of the STA of the medial and lateral epicondyle was estimated on the basis of a rigid thigh-shank CTF defined by markers on the shank, which are supposed to be more reliable than the thigh CTF in a knee-locked leg, in both upright posture and gait-simulated hip rotation. The STA model expressed as a function of the hip angles was hence used to correct the ALs trajectories during the level walking.

A quantitative validation of this method was performed with a patient wearing a single degree of freedom (DOF) knee prosthesis. When femur and

tibia poses were determined using a traditional least-squares optimal estimator, the knee joint translations and rotations were found to be affected by RMS errors up to 14 mm and 6 degrees, respectively. Using the proposed technique, these errors were reduced to less than 4 mm and 3 degrees, respectively. The technique is based on the confidence that STA during the dynamic target activity can be well reproduced during simulated trials of dynamic artefact assessment movements.

Point cluster technique

A further technique (Andriacchi et al. 1998) approached lower limb segment pose estimation by defining the CTF as the principal axes of inertia of the marker distribution and adjusting the mass of each marker at each step in order to minimize the effects of the marker cluster deformation.

The method was tested in a simulation model where systematic and random errors were introduced into a fixed cluster of points. The simulation demonstrated that the error due to non-rigid body movement could be substantially reduced. The method was also applied in a group of ten normal subjects during walking. The results for knee rotation and translation obtained from the point cluster method compared well with results previously obtained from normal subjects with intra-cortical pins inserted into the femur and tibia (Lafortune et al. 1992).

This method was extended (Alexander et al. 2001) to more general cases, providing transformation equations from assumed activity-dependent deformation models. This further method was tested in-vivo on a patient wearing an Ilizarov external fixation device on the shank. In the latter single trial test, the reduction of the error for overall pose was 33% and 25% respectively, though skin motion was likely to be restricted by the numerous pins of the device. Techniques for characterizing general cases of segment deformation have also been recently proposed (Alexander et al. 2003).

The techniques cannot cope with the rigid displacement of the array with respect to the underlying bone, and are also limited by the critical knowledge of the skin deformation models.

Global optimization

A recent innovative technique (Lu et al. 1999) was based on a global minimization, in a traditional least-squares sense, of the overall measurement errors when a simultaneous determination of the segment poses of a multi-link model of the locomotor musculo-skeletal system is performed. The hypothesis was that the consideration of joint constraints and global error compensation can significantly reduce the effects of STA on segment pose estimation, particularly on the critical values of Ab/Ad and In/Ex rotations.

The method was tested on 20 simulated gait trials where artificial noise was added into each 3D marker coordinate (Chèze et al. 1995). In Figure 2-9, results from four techniques, including the proposed "global optimization", employed in a typical simulated trial are reported. The errors in joint rotations were found to be significantly reduced by the use of the proposed method with respect to the traditional one. It was also noted that the inclusion of the weighting matrix in the optimization provides a more effective STA compensation.

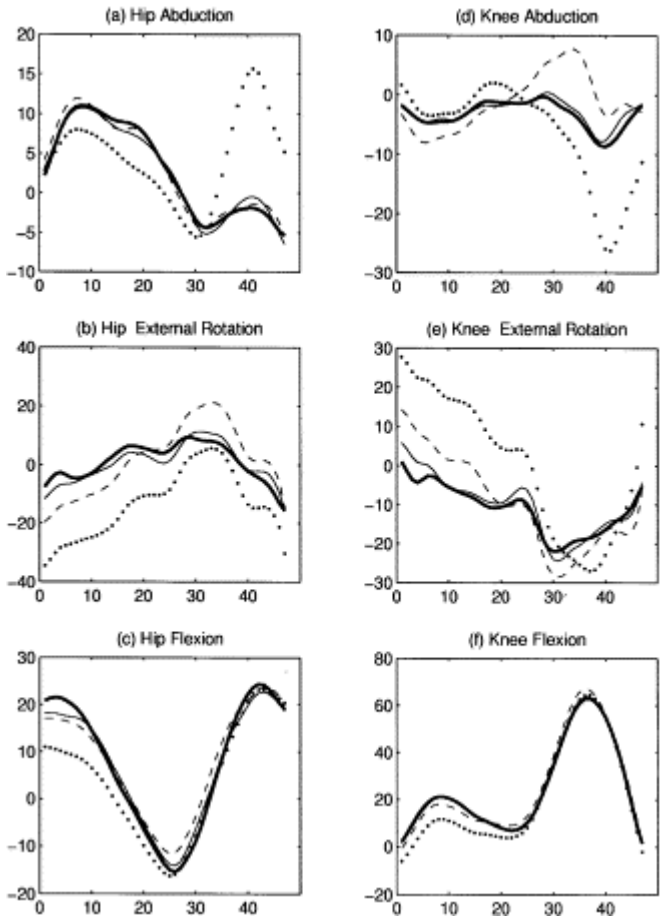

Figure 2-9 Results of the "global optimization" technique (Lu and O'Connor, 1999) from a typical simulated trial. Calculated angles in degrees at the hip (a–c) and knee (d–f) joints by using original true values (thick solid lines), a basic direct linking method (dotted lines), a traditional segment-based optimization method (dashed lines), and the proposed global optimization method (thin solid lines). (from Lu and O'Connor, 1999)

Spherical constraint at the hip, knee and ankle joints were also imposed on the Helen Hayes gait model for improving the reliability of the gait measurement (Charlton et al. 2004). The bony segment poses and the functional joint centres and axes are estimated in the same general iterative procedure also by utilizing specifically designed optimization and filtering techniques. Repeatability of these was tested on a single healthy subject by analyzing the gait cycles obtained from three physiotherapist. The standard deviation obtained in the inter- marker distance, bone segment dimension and angular kinematics was significant lower compared with the original gait model

STA reduction effects were claimed also by a similar technique (Cerveri et al. 2003; Cerveri et al. 2003). Using the collected original image points on the TV cameras and a multi-linkage ball-and-socket-joint model parameterised to the specific subject under analysis, joint kinematics is resolved by direct spatial reconstruction, trajectory tracking, joint angle determination, and derivative computation. Estimation is based on Kalman filters and on minimization of the summation of the distances on the 2D image plane between the measured marker traces and the corresponding back-projected markers of the 3D model. Although robustness of the technique against missing and phantom marker configurations was demonstrated, the ability to cope also with STA effects is to be further validated.

The application of global optimization (GO) methods on a large scale basis is limited by the controversial assumption of the ball-and-socket model for the knee and ankle joints, by the likely very complex analysis when more sophisticated joint models are included, and by applicability for patients with large joint instability or deformity. However, this method is the only one proposed so far that appropriately includes joint constraints in the overall estimation of the lower limb segment poses.

Two general approaches seem to represent well what has been proposed in the literature for STA minimization and compensation in bone pose estimation. These techniques can be distinguished between those modeling the external segment surface (Chèze et al. 1995; Andriacchi et al. 1998; Lucchetti et al. 1998; Alexander et al. 2001; Alexander et al. 2003) and those addressing also segment relative motion (Cappello et al. 1997; Lucchetti et al. 1998; Halvorsen et al. 1999; Lu et al. 1999; Cerveri et al. 2003; Cerveri et al. 2003; Charlton et al. 2004). The former, enhancing the traditional methods of segment pose optimal estimation (Spoor et al. 1980; Soderkvist et al. 1993) by explicitly addressing the random and systematic effects of STA, consider absolute and relative motion of the skin markers in a purely geometric view, irrespective of the physiological event generating the STA and irrespective of joint motion and constraints. The latter include in the analysis considerations about physiological joint motion, though very simple, for a more reliable final association between CTF and AF. However, two studies of this latter method

(Cappello et al. 1997; Lucchetti et al. 1998) involve the performance of an additional task necessary for subject-specific STA calibration. These two categories have both advantages and disadvantages, and should be chosen according to the specific application. It is the recommendation of the authors here that no a priori selection should be pursued among these different techniques, unless a general validation process is carried out based on a single set of consistent and realistic data.

It should also be concluded that the overall reliability obtained by addressing explicitly STA effects exceeds that obtained using traditional filtering and smoothing algorithms of single position data and other optimization techniques as reported in Chapter 2.2. One of the studies mentioned here (Lucchetti et al. 1998) is exemplary in this respect, reporting the root mean square of the estimates of five DOFs at the knee joint, known to be zero. These values, therefore representing errors for the corresponding DOFs, were found to decrease very differently when non-optimal, optimal and STA compensation techniques were applied: in AB/AD these were 5.5, 2.4 and 2.5 degrees respectively, in IN/EX 5.5, 4.1 and 2.4 degrees, in antero-posterior displacement 12.5, 11.9 and 3.6 mm, in vertical displacement 7.0, 6.7 and 4.5 mm, in medio-lateral displacement 13.5, 13.0 and 2.9 mm. Corresponding time-histories were reported in a recent paper (Cappozzo 2002).

In summary it has been recognized that STA is the most significant source of error in human movement analysis (Cappozzo 1991; Andriacchi et al. 2000). Any future investigation aimed at reliably estimating in-vivo human joint motion on a six-DOF-base certainly requires sophisticated techniques to cope with STA. The inaccuracies resulting from this source of error are definitely critical not only in joint mechanics investigations and in virtual reality applications, but also in routine clinical movement analysis. The interpretation of relevant results and the associated clinical decision-making process should therefore include awareness of this critical phenomenon and its effects.

Despite the numerous solutions proposed, the objective of a reliable estimation of bone pose in in-vivo experiments of human movement has not yet

been achieved satisfactorily. Theoretically, for an effective compensation of the STA, either ad-hoc exercises must be carried out in order to collect relevant subject-specific information, or a systematic general characterization of the artifact must be available. From this literature review, it is clear that this characterization is not only far from being completed but also far from being practicable, because large differences among subjects have been reported. It would, therefore, be desirable to identify structural models of the STA and to devise experiments that would allow for their calibration, i.e. model parameter determination, to be applicable to the specific subject and motor act under analysis.

2.4 Assessment of anatomical landmark mislocation and its effects on joint kinematics

2.4.1 Introduction

A major issue in human movement analysis is the identification of ALs and the reconstruction of their position in a selected set of axes, namely the AL calibration (Cappozzo et al. 1995; Cappozzo et al. 2005). ALs can be either internal or subcutaneous and the inaccuracy in their determination negatively affects AF definition and consequently, the estimation and interpretation of joint kinematics and kinetics.

This section reviews the information available in the literature regarding the precision and accuracy of the determination of the location of both internal and palpable ALs, and thus of the relevant AFs, as well as the sensitivity of joint kinematics variables to AF precision and accuracy.

2.4.2 Determination of subcutaneous palpable AL locations

The incorrect location of subcutaneous bony ALs through palpation can be caused by three main factors:

1) the palpable ALs are not points but surfaces, sometimes large and irregular;

2) a soft tissue layer of variable thickness and composition covers the ALs;

3) the identification of the location of the ALs depends on which palpation procedure was used.

White and colleagues, (White et al. 1989), first reported on the repeatability of the determination in vitro of pelvis and lower limb AL positions. A recent work (Piazza et al. 2000) focused the investigation on the medial (ME) and lateral (LE) femur epicondyles with the goal of estimating the

range of variability of the axis passing through them used to define the knee flexion/extension axis. The authors highlighted that AL position uncertainty and consequently the erroneous determination of AF axes may result in the observation of physiological knee motions such as the screw-home motion (external rotation of the tibia when the knee extends) even when such motion does not occur, leading to erroneous clinical interpretations of the estimation.

Della Croce et al. (Della Croce et al. 1999) presented an extensive study on the present issue, reporting:

a) precision of the lower limb ALs position determination,
b) its effects on AF orientation determination, and
c) the effects of errors in AF orientation on joint kinematics.

Intra- and inter-examiner AL precision values were determined using acquisitions carried out by physical therapists with gait laboratory experience on subjects with skin marker clusters attached to the pelvis and lower limb segments. The physical therapists were asked to palpate the ALs listed in Table 2-1 using detailed directions (Benedetti et al. 1994). In the same table, relevant precision values are reported expressed in an AF obtained from the mean values of AL positions. Intra-examiner precision was higher than the inter-examiner precision. This was interpreted as being caused by the different examiner interpretations of the procedure for locating ALs. Greater trochanter dispersion was the largest among the femoral ALs (root mean square value up to 18 mm). Tibial ALs were, on average, the most precise. A recent study (Rabuffetti et al. 2003) estimated the variability in identifying the location of ALs distributed over the whole body. Rabuffetti and co-workers estimated both the precision of AL identification of a so called “self-marking” procedure (the subject under examination performed AL identification and calibration on his/her own body) to be used for experimental motion analysis applications in space; and the intra- and inter-examiner precision of AL identification performed by movement analysis experts. In some cases, substantial differences in determining AL location between the expert and “self-marking” operators were found. For example, the GT location was found by the two groups of operators to be more than 20 mm apart and all pelvic ALs were determined with more than 10 mm difference. Inter-operator precision values

obtained in the two studies are highly consistent. The results reported in the Table 2-1 can also be used as guidelines for the choice of the ALs most suitable for AF definition so that the least precise ALs.

bones	AL	Intra-examiner [mm]				Inter-examiner [mm]			
		x	y	z	3D	x	y	z	3D
pelvis	LASIS	3.4	4.0	11.0	12.2	3.5	7.0	12.4	14.7
	RASIS	10.0	11.5	14.5	21.0	12.4	15.2	15.0	24.7
	LPSIS	2.8	8.3	7.5	11.5	9.5	10.8	14.6	20.5
	RPSIS	5.7	10.7	4.6	13.0	8.6	15.7	17.1	24.8
femur	GT	12.2	11.1	7.0	17.9	12.8	9.8	7.2	17.7
	ME	5.1	5.0	6.7	9.8	8.2	9.5	8.0	14.9
	LE	3.9	4.9	7.8	10.0	9.5	13.5	9.8	19.2
	LP	3.8	3.9	7.8	9.5	8.8	7.2	9.7	14.9
	MP	5.2	2.4	10.8	12.2	4.2	2.6	17.9	18.6
	LC	4.7	3.4	2.9	6.5	7.7	5.0	9.8	13.4
	MC	4.4	1.4	4.4	6.4	5.3	5.5	11.9	14.1
tibia fibula	TT	1.2	1.8	4.3	4.8	1.9	7.2	9.1	11.8
	HF	3.3	3.3	3.3	5.7	6.1	8.4	4.9	11.5
	MMP	3.4	4.4	6.6	8.6	12.1	6.6	14.1	19.7
	MLP	8.0	2.1	5.6	10.0	7.4	6.7	9.6	13.8
	MM	2.2	2.6	6.6	7.4	9.9	6.2	9.9	15.3
	LM	2.6	2.4	5.7	6.7	9.3	7.1	12.1	16.8
foot bones	CA	7.0	4.9	5.7	10.3	9.1	9.2	9.8	16.2
	FM	2.6	3.2	6.9	8.0	9.1	9.7	16.9	21.5
	SM	2.2	6.3	6.0	9.0	8.2	7.1	8.7	13.9
	VM	0.7	2.0	6.5	6.8	3.9	8.0	10.0	13.4

Table 2-2 Intra- and inter-examiner precision of the palpable anatomical landmark position components in the relevant mean anatomical frame obtained by Della Croce et al.(Della Croce et al. 1999) .

2.4.3 Determination of internal AL locations: hip and knee joint centers

Those ALs not representing palpable bony prominences are here called 'internal'. Among the lower limb internal ALs, the geometrical centres of the

femoral head is used the most. In human movement analysis, the articular surface areas of the femoral head and of the acetabulum are assumed to have spherical shapes and a common centre, therefore the hip is assumed to be a ball-and-socket joint. The accuracy and precision with which the hip joint centre (HJC) location is estimated are crucial in terms of error propagation to the kinematics and kinetics measurements of the hip and knee joints (Crowninshield et al. 1978; Kadaba et al. 1990).

The HJC location can be estimated using either a functional or a prediction approach. The former, originally proposed by (Cappozzo 1984), suggests that the HJC is the pivot point of a 3-D relative movement between the femur and pelvis. Recent experimental works performed with a stereophotogrammetry system and a ball-and-socket mechanical joint (Piazza et al. 2001; Camomilla et al. 2006) have demonstrated that the collection of an adequate hip range of motion is more important for a reliable estimation of the HJC than the type of motion. It was shown that, in the absence of soft tissue artefacts, the error in determining the pivot point location can reach 5 mm when performing a 30-deg rotation and 10 mm when performing a 15-deg rotation. In a later study (Piazza et al. 2004), the same authors tested the use of the functional method both on limited range ad hoc 3-D movements and on gait trials. They showed that a satisfactory estimation of the HJC requires hip motion both in the sagittal and frontal plane. Other authors focused on the mathematical approach to be used for determining the HJC location, and two novel algorithms were proposed (Halvorsen et al. 1999; Gamage et al. 2002). Recently, it was shown that under certain conditions the two mentioned algorithms are identical suggesting that the analytical method used play a limited role in the overall accuracy of pivot point location determination with respect to both the errors involved in the identification of the pelvis ALs and those resulting from skin motion artefacts (Cereatti et al. 2004). Several authors (Piazza et al. 2004; Camomilla et al. 2006; Ehrig et al. 2006) pointed out that the performance of the functional method can be strongly affected by variation in its implementation. The functional method requires acquisition of an additional task in the gait analysis session, it can be applied only on patients able to perform a significant hip motion, and it is affected by the soft

tissue artefacts. Nevertheless, with the limitations mentioned above, it remains at present the only clinically-feasible method potentially able to detect subject-specific location of the HJC, the alternative imaging-based techniques being inconvenient in most clinical settings.

The prediction approach uses regression equations with pelvis and anthropometric measurements as independent variables. Regression coefficients were obtained by using imaging techniques based on relatively small samples of living adult males (Crowninshield et al. 1978; Tylkowski et al. 1982; Bell et al. 1989; Bell et al. 1990; Davis et al. 1991) or by direct measurements on a larger sample of cadaver specimens (Seidel et al. 1995). Those provided in Bell et al. (1990) and Davis et al. (1991) are currently the most widely used. The mentioned prediction approaches are also based on a very limited and specific population of subjects, and their application to every clinical situation is therefore critical despite this fact similar regression equations are implemented in the major clinical gait software packages.

An attempt was made to combine kinematic data gathered from gait trials with morphological–based HJC location estimations aimed at enhancing the latter without the need for an ad hoc motion trial (Frigo et al. 1998; Charlton et al. 2004). Subject-specific HJC location was estimated using regression equations for an initial guess to be used in an iterative optimization algorithm. The repeatability of the combined method was reported to be better than that of its isolated parts, although the validation was limited by the lack of the actual HJC positions.

Several experimental works compared the performance of prediction and functional methods. The large majority of the studies (McGibbon et al. 1997; Leardini et al. 1999; Besier et al. 2003; Christopher et al. 2003) confirmed that the functional approach appears to be preferable when a considerable range of hip motion can be performed and to be still satisfactory when the hip range of motion is limited. Alternatively, prediction methods must be applied. There are few works (Bell et al. 1990) which claimed that the prediction method provide more accurate estimations than the functional method. The discrepancy between these two result can be related to the different implementation of the functional method(Camomilla et al. 2006).

In the work proposed by Leardini and colleagues, (Leardini et al. 1999), using eleven normal male volunteers, the functional method limited the mean estimation error to 12 mm, performing better than two popular prediction method (Bell et al. 1990; Davis et al. 1991), which produced mean errors of about 23 and 21 mm, respectively. Two different preliminary studies (Fieser et al. 2000; Jenkins et al. 2000) assessed the reliability of different prediction methods by comparing their estimations with actual measurements obtained from imaging techniques. (Jenkins et al. 2000) reported that the maximum discrepancy between predicted and measured HJC locations was 40 mm in a normal child and 85 mm in a child with CP. Mean HJC location errors were found to be significantly higher in children with CP (55 mm) than in normal children (22 mm) and adults (17 mm). This study strongly pointed out the necessity for specific regression parameters to better match age, gender or anthropometric typology and possibly pathological conditions.

For future progress, the use of the functional approach in large scale experimental campaigns in order to provide the gait analysis community with robust and detailed series of regression equations for HJC location, kinematics-based estimations, preventing large populations of volunteers from being exposed to radiation, has been suggested (Leardini et al. 1999; Camomilla et al. 2006; Camomilla et al. in press), and preliminarily performed (Shea et al. 1997).

All the current methods, however, are definitely expected to generate substantial errors in determining HJC location, and all the outcomes affected by these errors should therefore be considered very carefully in the clinical decision-making process (Stagni et al. 2000).

2.4.4 Determination of AF pose

The knowledge of the AL positions in the relevant CTF allows for the definition of AFs and the determination of their orientation. A precise determination of AF orientation is crucial for joint kinematics reliability. Della Croce et al. (Della Croce et al. 1999) used the AF definitions proposed by Cappozzo et al.(Cappozzo et al. 1996), which are in accordance with general

standard directions of reference axes (Wu et al. 2002). The experimental sessions provided observations of the AF orientation matrices and position vectors of the lower limb bones with respect to the relevant $\overline{AF}$ from which the orientation vectors were determined (Spoor et al. 1980). Their precision results are reported in Table 2-3. Pelvis and foot AF orientation errors were distributed roughly equally on the three axes. To the contrary, the femoral and tibial AF orientations resulted dispersed mostly about their longitudinal (y) axis. This was associated with the shape of these bones and consequent AL cluster geometry, characterized by an overwhelming contribution of the longitudinal dimension with respect to the other two dimensions. It was pointed out that the values in Table 2-3 are affected not only by the precision of the relevant ALs, but also by the AF definition rule adopted.

segment	intra-examiner [deg]			inter-examiner [deg]		
	θ_x	θ_y	θ_z	θ_x	θ_y	θ_z
hip bones	2.3	2.6	3.7	5.2	3.7	4.1
femur	0.9	4.7	0.9	2.5	5.1	3.0
tibia and fibula	1.4	3.5	0.3	4.2	9.4	2.6
foot bones	2.7	2.3	1.8	5.9	9.2	5.1

Table 2-3 Intra- and inter-examiner precision of the indicated anatomical frame orientation components along the antero/posterior (θ_x), longitudinal (θ_y), and medio/lateral (θ_z) directions.

Piazza and Cavanagh (Piazza et al. 2000) defined femur and tibia AFs using common definition rules (Cappozzo et al. 1995). They estimated the variability in determining the intercondylar axis orientation only and reported a mean angle of separation of 7.7 degrees.

Other studies did not deal with the precision of the AL location determination and its effects on AF orientation precision, but simply hypothesized a certain error in determining anatomical axes orientation (Kadaba et al. 1990; Fioretti et al. 1997; Cheze 2000; Manal et al. 2002) with the goal of observing the consequent variations in joint kinematics or dynamics representation.

2.4.5 Joint kinematics sensitivity to erroneous determination of AL location and AF orientation

Given the crucial role of the HJC in gait and locomotion analysis, the effects of the erroneous determination of its location have been investigated more than those of other AL location erroneous determinations (Kadaba et al. 1990; Stagni et al. 2000). Kadaba et al. (1990) observed the effects on joint kinematics when the HJC position was made to vary analytically over a 20 mm range in all directions. They observed an offset in joint kinematics curves without affecting the relevant patterns throughout the gait cycle. Stagni et al.

(2000) extended the quantification of the propagation of the erroneous determination of HJC location to hip and knee kinetics, as assessed on a group of five able-bodied subjects during level walking. Hip and knee angle and moment components were estimated for each experimental trial first using a nominal estimate of the HJC position, then adding a set of 3-D errors in HJC location taken within the range of the data reported in Leardini et al. (Leardini et al. 1999). It was observed that inaccuracies in the HJC coordinate estimates affect gait analysis results remarkably. The hip moments showed the largest propagation error, particularly in the flexion/extension component (propagated error of the mean of -22%, for HJC location determined with 30mm error on the anterior-posterior direction). The ab/adduction moment was found to be the second largest affected quantity, associated with medio-lateral HJC erroneous location. The effects of erroneous HJC location determination on knee angles and moments were found to be negligible.

Joint angle sensitivity to AF orientation variations has been shown to be high and particularly prejudicial to the reliability of those angles that undergo relatively small variations during movement. At least four different approaches to the estimation of the above mentioned sensitivity are found in the literature:

1) experimental error data applied to devices with controlled joint kinematics (Piazza et al. 2000);

2) experimental error data applied to simulated joint kinematics (Della Croce et al. 1999);

3) error simulation applied to human joint kinematics or dynamics, (Kadaba et al. 1990; Stagni et al. 2000) and

4) a mathematical approach (sensitivity analysis) (Woltring 1994).

Piazza and Cavanagh (Piazza et al. 2000) used two custom devices simulating knee kinematics with 1 and 2 degrees of freedom, respectively. The kinematics of the devices was controlled by the experimenters. Their test allowed for the estimation of the cross-talk in knee kinematics representation. Interestingly, a cross-talk was also found when no remarkable error was introduced in locating the fiducial “anatomical” landmarks of the devices. The authors concluded that joint kinematics representation is extremely sensitive

to rotation axis location in space, and recommended a limited use of "minor" angle data.

Della Croce et al. estimated the propagation of AL position precision to joint kinematics by simulating the joint movement. Using the AF orientation observations of the proximal and distal segments of each lower limb joint, and analytically aligning proximal and distal $\overline{AF}$, the effect of AF orientation errors was computed. A flexion for hip and knee and dorsi-flexion for the ankle were then simulated through an adequate rotation of the relevant distal $\overline{AF}$ about the medio-lateral axis of the proximal $\overline{AF}$. This reproduced a situation similar to that found during gait, whereby one rotational component is significantly greater than the others. The three Cardan angles, as defined by Grood and Suntay (1983), were calculated to describe the joint orientation in terms of flexion/extension, ab/adduction and internal/external rotations. These results are reported in Table 2-4 for joint angle precision when proximal and distal mean $\overline{AF}$ are aligned. Internal/external rotation components were the least precise. Precision propagation to knee ab/adduction and internal/external angles was shown to be dependent on the degree of knee flexion. The values of both ab/adduction and internal/external angles, were considered to be large enough to affect the reliability of the intrinsically small values of these angles. The same did not hold true for hip and ankle.

joint	**intra-examiner [deg]**			**inter-examiner [deg]**		
	ab/adduction	int/external rot	flex/extension	ab/adduction	int/external rot	flex/extension
hip	2.5	5.3	3.9	5.2	5.6	5.0
knee	1.7	5.8	1.0	5.2	10.4	3.7
ankle	3.5	3.9	1.6	10.9	10.3	3.3

Table 2-4 Intra- and inter-examiner precision of the joint angles during upright posture.

Kadaba et al.(Kadaba et al. 1990) performed a sensitivity analysis of joint kinematics representation to variations of flexion/extension axis orientation. Joint kinematics of one subject was used to perform the analysis. The knee flexion/extension axis was made to vary analytically within a range of 30 deg and errors in knee internal/external and ab/adduction were plotted against the flexion/extension angle. This showed a dependency of the minor angle error on

the degree of flexion. Among other observations, they concluded that ab/adduction and internal/external rotation angles must be interpreted with caution, especially at the knee. Chèze (Cheze 2000) performed a test with the goal of identifying the joint kinematics representation the least sensitive to both AL location determination and skin artefacts. A time variant periodic error was added to the AL positions recorded during a gait cycle performed by a subject, to represent both skin movement artefacts and AL location errors. Unfortunately, the study did not report the details of the analysis methods. Interestingly, however, the results showed that internal/external rotations are the most sensitive to the AL instantaneous position errors. Fioretti et al. (Fioretti et al. 1997) tested the sensitivity to incorrect determination of the direction of the knee flexion/extension axis, of four different methods used to describe joint kinematics: a) the Cardanic convention introduced by Grood and Suntay (1983); b) the non-orthogonal projections of the orientation vector on the joint axes defined by Grood and Suntay (Grood et al. 1983), as proposed by (Meglan et al. 1990) ; c) the orthogonal projections of the orientation vector on the proximal (thigh) AF (Woltring 1994), and d) the joint angles obtained following the geometric approach described by Paul (Paul 1992). The flexion/extension axis direction was analytically made to vary ±15 deg both internally and externally in increments of 5 deg. This resulted in changes affecting the orientation matrix and, consequently, the angles.

Woltring (Woltring 1994), while proposing the orientation vector to describe joint kinematics, performed a mathematical sensitivity analysis of both the orientation vector and Cardan angles (Grood et al. 1983). It was shown that Cardan convention was affected by more cross-talk among components as the major angle increases. He concluded that the orientation vector was more suitable for describing joint kinematics than any Cardanic convention. However, the use of this representation for joint kinematics has not been successful, mainly because it is considered to be lacking in physiological interpretability.

The original figures reported below (Figure 2-10 -- Figure 2-13) illustrate the effects of AF orientation changes on knee kinematics obtained during the gait cycle of a healthy subject and described using the four methods mentioned

above. In Figure 2-10 and Figure 2-11 the proximal AF is made to rotate about the anterior/posterior axis of the femur within a ±10 deg range. Figure 2-10 shows the effects of the AF rotations on the ab/adduction angle calculated with the four methods (Figure 2-10 a-d). The four methods show about the same sensitivity to proximal AF rotations until the knee is maximally flexed. In this situation, methods (a) and (b) show a reduced sensitivity, while method (d) becomes more sensitive. Figure 2-11 shows the effects of the same AF rotations reported in Figure 2-10 on the internal/external angles calculated with the four methods. Interestingly, the method (d) internal/external angle is not affected by rotations about the AF anterior/posterior axis. The internal/external angles calculated with the other three methods are more sensitive when the knee is maximally flexed.

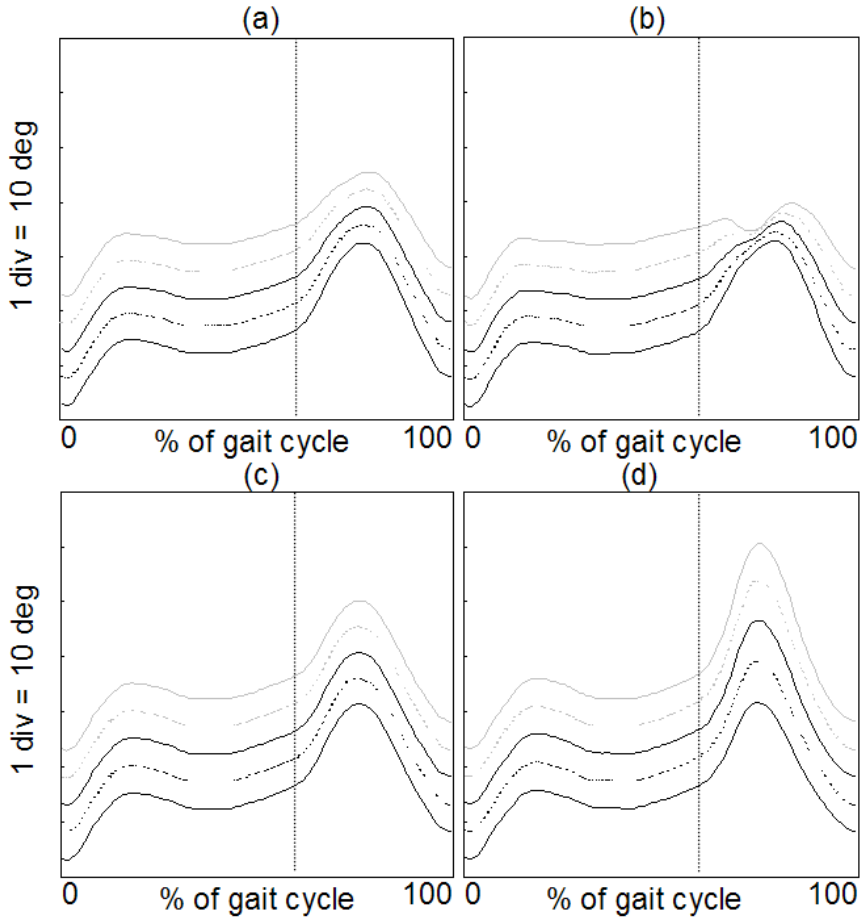

Figure 2-10 Effects of proximal AF orientation variations on ab/adduction angle (adduction angles are positive) during a whole gait cycle (dotted vertical lines indicate toe off timing). The proximal AF orientation is made to vary about the AF anterior/posterior axis: -10 deg (solid grey line), -5 deg (dotted grey line), +5 deg (dotted black line) and +10 deg (solid black line) with respect to the nominal orientation (thick solid line). Ab/adduction angle is calculated using four joint kinematics description methods: a) the Cardanic convention proposed by Grood and Suntay (Grood et al. 1983); b) the orientation vector projected on the joint axes proposed in Grood and Suntay, 1983; c) the orientation vector components in the proximal AF as proposed by Woltring (Woltring 1994) and d) the geometric method proposed by Paul (Paul 1992).

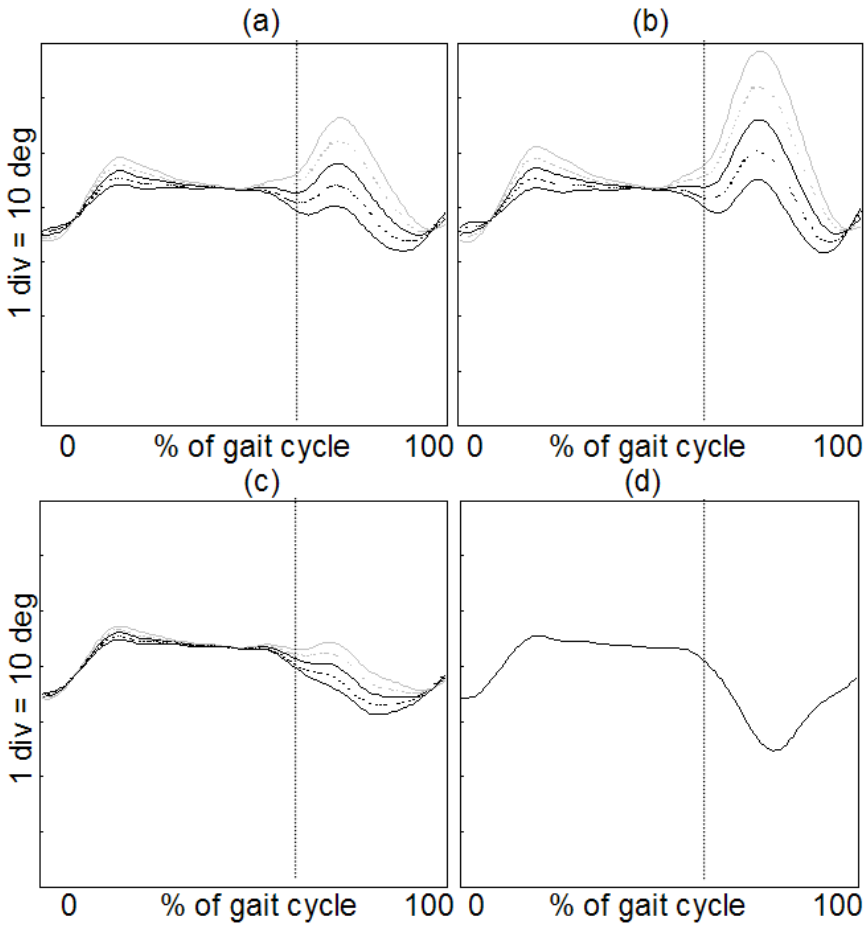

Figure 2-11 Effects on internal/external rotation angle (internal rotations angles are positive) during a whole gait cycle of variations of the proximal AF orientation made to vary ±10 deg (increments of 5 deg) about the AF anterior/posterior axis. Internal/external angle is calculated using four joint kinematics description methods (see caption Figure 2-10 for details).

In Figure 2-12 and Figure 2-13 the knee proximal AF is made to rotate about its longitudinal axis within a ±10 deg range. Figure 2-12 shows the sensitivity of ab/adduction calculated with the four methods to AF orientation changes. Similar to what was found in Figure 2-11, method (d) is not sensitive to rotations of the proximal AF about its longitudinal axis. Among the remaining three methods, method (c) is the least sensitive. The same comments as those for Figure 2-10 can be extended to Figure 2-13, which reports the sensitivity of the internal/external rotation to the proximal AF rotation. An additional remark can be made about method (d) that, during the swing phase, shows a pattern sensitive to the amount of rotation of the

proximal AF about its longitudinal axis. The results shown here highlight that none of the four methods is a best choice for describing joint kinematics. However, a method has to be chosen if results of different tests are to be compared.

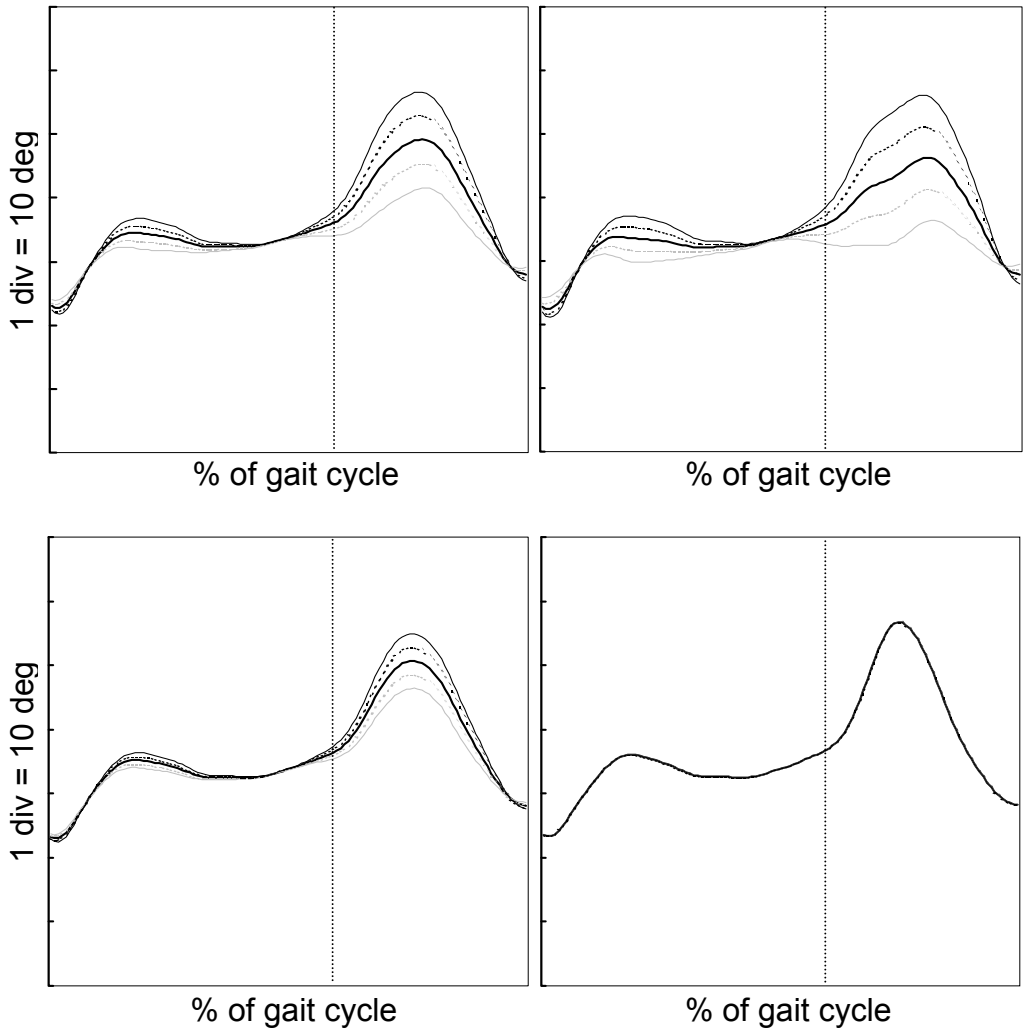

Figure 2-12 Effects on ab/adduction angle (adduction angles are positive) during a whole gait cycle of variations of the proximal AF orientation made to vary ±10 deg (increments of 5 deg) about the AF longitudinal axis. Ab/adduction angle is calculated using four joint kinematics description methods (see caption Figure 2-10 for details).

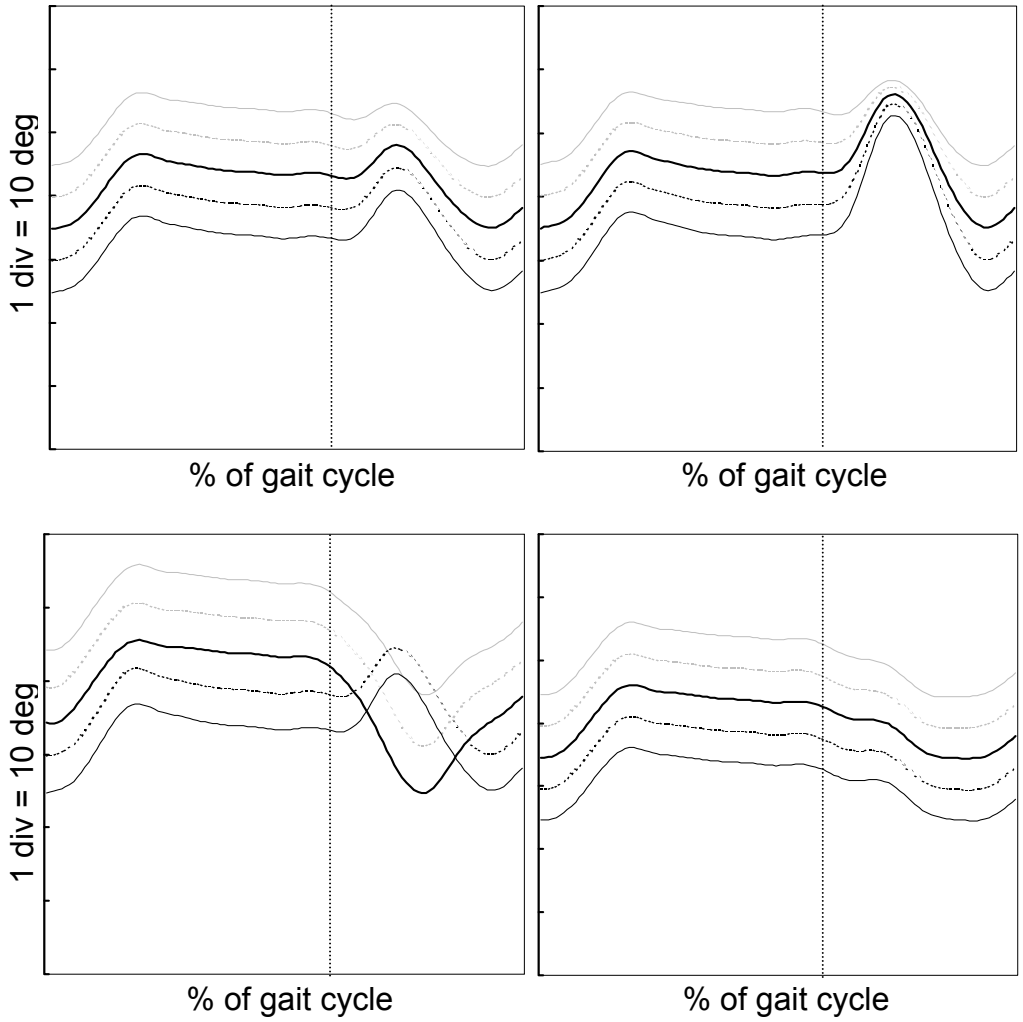

Figure 2-13 Effects on internal/external rotation angle (internal rotation angles are positive) during a whole gait cycle of variations of the proximal AF orientation made to vary ±10 deg (increments of 5 deg) about the AF longitudinal axis. Internal/external angle is calculated using four joint kinematics description methods (see caption Figure 2-10 for details).

2.4.6 Reduction of AL uncertainty effects on joint kinematics

As reported in the previous section, only a limited number of studies dealt with the effect of incorrect definition of joint axes and ultimately of AL location uncertainty on joint kinematics description. Moreover, the conclusions of those studies were limited to a "warning" to the biomechanical community about using information regarding the minor angles of joint kinematics data. No technique was proposed to reduce the mentioned effects. Recently, a first

attempt in this direction was proposed by Della Croce et al.(Della Croce et al. 2003). They tested 12 rules for femur AF definition based on the position of a certain number of femur ALs with the goal of determining a rule that is minimally sensitive to AL position imprecision. The rules differed both in the number of ALs involved in the definition of the AF, and in the geometric algorithm used to identify AF axes from the AL positions. Some AF definition rules used up to eight femoral ALs, together with optimisation algorithms such as SVD, with the hypothesis that redundant information would allow for a more repeatable AF determination. Errors with a standard deviation obtained from the results of a previous study (Della Croce et al. 1999) were added to the positions of the femur ALs. The twelve AF definition rules were applied and the orientation errors of the AFs were determined, allowing for a first selection of the rules that were the least sensitive to AL position uncertainty. The authors concluded that a higher number of ALs and more advanced AF definition techniques making a combined use of CTFs and morphology technical frames (Cappozzo et al. 2005), may contribute in reducing the errors in joint kinematics due to AL uncertainty.

The studies reviewed in this section led to a quantitative description of the precision of AL position determination and its effects on joint kinematics. Although following different approaches, these have shown that reliability and interpretability of joint kinematics are largely dependent on the precision of the determination of AF orientation. It was also shown that the non-linear nature of this dependency renders the effects on joint kinematics unpredictable. Reduction of these errors can be obtained by improving the AL identification procedure. This reduction can be obtained, for instance, by using imaging techniques, by including in the AF definition a higher number of ALs than the three or four normally used, and by using AF definition rules less sensitive to AL uncertainty. Correct interpretation of joint kinematics remains limited to major angles until the above mentioned improvements are achieved and a standard joint kinematics description method is chosen for every joint.

The data acquisition protocols developed for, and generally used in, clinical gait analysis often had the reduction of the number of markers and of

the complexity of data acquisition as the main objective. However, as was shown in this and in the previous sections of this Chapter, additional objectives need to be introduced in order to obtain more reliable gait data and, more generally, human movement data. In particular, it was shown that the absence in the above mentioned protocols of procedures aimed at reducing error effects on output data limits the reliability of the analysis results. On the other hand, data reliability can be remarkably improved if slightly more complex and error-reduction-oriented protocols are used.

CHAPTER 3. SOFT TISSUE ARTIFACT ASSESSMENT AND COMPENSATION

3.1 Introduction

In the analysis of a physical exercise, each segment of interest is usually considered non-deformable and, therefore, modelled as a rigid body. Active and passive soft tissues may or may not be considered deformable. Most of the literature chooses the latter option. In recent years, however, some authors have advocated closer attention to soft tissue deformability in human movement modelling. Ignoring this deformability, bony segment kinematics, reconstructed by using non-invasive photogrammetric data and skin-markers, is so inaccurate that the results are unable to be used (Andriacchi et al. 2000).

The description of the bone movement relative to a global reference frame requires the reconstruction of the instantaneous position and orientation (referred to as pose) of a local system of axes (technical frame - TF) rigidly associated with the bone. Reconstructed marker position vectors can be characterized by three components: the position vector of the target point rigidly associated with the bone, the displacement vector caused by the deformation of the soft tissues interposed between bone and skin (soft tissue artefact - STA), and an apparent displacement, due to photogrammetric error (Cappozzo et al. 2005).

Soft tissue artefact is due to the contribution of inertial effects, skin deformation and sliding, gravity, and muscle contraction with a frequency content similar to that of bone movement (Leardini et al. 2005). Its propagation to the end results is far more disruptive than photogrammetric error (Leardini et al. 2005), which is easily minimized by means of frequency-based filtering techniques (Chiari et al. 2005). In the movement analyst community, the assessment of STA is considered to be a priority, especially with reference to the thigh (Andriacchi et al. 2000; Leardini et al. 2005). Once this error is accurately described, quantified, and modelled then steps can be

taken towards modifying the data and acquisition methods in order to compensate for its detrimental effects on the end results.

A number of studies that describe patterns and magnitudes of STA have been reported (Leardini et al. 2005). Considerable discrepancies are present between the values reported, due to the large variability of the subjects analyzed, the tasks performed, and the locations of the skin-mounted markers. However, there is agreement on the following points: the pattern of the artefact is dependent on the task; STA is reproducible within, but not among, subjects; for the lower limb, the STA associated with the thigh is the largest. (Leardini et al. 2005).

Most of the techniques used in the past were either invasive, like intra-cortical pins, external fixators, and roentgen photogrammetry, or they did not allow the physiological movement of soft tissues with respect to the bone, like percutaneous skeletal trackers. Recently, a minimally invasive method, based on the combination of 2D fluoroscopy and of a model of the bone under analysis, was used by different authors (Banks et al. 1996; Fregly et al. 2005; Stagni et al. 2005; Zihlmann et al. 2006). Another method, based on MRI, was lately proposed by Sangeux et al. (Sangeux et al. 2006) in order to evaluate the magnitude of the STA. However, none of these assessments have led to a general structured description of soft tissue artefacts, that would allow their modeling as a function of the marker location and the movement performed. The objective of Chapter 3.1 was thus to obtain a non-invasive method for STA assessment, both subject-specific and task-specific.

In Alexander and Andriacchi an artefact model, function of the marker anatomical location and partly of the movement being performed, has been provided in order to compensate for it. STA was modelled as if consisting of a functional form, deformed over the observation interval, plus additive noise The functional form is imposed on the marker trajectories relative to the bone system and inferring that the observation of the cluster system in the reference position is also an observation of the bone system. The functional form can be selected on the basis of a priori knowledge of the activity being studied; for example, the step-up activity, where the subject starts and stops in the same relative position of the body segments, can be modelled as a

Gaussian function. However the functional forms proposed do not take into account all possible task in HMA. A further step towards an improved modelling that solves this problem was taken in Chapter 3.2. In fact, there is the evidence in the literature (Cappozzo et al. 1996) that STA is correlated with joint kinematics; therefore a linear combination of joint kinematics was used as a functional form for the model proposed by Alexander and Andriacchi. The STA that can affect markers located on the thigh during active movements of the hip and of the knee, in the relevant range of motion, were modelled and compensated as a function of the four joint angles involved (three at the hip and one at the knee).

In order to compare the effectiveness of the method proposed, a validation procedure was needed. No general validation process has never been carried out on a single set of consistent and realistic data. To this aim, in Chapter 3.3 a simulation procedure was built and tested on various HMA data. The artifact trajectories generated according to the method in Chapter 3.1 were added to nominal trajectories, generated moving "rigid" body segments with the real joint kinematics. The compensated trajectories, obtained from simulated data after the application of the compensation method described in Chapter 3.2, were compared with the nominal trajectories to assess the quality of the method.

3.2 Non-invasive assessment of skin marker to bone movements in the human thigh

3.2.1 Introduction

In order to correctly describe the movement of the skin markers relative to the bone, an observer rigid with the bone would be required. Such an observer could be provided either by invasive experimental techniques, unsuitable for routine assessments, or in combination with fluoroscopy limited to a single joint. Using the latter requires a joint model and extensive image data processing, in addition it is usually unavailable when using stereophotogrammetry. This measurement system provides observers using only skin markers, i.e. observers in motion relative to the bone, which are therefore affected by STA as well. The position vector of a marker reconstructed in such observers (TF) is made of two vectors, which are both time-variant: one describes the movement between the bone and the TF used to observe the marker; the other describes the movement between the marker and the bone. While the former changes depending on the observer, the latter is observer-independent.

According to the coherent averaging principle (Goovaerts et al. 1991), the observer-independent contribution could be enhanced. If there is a high number of observers, and several of them move with respect to the bone in an uncorrelated fashion, and if this movement is negligible with respect to the movement of the marker with respect to the bone, then, the average of the marker position vectors, reconstructed using such observers, would represent a reasonable estimate of STA.

The aim of this section is to develop a method, based on the coherent averaging principle, for a general structured characterization of STA that:

- is non-invasive (based on stereophotogrammetry only);
- can be carried out on a subject-specific base;

- can be carried out during the execution of specific motor tasks;
- allows for the modeling of STA as a function of the marker location and the movement being performed.

3.2.2 Methods

In order to obtain a high number of observers (N_n) and to effectively describe STA in all areas of the segment under analysis, a high number of markers (N_m) must be placed on a wide portion of the segment. On the other hand, the number of observers that can be used is limited by computing time. Sixteen markers were considered as a satisfactory compromise between the two necessities. Markers were clustered in groups of four to obtain the observers (Cappozzo et al. 1997).

The i-th marker can be observed by a number N_n of all possible clusters of 4 markers, ${}_j\overset{a}{\mathbf{C}}_i$, that do not include the i-th marker.

$$ {}_j\overset{a}{\mathbf{C}}_i = \left[{}^g\mathbf{p}_{j1}, {}^g\mathbf{p}_{j2}, {}^g\mathbf{p}_{j3}, {}^g\mathbf{p}_{j4} \right]; \quad j1,..,j4 \neq i; \quad j = 1..\ N_n; \quad N_n = \begin{pmatrix} N_m - 1 \\ 4 \end{pmatrix} \quad (3.1) $$

where the superscript 'a' refers to the artefact estimate. Each ${}_j\overset{a}{\mathbf{C}}_i$ is associated to a TF built using a geometric rule.

In each instant of time, the pose of the TF_j can be described with respect to the global TF using the following transformation matrix:

$$ {}^j\mathbf{T}_g = \begin{bmatrix} & {}^j\mathbf{R}_g & & {}^j\mathbf{o}_g \\ 0 & 0 & 0 & 1 \end{bmatrix} \quad (3.2) $$

where ${}^j\mathbf{o}_g = \frac{1}{4}\sum_{n=1}^{4} {}^g\mathbf{p}_{jn}$ and ${}^j\mathbf{R}_g$ is the rotation matrix from the global TF to TF_j.

For each j-th observer, the trajectory of the i-th marker can be represented with respect to the femoral AF through a time-variant rigid transformation of the marker trajectory, ${}^g\mathbf{p}_i$, from the global frame to TF_j

$$ {}^{j}\mathbf{p}_i = {}^{j}\mathbf{T}_g \cdot {}^{g}\mathbf{p}_i \tag{3.3} $$

and a subsequent time-invariant rigid transformation from TF_j to AF, obtained in a reference position:

$$ {}^{AF}_{j}\mathbf{p}_i = {}^{AF}\mathbf{T}_j(0)\,{}^{j}\mathbf{p}_i \tag{3.4} $$

Identification of non-correlated observers

To identify the observers that move with respect to the bone in an uncorrelated fashion, the deformation of the j-th cluster is described using the variation during time of the singular values, ${}^{U}\boldsymbol{\gamma}$, obtained from the following matrix:

$$ {}_{j}\overset{a}{\mathbf{K}}_i = {}_{j}\overset{a}{\mathbf{C}}_i \cdot \mathbf{I} \cdot {}_{j}\overset{a}{\mathbf{C}}'_i - {}^{j}\mathbf{o}_g\,{}^{j}\mathbf{o}'_g \tag{3.5} $$

through an SVD procedure (Hanson et al. 1981)

$$ \overset{a}{\mathbf{K}} = \overset{a}{\mathbf{U}}\,\overset{a}{\mathbf{S}}\,\mathbf{V}' \tag{3.6} $$

$$ {}^{U}\boldsymbol{\gamma} = diag\left(\overset{a}{\mathbf{S}}\right) \tag{3.7} $$

The singular values ${}^{U}\boldsymbol{\gamma}$ are then projected along the anatomical axes:

$$ {}^{AF}\boldsymbol{\gamma} = {}^{AF}\mathbf{R}_g(0) \cdot \overset{a}{\mathbf{U}}(0) \cdot {}^{U}\boldsymbol{\gamma} \tag{3.8} $$

For each coordinate k=[x,y,z] of the AF system, the following steps are taken. First, an N_n x N_n matrix is determined, each element of which, r_{jh}, is the correlation coefficient among ${}^{AF}_{j}\boldsymbol{\gamma}^{k}_{i}$, ${}^{AF}_{h}\boldsymbol{\gamma}^{k}_{i}$. Second, a graph is constructed, $\overset{a}{\mathrm{G}}\left(\overset{a}{\mathrm{C}},\overset{a}{\mathrm{E}}\right)$, having the $\overset{a}{\mathrm{C}}$ as vertices and edges, $\overset{a}{\mathrm{E}}$, linking only pairs of $\overset{a}{\mathrm{C}}$ characterized by r_{jh} lower than a non-correlation threshold (0.5).

$$ \overset{a}{\mathrm{E}} = \left\{ \exists\, \mathrm{e}_{jh} \Leftrightarrow r_{jh} < 0.5 \right\} \tag{3.9} $$

Third, the vertices $\overset{a}{C}'$ of a graph belonging to a maximal sub-graph completely connected (maximal clique), $\overset{a}{G}'=\text{maxClique}(\overset{a}{G})$, are found using a heuristic algorithm (Bomze et al. 1999):

$$\overset{a}{C}' = {}_{ja}\overset{a}{\mathbf{C}}, \quad ja \in vertices(\overset{a}{G}') \tag{3.10}$$

Among the uncorrelated observers included in $\overset{a}{C}'$, a further selection is performed in order to exclude those observers whose movement with respect to the bone is much greater compared to the marker to bone movement, since they would conceal the searched information. Thus, only the observations correlated with a model of the pattern of the marker to bone movement were included in the coherent averaging.

Generation of the artefact model

The model of the artefact pattern in the area of each marker was found by analysing the deformation of all the clusters, ${}_{j}\overset{m}{\mathbf{C}}_{i}$, that include the i-th marker under analysis.

$$\begin{aligned} {}_{j}\overset{m}{\mathbf{C}}_{i} &= \left[{}^{g}\mathbf{p}_{i}, {}^{g}\mathbf{p}_{j1}, {}^{g}\mathbf{p}_{j2}, {}^{g}\mathbf{p}_{j3} \right]; \; j = 1..N_{w} \\ N_{w} &= \binom{N_{m}}{4} - \binom{N_{m}-1}{4} = 4!\binom{N_{m}-1}{4-1} \end{aligned} \; ; \tag{3.11}$$

where the superscript 'm' refers to the artefact model.

A weighting matrix **W** is defined in order to enhance the contribution of the marker to the overall cluster deformation.

$$\mathbf{W}=\begin{bmatrix} w_1 = 0.77 & & & 0 \\ & w_2 & & \\ & & w_3 & \\ 0 & & & w_4 \end{bmatrix}, \; \sum_{n=1}^{4} w_n = 1 \tag{3.12}.$$

Each ${}_{j}\overset{m}{\mathbf{C}}_{i}$ is associated to a TF having its origin in the centroid of the weighted markers, ${}^{g}_{j}\overline{\mathbf{p}}_{i}$, and the axes equal to the principal axes of the weighted marker distribution.

$$ {}^{g}_{j}\bar{\mathbf{p}}_{i} = \left[{}^{g}\mathbf{p}_{i}, {}^{g}\mathbf{p}_{j1}, {}^{g}\mathbf{p}_{j2}, {}^{g}\mathbf{p}_{j3} \right] \cdot diag(\mathbf{W})' = w_1 \cdot {}^{g}\mathbf{p}_{i} + \sum_{n=1}^{3} w_n \cdot {}^{g}\mathbf{p}_{jn} \quad (3.13). $$

The deformation of the j-th cluster is described using the variation during time of the singular values, ${}^{U}\boldsymbol{\lambda}$, obtained from a weighted version of the matrix **K**:

$$ {}^{m}_{j}\mathbf{K}_{i} = {}_{j}\mathbf{C}_{i} \cdot \mathbf{W} \cdot {}_{j}\mathbf{C}'_{i} - {}^{g}_{j}\bar{\mathbf{p}}_{i} \cdot {}^{g}_{j}\bar{\mathbf{p}}'_{i} \quad (3.14) $$

through an SVD procedure (Hanson et al. 1981):

$$ \mathbf{K} = \mathbf{U}\,\mathbf{S}\,\mathbf{V}' \quad (3.15) $$

$$ {}^{U}\boldsymbol{\lambda} = diag\left(\mathbf{S} \right) \quad (3.16) $$

In order to evaluate the marker movement along each anatomical axis, the singular values ${}^{U}\boldsymbol{\lambda}$ are projected onto the AF:

$$ {}^{AF}\boldsymbol{\lambda} = {}^{AF}\mathbf{R}_{g}(0) \cdot \mathbf{U}(0) \cdot {}^{U}\boldsymbol{\lambda} \quad (3.17) $$

For each marker and each coordinate k= [x,y,z] of the AF, the ${}_{j}\mathbf{C}_{i}$ characterized by a similar deformation are selected and the average of the relevant singular values, ${}^{AF}_{j}\boldsymbol{\lambda}^{k}_{i}$, is assumed to be a model of the artefact behaviour. An $N_w \times N_w$ matrix is determined, each element of which, r_{jh}, is the correlation coefficient among ${}^{AF}_{j}\boldsymbol{\lambda}^{k}_{i}$, ${}^{AF}_{h}\boldsymbol{\lambda}^{k}_{i}$. A graph is constructed, $G\left(\mathrm{C}, \mathrm{E} \right)$, having the N_w clusters as vertices ($\mathrm{C} = {}_{j}\mathbf{C}$) and edges linking only pairs of vertexes characterized by r_{jh} higher than a correlation threshold (0.9):

$$ \mathrm{E} = \left\{ \exists\, \mathrm{e}_{jh} \Leftrightarrow r_{jh} > 0.9 \right\} \quad (3.18) $$

The vertices $\overset{m}{C'}$ of a graph belonging to a maximal sub-graph completely connected (maximal clique), $\overset{m}{G'}=\text{maxClique}(\overset{m}{G})$, are found using a heuristic algorithm (Bomze et al. 1999):

$$\overset{m}{C'} = {}_{jm}\overset{m}{C}, \quad jm \in vertices(\overset{m}{G'}) \tag{3.19}$$

The clusters belonging to the clique $\overset{m}{C'}$ are characterized by singular values which are mutually correlated.

The model of the artefact behaviour of the i-th marker along the k-th direction is obtained as the average of these singular values:

$${}^{AF}\tilde{p}_i^k = \sum_{jm \in vertices(\overset{m}{G'})} {}^{AF}_{jm}\lambda_i^k \tag{3.20}$$

Artefact assessment

Prior to the application of the coherent averaging on the uncorrelated observers, the ${}^{AF}_{ja}p_i^k$ time histories are characterized by their correlation with the model ${}^{AF}\tilde{p}_i^k$:

$$r_{i\text{-}ja} = corr({}^{AF}\tilde{p}_i^k, {}^{AF}_{ja}p_i^k) \tag{3.21}$$

The time histories correlated with the model are selected using a threshold for the correlation coefficient $r_{i\text{-}ja}$ (0.9). Its sign is used as a weighting term, so that all contributions are in-phase with the model.

$${}_{ja}w = \begin{cases} r_{i\text{-}ja} / |r_{i\text{-}ja}| \Rightarrow |r_{i\text{-}ja}| > 0.9 \\ 0 \Rightarrow |r_{i\text{-}ja}| < 0.9 \end{cases} \tag{3.22}$$

$${}^{AF}\hat{p}_i^k = \frac{\sum_{ja=1}^{Nja} \left[{}_{ja}w \cdot ({}^{AF}_{ja}p_i^k - {}^{AF}_{ja}p_i^k(0)) \right]}{\sum_{ja=1}^{Nja} |{}_{ja}w|} + \frac{1}{Nja} \sum_{ja=1}^{Nja} \left[{}^{AF}_{ja}p_i^k(0) \right] \tag{3.23}$$

Such weighted average of the *i*-th marker descriptions can be considered to carry reliable information about the real artefact.

3.2.3 Validation

To test the performance of the method, a data set that allows for the estimate of the thigh artefacts was used. It included synchronized measurements of skin marker trajectories and corresponding bone poses during the execution of step up/down (SUD) motor tasks (Stagni et al. 2005). Bone poses were assessed using 3-D fluoroscopy, marker trajectories using stereophotogrammetry. In this way STA was characterized non-invasively, in-vivo and with no restriction to skin motion on two subjects treated for a total knee replacement (subject 1 age 67, height 1.55 m, weight 58 kg, body mass index 24 kg/m^2, subject 2 age 64, height 1.64 m, weight 60 kg, body mass index 22 kg/m^2 see Stagni et al, 2005 for other details) The accuracy of this data set is limited by the accuracy of the method used for bone pose estimation. The 3-D positions of the two prosthesis components were reconstructed from each 2-D fluoroscopic projection in the fluoroscope reference system based on the knowledge of corresponding CAD models (Banks et al. 1996). Previous validation work (Banks et al. 1996) had shown that the position and orientation of the femoral component on the sagittal plane could be estimated with an accuracy of 0.5 mm and 1 degree, respectively, while the translational error along the axis orthogonal to the sagittal plane was 8.3 mm. For the subjects assessed, the artefact maximal rms values estimated using this method were 19.6, 23.6 , and 31.2mm. Therefore, only the data-set relative to the sagittal plane was considered reliable for validation purpouse, being of at least an order of magnitude greater than the inaccuracies typical of the method itself.

For each trial, marker, and coordinate, the quality of the estimate was assessed in terms of the correlation with the fluoroscopic values and normalized RMS error.

In order to evaluate the performance of the method, the estimates of artifact obtained with the proposed method (NICA), ${}^{AF}\hat{p}_i^k$, and through fluoroscopy, ${}^{AF}\mathbf{p}_i^{Fl\,k}$, were compared. To evaluate pattern similarity the correlation coefficient was used.

$$r_i^k = corr({}^{AF}\tilde{p}_i^k, {}^{AF}\mathbf{p}_i^{Fl\,k}) \tag{3.24}$$

The RMS error between the fluoroscopic artefact and an estimate of the NICA artefact in-phase with the fluoroscopic pattern was used to quantify the magnitude of the error

$${}^{AF}_{ph}\hat{p}_i^k = \frac{r_i^k}{\left|r_i^k\right|} \cdot {}^{AF}\hat{p}_i^k + {}^{AF}\hat{p}_i^k(0)\left(1 - \frac{r_i^k}{\left|r_i^k\right|}\right) \tag{3.25}$$

3.2.4 **Results**

The magnitude of both estimates was characterized in terms of rms. The RMS of the Fluoro-artefact ranged between 4.6 and 23.6 mm for subject 1 and between 3 and 17.5 mm for subject 2, while the NICA-artefacts were in the range 4.5-18.5 mm for subject 1 and 4 – 14.7 for subject 2.

The average RMS over all markers and coordinates was approximately 30% for subject 1 and 25% for subject 2.

The correlation coefficient for the coordinate X ranged between 0.55 and 0.93 (mean 0.82) and between 0.61 and 0.98 (mean 0.88) for subject 1 and 2, respectively. Regarding the Y coordinate the correlation coefficient averaged over all markers was 0.73 (range:0.08-0.97) for subject 1 and 0.80 (range:0.27-0.97) for subject 2

Subject 1	RMS				RMSD NICA-Fluoro		R NICA-Fluoro	
	X		Y		X	Y	X	Y
	Fluoro	NICA	Fluoro	NICA				
M01	10.8	7.4	22.9	12.4	20.7%	27.7%	0.55	0.94
M02	16.0	10.8	10.3	5.2	18.8%	40.0%	0.77	0.07
M03	15.0	8.9	21.7	10.6	19.3%	29.8%	0.82	0.93
M04	10.1	9.0	8.9	12.8	19.9%	29.8%	0.60	0.93
M05	14.8	11.2	7.8	10.0	17.2%	38.4%	0.79	0.89
M06	19.6	8.3	10.0	4.9	24.2%	36.7%	0.91	0.27
M07	10.6	9.4	6.4	8.1	18.6%	40.7%	0.84	0.79
M08	12.8	6.2	20.3	9.4	22.8%	32.0%	0.86	0.94
M09	13.2	7.7	6.3	7.6	19.5%	63.0%	0.87	0.64
M10	9.7	14.8	20.4	8.9	25.7%	34.2%	0.91	0.95
M11	9.3	10.4	6.0	6.9	16.1%	43.5%	0.89	0.72
M12	12.1	11.9	12.4	4.5	12.9%	42.8%	0.87	0.79
M13	4.6	17.3	5.6	9.9	98.0%	40.4%	0.73	0.81
M14	9.1	19.8	23.6	12.4	52.5%	29.5%	0.93	0.97
M15	9.6	16.6	16.2	6.7	36.5%	38.5%	0.85	0.93
M16	10.6	18.5	6.7	5.4	36.1%	31.2%	0.93	0.17

Subject 2	RMS				RMSD NICA-Fluoro		R NICA-Fluoro	
	X		Y		X	Y	X	Y
	Fluoro	NICA	Fluoro	NICA				
M01	12.9	10.6	16.2	14.7	14.9%	9.5%	0.91	0.97
M02	9.7	8.6	3.0	5.4	19.1%	37.6%	0.80	0.28
M03	6.5	6.3	12.4	5.8	20.4%	26.5%	0.65	0.90
M04	5.7	5.4	17.5	8.2	17.9%	25.8%	0.61	0.97
M05	8.1	8.0	17.5	8.4	19.1%	24.3%	0.65	0.98
M06	10.8	4.2	10.8	4.7	21.1%	27.1%	0.90	0.90
M07	14.6	5.3	3.3	4.0	24.0%	32.7%	0.94	0.27
M08	7.3	5.9	15.3	6.7	16.7%	26.6%	0.82	0.96
M09	13.1	5.1	9.0	4.5	21.3%	24.1%	0.95	0.85
M10	13.6	7.5	9.8	9.4	18.3%	12.6%	0.96	0.93
M11	8.1	7.3	12.9	5.6	10.4%	29.3%	0.93	0.88
M12	12.8	5.6	9.1	4.1	20.8%	26.7%	0.96	0.82
M13	11.4	12.2	8.5	9.3	12.4%	14.8%	0.95	0.93
M14	12.5	7.7	3.5	7.2	22.1%	53.8%	0.98	0.46
M15	9.5	12.7	15.9	8.1	28.5%	28.1%	0.96	0.94
M16	16.4	14.5	8.8	5.0	17.1%	32.9%	0.98	0.75

Table 3-1 Subject 1 and 2: RMS of the NICA and fluoroscopic estimated artifact; RMS difference normalized with respect of the peak-to-peak of the fluoroscopic artifact(RMSD); correlation coefficient between the two estimates.

In Figure 3-1 a graphical representation of the table data is reported for subject 1 and subject 2

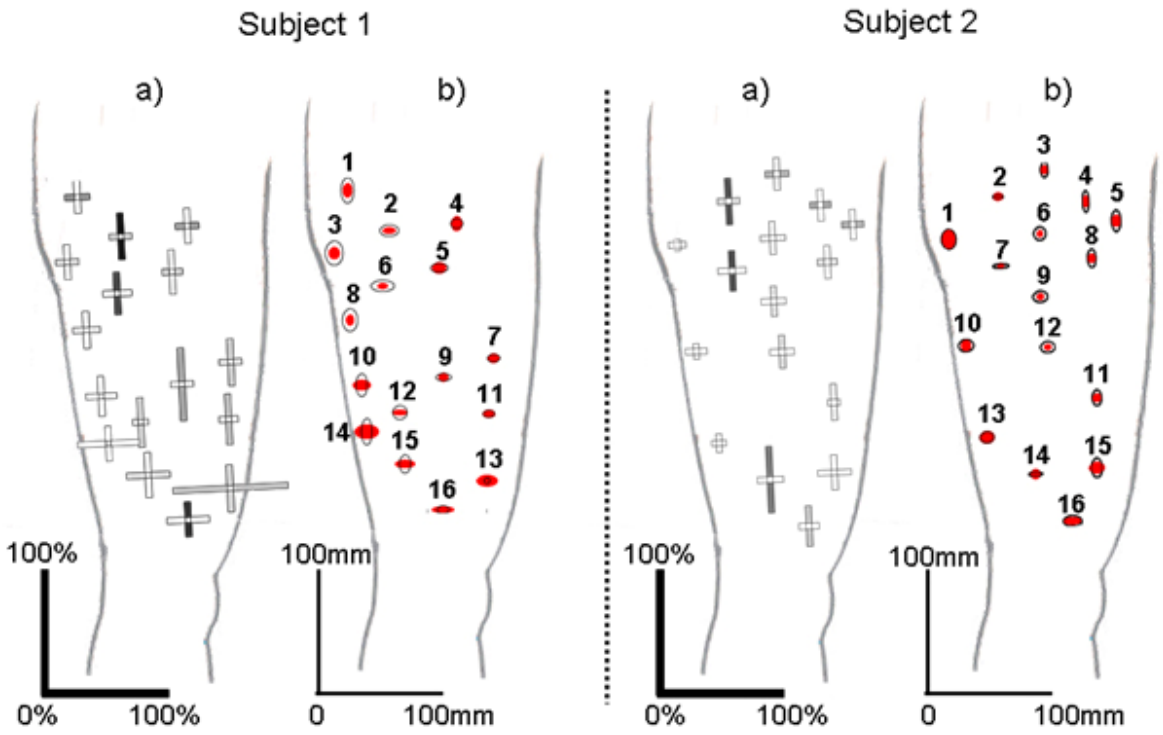

Figure 3-1: A graphical representation of the comparison of the two estimates of the artifact for each subject: a) the length of each line is proportional to the RMSD of the estimates, the color of the lines is related to the correlation (white: 1, black: 0). b) the size of the ellipses describe the RMS of the artifact for the labeled markers in the two directions: red for NICA artifact, black for the Fluoroscopic artifact.

In Figure 3-2 estimated STA are depicted for 2 markers on the thigh, during the step up/down movement.

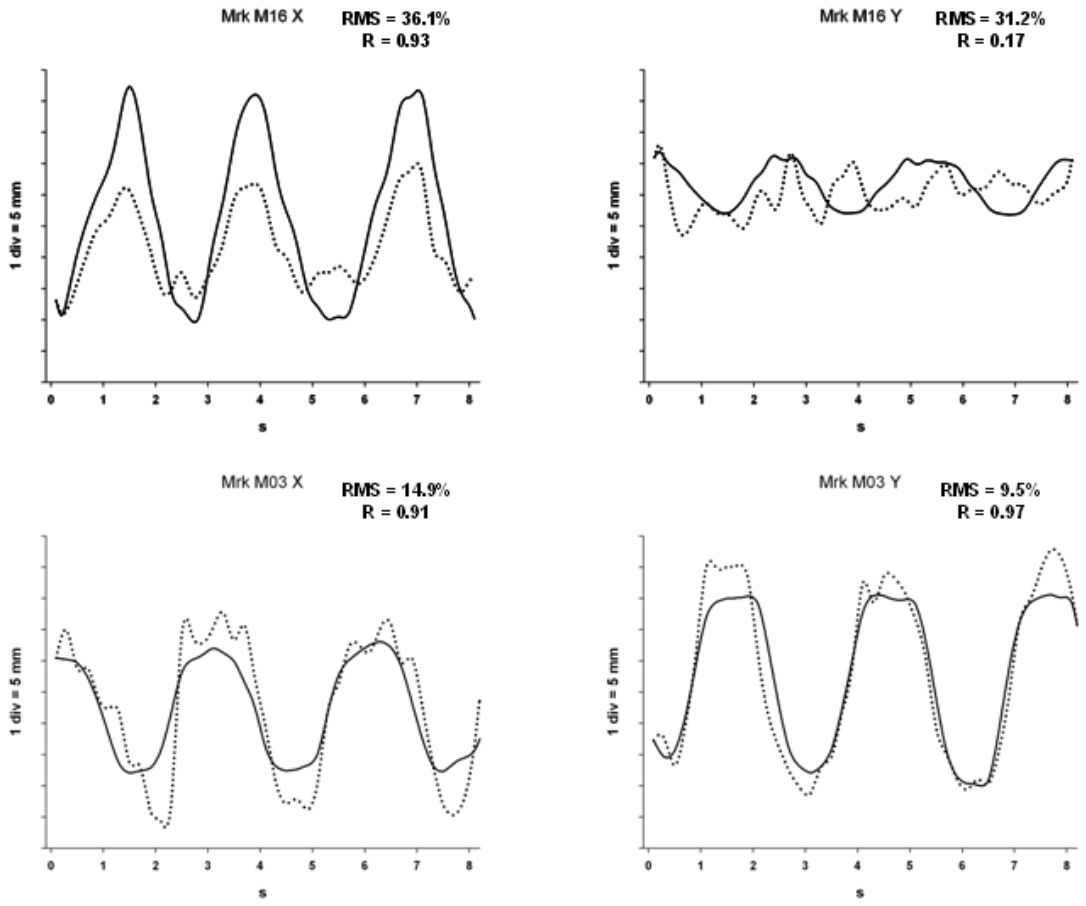

Figure 3-2 estimated NICA STA (solid line) and estimated fluoroscopic STA (dashed line) for 2 markers; M16 for subject 1 and M03 for subject 2.

3.2.5 Discussion

In this chapter a method was proposed for non invasive in vivo assessment of soft tissue artifact with no restriction to skin motion using stereophotogrammetry. The method was tested on the same data set that was used in previous research to characterize STA using synchronized measurements of skin marker trajectories and corresponding bone poses obtained from fluoroscopy (Stagni et al. 2005). Consistency of our and previous results, achieved on the same data, allows to consider the present assessment a reliable representation of the phenomenon.

Most of the authors that quantified STA used external fixators, or intracortical pins, or percutaneous trackers (Leardini et al. 2005); such devices strongly limit the realistic quantification of STA. The present technique does not impose restrictions to skin motion. While comparison with results reported in the literature is made difficult by the different techniques used, the great variability in the subjects analysed and the different motor tasks and skin marker clusters taken into consideration, our results are consistent with some of the results obtained in similar, unconstrained, conditions. The range estimated with NICA for the thigh artifact of two subjects who underwent knee total replacement, performing a step-up task, was 4.0 – 18.5 mm. A similar range (from 2.1 to 17.1 mm RMS) was reported by Sati et al that quantified the artefact using fluoroscopy during approximately 65° of active knee flexion from upright posture in healthy subjects. Comparably, during a similar passive knee flexion, Sangeux and colleagues (Sangeux et al. 2006) using a method based on the MRI, showed an average rms displacement of 12.5 mm between the bone and the centroid of a marker cluster mounted on a thigh plate. This displacement is to some extent smaller, probably due to the observation of markers mounted on a rigid plate compared to markers placed directly on the skin and to the comparison between passive and active movement.

The effectiveness of the coherent averaging and, thus, of the method, is based on the number of non correlated observers available, dependent from the number of existing observers. A cluster of 16 markers grants for at least 15 non correlated observers; a greater number of markers could ensure a less noisy coherent averaging, but at the cost of a much greater computational time, therefore it is not deemed essential. The method provides an estimate only for the artifact pattern and magnitude, while no information is provided on the phase of the signal. This limitation is intrinsic to the method, since the cluster deformation used to generate the artifact model does not contain information about the direction in which the deformation occurs, but only relative to whether the cluster is enlarging or shrinking. Nevertheless, the artifact pattern and magnitude can be considered alone a valuable information, if the characterization of the artifact aims at developing a compensation procedure for its negative effects. With this respect, the required high number of markers is not to be considered a practical drawback.

Validation results proved the similarity of the present and the fluoroscopic estimated patterns, the average correlation coefficient being greater than 0.76 for both coordinates and subjects, and the average RMSD being lower than 30%. Only three markers for each subject showed a vertical component whose correlation was lower than 0.4; the fluoroscopic estimates of these artifact components were characterized by discontinuities due to the low sampling frequency and the possible higher frequency oscillations of the real artifact, while the averaging performed in the NICA method always determines smoother data (Figure 3-2). As expected, the highest RMSD values were obtained for smaller artefacts, since the RMSD emphasises the difference between the estimates more than the absolute amplitude of the curves. As far as the amplitudes are concerned, the two artifact estimates were generally comparable except for the markers located in the posterior part of the thigh of subject 1 whose NICA artifacts were lower. This could be due to the fact that subject 1 is less tonic than subject 2 and the posterior markers are probably the most affected by inertial effects, whose main frequency, reported as being around 10Hz (Wakeling et al. 2003), might be too high to be well estimated by

fluoroscopy (frame rate 5 images/second). An additional negative influence of this low frame rate can be hypothesised in the comparison of the two estimates obtained for subject 1. For this subject, a two frames discontinuity occurred in the fluoroscopy data, entailing a 0.4s interruption in the trajectories. Such interruption probably worsened the NICA results, because this method does not follow a frame by frame philosophy, but uses the patterns of all markers as a whole.

In summary, the NICA assessment gave results reasonably comparable to those obtained with the fluoroscopic method, that is completely different from NICA while similarly not invasive and with no restriction to skin motion. Whereas a definite proof of the validity of the method cannot be provided, coherence of the results constitutes a supportive evidence of the credibility of the obtained estimates. Such assessment could provide information on the artefact in different locations of the thigh and during different motor tasks; therefore, it could allow for optimal marker placement and constitues an indispensable prerequisite for bone pose estimator design and assessment.

3.3 A new method for soft tissue artefact compensation

3.3.1 Introduction

In (Alexander et al. 2001) an artefact model, function of the marker anatomical location and partly of the movement being performed, has been provided. STA was compensated for by modelling it as if consisting of a functional form, deformed over the observation interval, plus additive noise The functional form is imposed on the marker trajectories relative to the bone system and inferring that the observation of the cluster system in the reference position is also an observation of the bone system. This functional form can be selected on the basis of a priori knowledge of the activity being studied. However the functional forms available cannot take into account all possible task in HMA. There is evidence in the literature (Cappozzo et al. 1996) that STA is correlated with joint kinematics. A further step towards modelling can be taken, by using a linear combination of joint kinematics as a functional form for the model proposed by Alexander and Andriacchi. Aim of this Chapter is to model the STA that can affect markers located on the thigh during active movements of the hip and of the knee, in the relevant range of motion, as a function of the four joint angles involved (three at the hip and one at the knee). The model, calibrated on the specific subject, can be used to compensate for STA.

3.3.2 Materials and method

Four healthy young adults participated in the study (1 female and 3 males). Average age, mass and height of the subjects were 28±2years, 71±14kg, and 1.80±0.11m, respectively.

Marker placement:

The subjects were equipped with 4 markers on the pelvis (PSIs and ASIs), 15 on each thigh (12 technical marker, in yellow, along three longitudinal lines in antero-medial, lateral, and posterior positions, avoiding the muscle bellies, 3 anatomical on the lateral and medial epicondyles, LE and ME, and on the greater trocanther, GT), 4 on each shank (head of the fibula, HF, tibial tuberosity, TT, lateral and medial malleoli, LM and MM), and 2 on each foot (calcaneum, CA, and first metatarsal head, FM), Figure 3-3. One subject was equipped with markers on both thighs. Technical markers were divided into subgroups, proximal if numbered 1 or 2, distal if numbered 3 or 4.

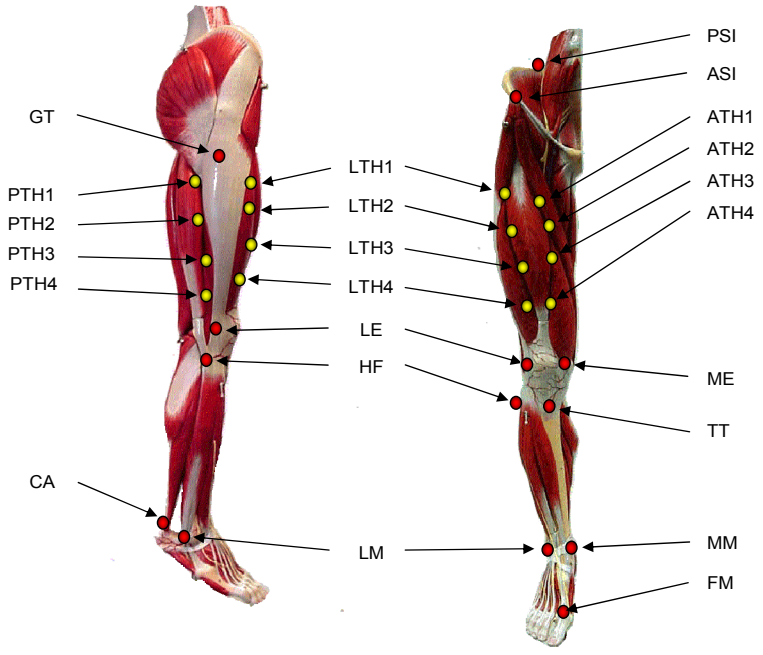

Figure 3-3 Marker placement is shown on the right leg. Technical markers, depicted in yellow, were placed on the thigh, along three longitudinal lines in antero-medial, ATH, lateral, LTH, and posterior position, PTH, four markers for each line. Anatomical markers, depicted in red, were placed on pelvis (PSIs and ASIs), thigh (LE and ME), shank (HF, TT, LM and MM), and foot (CA and FM).

Measurement system

A nine-camera photogrammetric system (Vicon 612®) tracked the markers at 120 frames/s. The acquisition volume was set to 1.5m x 1.5 x 2m.

Movements performed

Subjects were asked to perform each of the following movements for three times:

1. upright posture;
2. hip movement aiming at hip joint centre estimation (see detailed description in Figure 3-4;
3. while keeping the knee rigidly extended:
    a. hip flexion from full extension,
    b. hip adduction from full abduction,
    c. hip external rotation from full internal rotation;
    d. rear foot impact on the ground;
    e. while keeping the hip in a neutral position, knee flexion from full extension.

Pure flexion
Back to the reference position without touching the ground
Hip flexion combined with a slight abduction
Back to the reference position without touching the ground
Hip flexion combined with a wide abduction
Back to the reference position without touching the ground
Hip extension combined with a slight abduction
Back to the reference position without touching the ground
Hip extension combined with a wide abduction
Back to the reference position without touching the ground
Pure extension of the hip towards his back
Return to a flexion position by performing half a circumduction
The foot comes back to the reference position

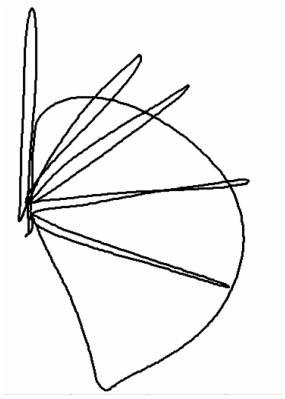

Figure 3-4 Movement performed by the subjects. The toe projection on the floor, during the movement, is depicted.

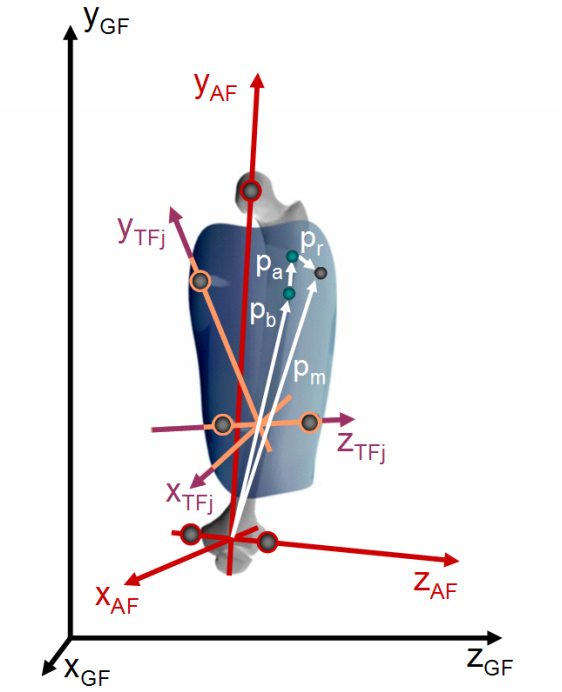

Figure 3-5 The global frame, GF, the femoral frame, AF, built on LE, ME and the hip joint centre, and the j-th technical frame, TFj, are shown. For a marker four vectors are depicted: the reconstructed position vector, $\mathbf{p}_m$; the position vector rigidly associated with the bone, $\mathbf{p}_b$; the displacement vector caused by STA, $\mathbf{p}_a$; and the displacement vector

data processing

The Interval Deformation Technique (IDT) aims at estimating, and thus compensating, the relative movement between points of the skin and the underling bone (soft tissue artifact), ${}^{a}\mathbf{P}(i,n)$ for the i-th marker in the n-th sampled instant of time. The estimate, ${}^{a}\hat{\mathbf{P}}(i,n)$, is achieved by modelling the skin deformation during activities of daily living using a set of activity-dependent functional forms (the deformation model) deformed over the observation interval. The model is represented in the technical reference frame defined by the principal axes of inertia of the marker cluster, ${}^{pa}\hat{\mathbf{P}}(i,n)$, through a rigid transformation between the technical and the anatomical reference system, determined during a reference trial. The marker trajectories relative to the studied movement are represented in the same technical reference frame, ${}^{pa}\mathbf{P}(i,n)$, through a time variant transformation from the global to the

technical frame. The parameters of the subject-specific model are thus calibrated, using a chi-squared estimate, by fitting the model to these marker trajectories.

A. Description of the markers in the anatomical reference system

The position vector ${}^{a}\mathbf{P}(i,n)$ representing the relative movement between skin and bone in the anatomical reference frame, can be represented in the global reference frame as follows:

$$ {}^{g}\mathbf{P}(i,n) = {}^{g}\mathbf{T}_{a}(n) + {}^{g}\mathbf{R}_{a}(n) \cdot {}^{a}\mathbf{P}(i,n) \tag{3.26} $$

where ${}^{g}\mathbf{T}_{a}(n)$ is the origin of the anatomical reference system and ${}^{g}\mathbf{R}_{a}(n)$ the rotation matrix of the anatomical reference system with respect to the global reference system, Figure 3-5.

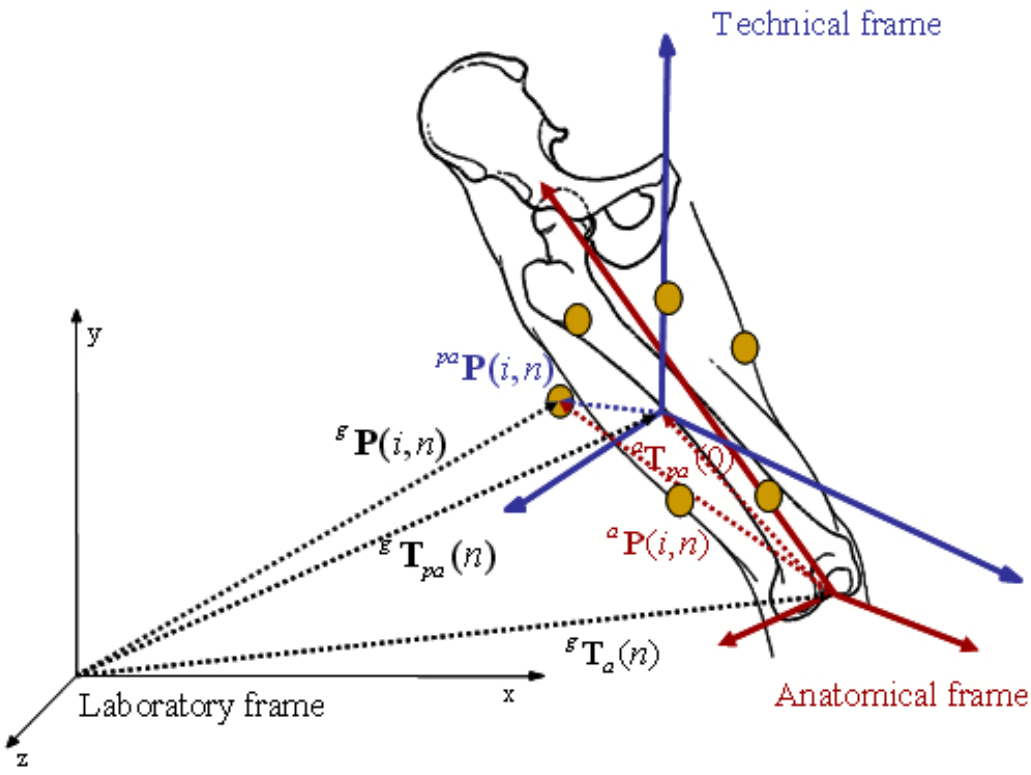

Figure 3-6 Reference frames used in marker observation. Vectors indicated with subscripts are relative to the i-th marker and/or the n-th sampled instant of time. Laboratory frame and relevant vectors are in black, anatomical frame in red, technical frame (principal axes of inertia) in blue. ${}^{g}\mathbf{T}_{a}(n)$ **is the moving origin of the anatomical frame;** ${}^{g}\mathbf{T}_{pa}(n)$ **is the moving origin of the technical frame in the global frame;** ${}^{a}\mathbf{T}_{pa}(0)$ **is the origin of the technical reference system as observed from the anatomical frame in a reference trial.** ${}^{a}\mathbf{P}(i,n)$ **is the position vector of the i-th marker in the anatomical frame;** ${}^{g}\mathbf{P}(i,n)$ **is the position vector of the marker in the global frame;** ${}^{pa}\mathbf{P}(i,n)$ **is the position vector of the marker in the technical frame.**

A parametric expression for ${}^{g}\mathbf{T}_{a}(n)$ and ${}^{g}\mathbf{R}_{a}(n)$ can be obtained through the following steps:

A1. Description of the markers in the principal axes reference system

The same marker can be observed from the technical reference system, the equation relating global and technical vectors is similar to (3.26):

$$ {}^{g}\mathbf{P}(i,n) = {}^{g}\mathbf{T}_{pa}(n) + {}^{g}\mathbf{R}_{pa}(n) \cdot {}^{pa}\mathbf{P}(i,n) \tag{3.27} $$

where ${}^{g}\mathbf{T}_{pa}(n)$ is the centre of mass of the cluster of markers; ${}^{g}\mathbf{R}_{pa}(n)$ is the rotation matrix (the principal axes of the inertia tensor of the cluster) from the technical to the global frame; ${}^{pa}\mathbf{P}(i,n)$ is the position vector of the i-th marker in the principal axes reference frame, Figure 3-5.

A2. Definition of a transformation from technical to anatomical reference system in posture

The core assumption of the algorithm is that, given a proper reference position, for example the first frame of the trial, the observation of the cluster system in the reference position is also an observation of the bone system. A transformation matrix that leads from the technical to the anatomical frame in the reference frame is here represented:

$$ {}^{a}\mathbf{P}(i,0) = {}^{a}\mathbf{T}_{pa}(0) + {}^{a}\mathbf{R}_{pa}(0) \cdot {}^{pa}\mathbf{P}(i,0) \tag{3.28} $$

where ${}^{g}\mathbf{T}_{pa}(0)$ is the origin of the technical reference system as observed from the anatomical frame in the reference trial; ${}^{g}\mathbf{R}_{pa}(0)$ is the rotation matrix from the technical to the anatomical frame in the reference position.

A3. Parametric expression of the global to anatomical frame transformation.

The transformation between technical and anatomical frame thus obtained can be applied to all sampled instants of time:

$$ {}^{a}\mathbf{P}(i,n) = {}^{a}\mathbf{T}_{pa}(0) + {}^{a}\mathbf{R}_{pa}(0) \cdot {}^{pa}\mathbf{P}(i,n) \tag{3.29} $$

The position vector of the i-th marker in the technical frame, using (3.29), can be expressed as:

$$ {}^{pa}\mathbf{P}(i,n) = {}^{a}\mathbf{R}_{pa}(0)^{'} \cdot ({}^{a}\mathbf{P}(i,n) - {}^{a}\mathbf{T}_{pa}(0)) \tag{3.30} $$

Substituting equation (3.30) in equation (3.27) we can obtain:

$$ \begin{aligned} &{}^{g}\mathbf{P}(i,n) = {}^{g}\mathbf{T}_{pa}(n) + {}^{g}\mathbf{R}_{pa}(n) \cdot {}^{pa}\mathbf{P}(i,n) = \\ &= {}^{g}\mathbf{T}_{pa}(n) + {}^{g}\mathbf{R}_{pa}(n) \cdot {}^{a}\mathbf{R}_{pa}(0)^{'} \cdot ({}^{a}\mathbf{P}(i,n) - {}^{a}\mathbf{T}_{pa}(0)) = \\ &= {}^{g}\mathbf{T}_{pa}(n) - {}^{g}\mathbf{R}_{pa}(n) \cdot {}^{a}\mathbf{R}_{pa}(0)^{'} \cdot {}^{a}\mathbf{T}_{pa}(0) + {}^{g}\mathbf{R}_{pa}(n) \cdot {}^{a}\mathbf{R}_{pa}(0)^{'} \cdot {}^{a}\mathbf{P}(i,n) \end{aligned} \tag{3.31} $$

${}^{g}\mathbf{R}_{a}(n)$ and ${}^{g}\mathbf{T}_{a}(n)$ can be determined by comparing equation (3.31) to equation (3.26):

$${}^{g}\mathbf{R}_{a}(n) = {}^{g}\mathbf{R}_{pa}(n) \cdot {}^{a}\mathbf{R}_{pa}(0)' \tag{3.32}$$

$${}^{g}\mathbf{T}_{a}(n) = {}^{g}\mathbf{T}_{pa}(n) - {}^{g}\mathbf{R}_{a}(n) \cdot {}^{a}\mathbf{T}_{pa}(0) \tag{3.33}$$

B. Modelling of markers movement in the anatomical reference system

The model of skin deformation estimate, ${}^{a}\hat{\mathbf{P}}(i,n)$, is achieved associating a set of activity-dependent functional forms (the deformation model) to marker trajectories in the anatomical system. These a priori forms are assumed to represent the general characteristics of the deformation anticipated for the particular activity. The final aim is to track the real movement, an estimate of which is reproduced in Figure 3-7 for the movement used for HJC estimation (Figure 3-4).

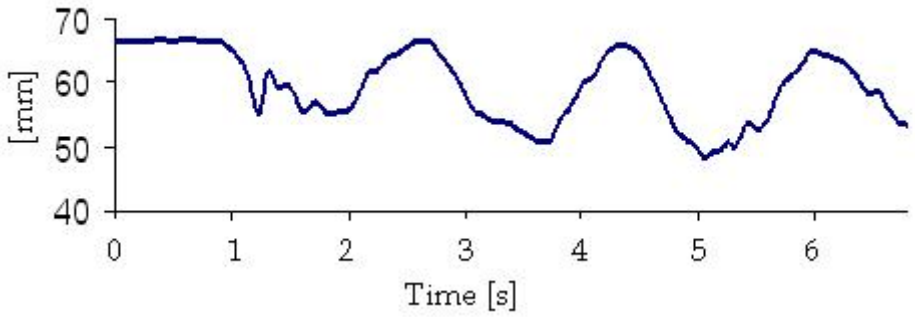

Figure 3-7 A possible artifact trajectory in the anatomical reference frame, as modelled in Chapter 3.1 during the execution of a movement aiming at HJC estimate, described in Chapter 4.2.

The functional form can be selected on the basis of a priori knowledge of the activity being studied; for example, the step-up activity, where the subject starts and stops in the reference position, can be modelled as a Gaussian function, whose parameters were its amplitude, mean and variance, as denoted by equation (3.34):

$$y = \delta \exp\left[-\frac{1}{2}\left(\frac{x-\varepsilon}{\xi}\right)^2\right] \tag{3.34}$$

In level walking, a periodic activity, the marker motion relative to the underlying bone can be modelled as a sinusoid. An exponential curve or combination of different exponential curves is a valid alternative to these shapes. (Figure 3-8)

Figure 3-8 Possible functional forms that can be assumed to represent the characteristics of the deformation.

However, less simple movements can't be satisfactorily modelled by these functional forms; this is the case, for example, for HJC movement. The model was thus improved by identifying a functional form subject- specific and task-specific. It has been shown that the artifact is correlated with joint angles (Lucchetti et al. 1998), a linear interpolation of joint kinematics partially represents the artifact, though without modelling inertial and impact effects. The relevant parameters in this case are the coefficients of the linear interpolation. The movement for HJC estimation is performed with the knee in full extension, and can be compensated for artifact by taking into account only hip joint angles. Hip flexion extension, ab-adduction, and internal-external rotation ($\alpha_h, \beta_h, \gamma_h$) and knee flexion-extension (α_h) angles were estimated using the anatomical frames (AFs) defined in Chapter 3.1 and the Cardanic convention. To this purpose all available markers and a least squares approach were used. STAs were represented as linear combinations of hip angles:

$$\mathbf{m}_{ij}^{h} = h_1^{ij}\alpha_h + h_2^{ij}\alpha_h + h_3^{ij}\alpha_h + h_4^{ij} + \sigma_{i,j}\ ;\ \text{j=1..3; i=1..M} \tag{3.35}$$

In movements involving knee movements only, STAs were represented as linear function of knee flexion-extension angle:

$$\mathbf{m}_{ij}^{h} = k_{12}^{ij}\alpha_h + k_3^{ij} + \sigma_{i,j} \quad \text{j=1..3; i=1..M} \tag{3.36}$$

Instrumental errors were also taken into account by adding a random noise, with given standard deviation, $\sigma_{i,j}$.

C. Cost function determination

If the random noise in the artifact model is composed by normal distributions independent of each other, the probability of the data for the i-th marker, j-th coordinate being a realization of the stochastic process is given by:

$$\text{Prob}(i,j) = \prod_{i=1}^{M}\prod_{j=1}^{3}\prod_{n=1}^{N}\exp\left[-\frac{1}{2}\left(\frac{{}^{pa}\mathbf{P}(i,j,n) - {}^{pa}\hat{\mathbf{P}}(i,j,n)}{\sigma_{i,j,n}}\right)^2\right] \tag{3.37}$$

Maximizing this probability is equivalent to minimizing the negative of its logarithm, yielding to the chi-square criteria:

$$\chi^2 = f(\mathbf{p}) = \sum_{i=1}^{M}\sum_{j=1}^{3}\sum_{n=1}^{N}\left(\frac{{}^{pa}\mathbf{P}(i,j,n) - {}^{pa}\hat{\mathbf{P}}(i,j,n)}{\sigma_{i,j,n}}\right)^2 \quad \text{(parametric)} \tag{3.38}$$

In other words, the model was calibrated minimizing the quadratic distance between the model and the artifact, as represented in the technical reference frame.

C1. Representation of the modelled data in the principal reference system

${}^{pa}\hat{\mathbf{P}}(i,n)$ can be determined from the model, ${}^{a}\hat{\mathbf{P}}(i,n)$, using equation (3.30).

$${}^{pa}\hat{\mathbf{P}}(i,n) = {}^{a}\mathbf{R}_{pa}(0)' \cdot ({}^{a}\hat{\mathbf{P}}(i,n) - {}^{a}\mathbf{T}_{pa}(0)) \quad \text{(parametric)} \tag{3.39}$$

C2. Representation of the measured data in the principal reference system

${}^{pa}\mathbf{P}(i,n)$ can be determined in the same technical reference frame from marker trajectories of the studied movement, using equation (3.27).

$${}^{pa}\mathbf{P}(i,n) = {}^{g}\mathbf{R}_{pa}(0)' \cdot ({}^{g}\mathbf{P}(i,n) - {}^{g}\mathbf{T}_{pa}(0)) \quad \text{(known)} \tag{3.40}$$

D. Chi-squared estimate problem

An annealing optimization algorithm was used in order to solve the minimization problem and to estimate the subject-specific parameters of the model. Consequently the orientation matrix ${}^{pa}\hat{\mathbf{R}}_a(n)$ and translation vector ${}^{pa}\hat{\mathbf{T}}_a(n)$ between the principal axes and anatomical frame were inferred.

E. Deformation correction

An estimate of the deformation correction was then generated by subtracting the estimated signal to the measured signal in the principal axes reference system.

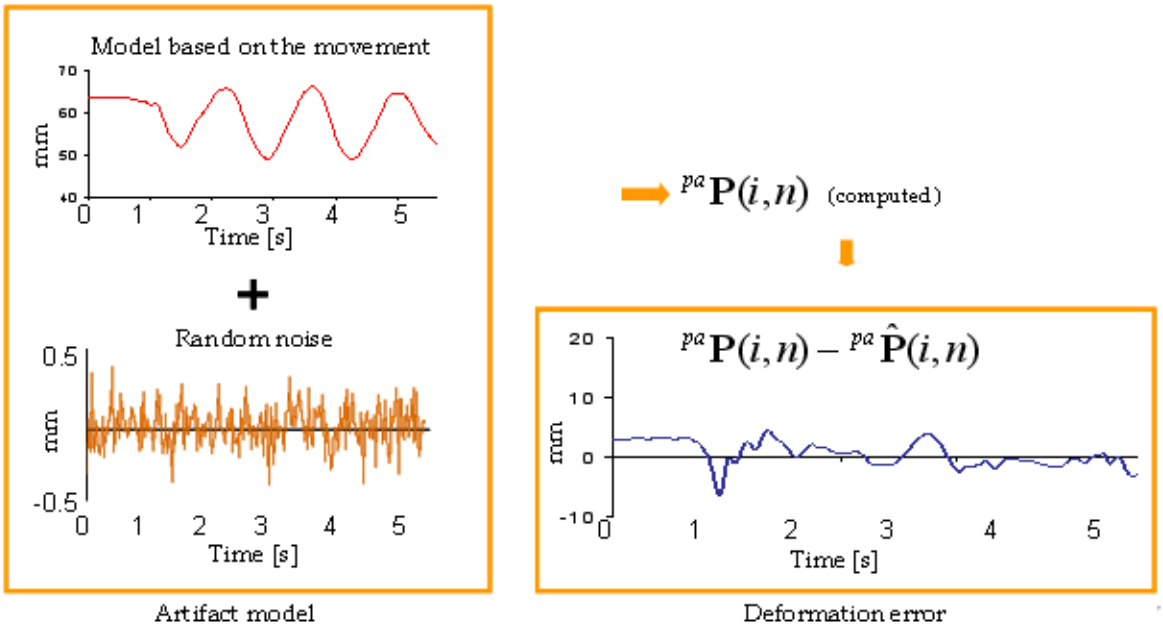

Figure 3-9 Modelled artifact and deformation error are reported, as an example, for the signal in Figure 3-7.

PHASE		VARIABLES	MEASURE, COMPUTATION OR ESTIMATE?	TIME FRAME
A	DESCRIPTION OF THE MARKERS IN THE PRINCIPAL AXES AND IN THE ANATOMICAL REFERENCE SYSTEM	$^{g}\mathbf{P}(i,n)$	MEASURED	(N=0..N-1)
		$^{g}\mathbf{R}_{pa}(n),\ ^{g}\mathbf{T}_{pa}(n)$	COMPUTED	(N=0..N-1)
		$^{a}\mathbf{P}(i,0)$	MEASURED IN POSTURE	(N=0)
		$^{a}\mathbf{T}_{pa}(0),\ ^{a}\mathbf{R}_{pa}(0)$	COMPUTED RELATIVE TO POSTURE	(N=0)
		$^{g}\mathbf{R}_{a}(0),\ ^{g}\mathbf{T}_{a}(0)$	COMPUTED RELATIVE TO POSTURE	(N=0)
B	MODELLING OF MARKERS MOVEMENT IN THE ANATOMICAL REFERENCE SYSTEM	$^{a}\hat{\mathbf{P}}(i,n)$ (PARAMETRIC)	ESTIMATED ACCORDING TO THE CHOSEN MODEL (SIN, EXP, JOINT ANGLES…)	(N=0..N-1)
C	COST FUNCTION DETERMINATION	$^{pa}\hat{\mathbf{P}}(i,n)$ (PARAMETRIC)	COMPUTED USING $^{a}\hat{\mathbf{P}}(i,n)$	(N=0..N-1)
		$^{pa}\mathbf{P}(i,n)$	COMPUTED USING $^{g}\mathbf{P}(i,n)$	(N=0..N-1)
D	MODEL PARAMETER COMPUTATION	$\min \sum_{i=1}^{M}\sum_{j=1}^{3}\sum_{n=1}^{N}\left(\frac{^{pa}\mathbf{P}(i,j,n) - {}^{pa}\hat{\mathbf{P}}(i,j,n)}{\sigma_{i,j,n}}\right)^{2}$		
		$^{pa}\hat{\mathbf{R}}_{a}(n),\ ^{pa}\hat{\mathbf{T}}_{a}(n)$	COMPUTED USING $^{a}\hat{\mathbf{P}}(i,n)$ AND $^{pa}\mathbf{P}(i,n)$	(N=0..N-1)
E	DEFORMATION CORRECTION	$^{pa}\mathbf{P}(i,n) - {}^{pa}\hat{\mathbf{P}}(i,n)$	COMPUTED	(N=0..N-1)

Table 3-2

3.3.3 **Results**

In order to assess the effectiveness of the method, the hip exercise previously described was used. In fact, in this case it is known that the linear displacement of the femur relative to the pelvis may be considered nil. The hip linear degrees of freedom were thus estimated using both non-artefact-compensated and artefact-compensated data. Results in Figure 3-10 show that the method remarkably reduces the artefact propagation.

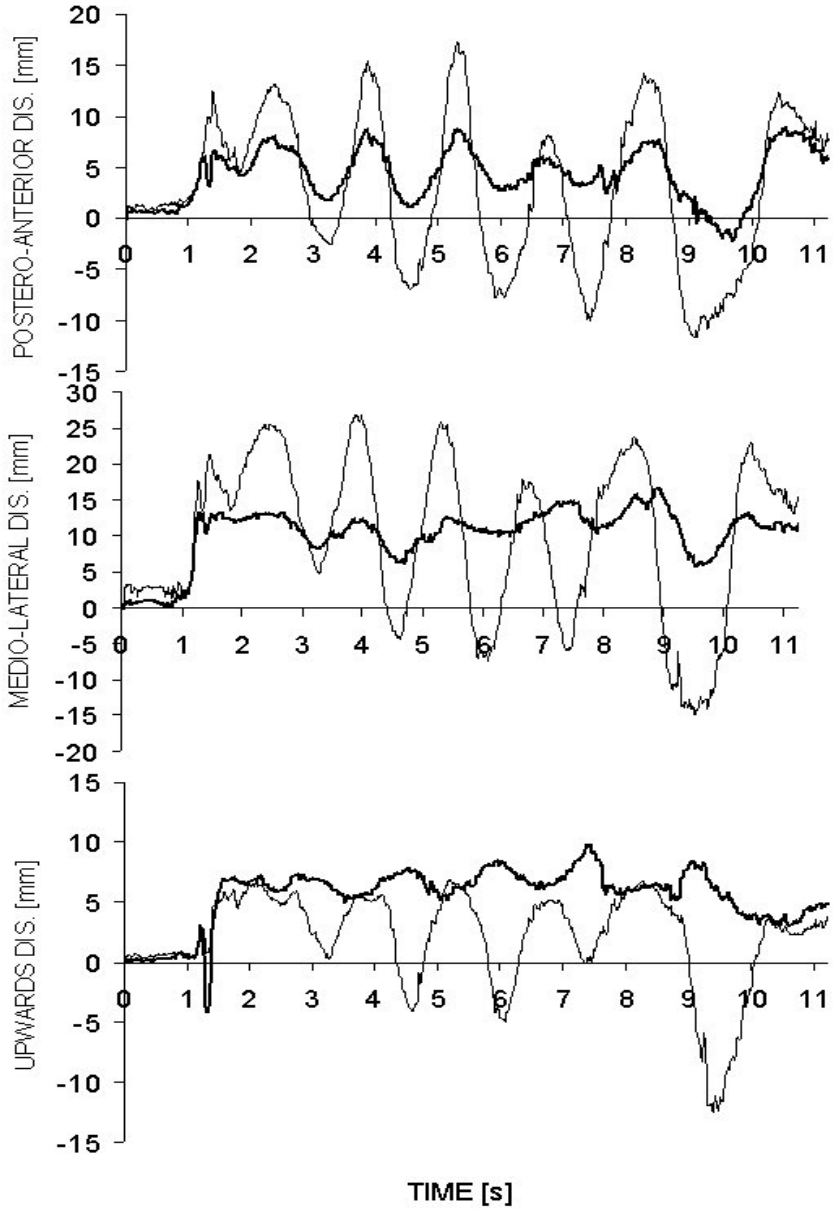

Figure 3-10 Displacement between femur and pelvis (relative to the pelvic anatomical frame) during the hip exercise as obtained implementing the STA compensation procedure (thick lines) and without (thin lines).

The mean and the root mean square (rms) distance between the trajectories, normalized with respect to the duration of the trial and averaged among coordinates, used as quantitative indexes for this spot check were 5 and 6mm, before compensation, 6 and 2mm, after compensation. However, it should be noted that the STA component occurring at the beginning of the movement, when muscles are first contracted, is not compensated for. This is evident from Figure 3-10 and may be associated with the fact that, in this phase, the marker cluster undergoes a quasi-rigid movement which is not related to joint movement as assumed in the STA model. This is a matter that calls for further investigation.

The parameters obtained may be used to synthesize the STAs in simulation exercises. Note that this model, being a function of the joint angles, may be used for reconstructing STAs associated with any motor task.

3.4 A simulation method for the assessment of compensation methods for soft tissue artifact.

3.4.1 Introduction

The relevance of STA as a source of error in human motion analysis, led several authors to suggest methods in order to model and to compensate STA. No a priori selection can be pursued among those techniques compensating for STAs, unless a general validation process is carried out. This latter exercise is particularly solicited by human analysis specialists (Leardini et al. 2005).

Stagni et al.(Stagni et al. 2003) evaluated the performance of some of the most recent compensation methods using experimental data acquired combining stereophotogrammetry and 3D video-fluoroscopy. This test allowed for the assessment of the techniques in real conditions, without any restriction to skin motion, and with the knowledge of the reference motion of the underlying bone. However, this motion can be obtained only on subjects who underwent total knee replacement. The 3D pose of the prosthesis components was reconstructed by means of single-plane lateral 2D fluoroscopic projections and CAD models. Thus, this validation process can not be considered general and used to test different methods, unless nominal and corrupted trajectories obtained through the described procedure are provided.

In order to evaluate the effectiveness of the method proposed in Chapter 3.2, a validation procedure is here proposed. This procedure was carried out through a simulation study that can be reproduced on a subset of usual HMA tasks, of a specific subject. Nominal trajectories, generated moving “rigid” body segments with the real joint kinematics, were obtained from HMA data. The artifact trajectories generated in Chapter 3.1 were assumed to represent STA and were added to nominal trajectories, obtaining simulated data affected by STAs. Test trajectories were thus compensated with the new compensation method. Compensated trajectories were compared with the nominal trajectories in order to assess the quality of the method. This test allows

for the assessment of the technique in real conditions, without any restriction to skin motion, and with the knowledge of the reference motion of the underlying bone.

3.4.2 Materials and methods

Simulation model

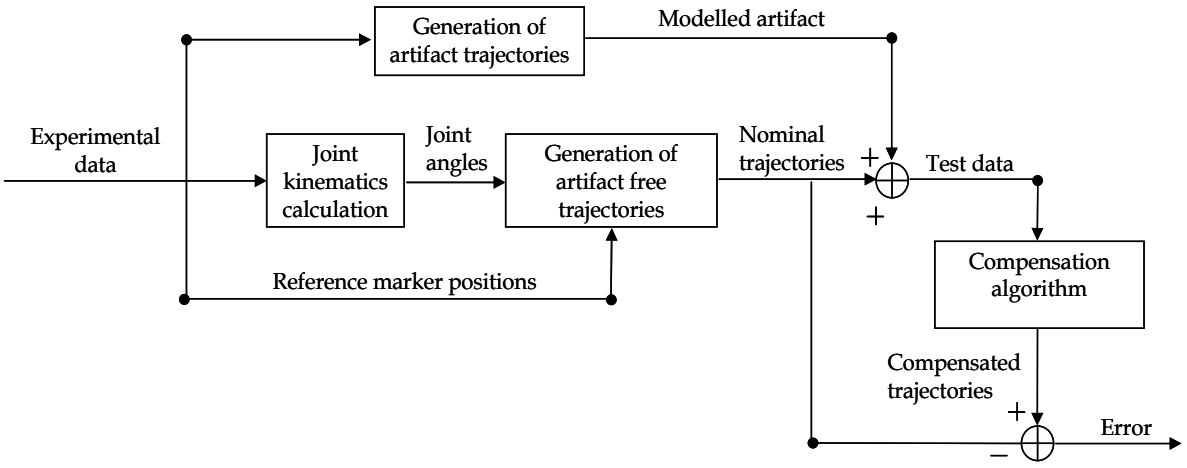

Figure 3-11 The simulation model

The compensation method proposed in Chapter 3.2 was validated by analyzing experimental data obtained during a trial aiming at estimating the hip joint centre (Figure 3-4). Joint kinematics was computed according to Grood and Suntay convention. Nominal trajectories of thigh markers were obtained by defining marker positions in the thigh AF during a static reference trial and then moving the thigh AF according to joint kinematics. Artifact trajectories were generated, using the same movement, as described in Chapter 3.2. Test data were compensated using the modified IDT method, described in the previous Chapter. Results were compared with the nominal trajectories, obtaining an assessment of the efficacy for the method under test.

Quality assessment

Results relative to hip joint centre estimate were evaluated by quantifying the accuracy of this estimate. The accuracy was evaluated as difference between nominal and estimated value, averaged over HJCs estimated in 8 different trials. For each trial the determination was repeated using 3 different clusters and 3 algorithms for centre of rotation determination (see Chapter 4.2).

3.4.3 Results

The average error in determining HJC, using different thigh clusters and the best algorithms available, was of 7 mm, 10 mm e 7 mm, for X, Y and Z respectively. This error was reduced of one order of magnitude when compensation was applied, as reported in Table 3-3.

		NC	C
Simulated data	**X**	7.1	0.6
	Y	9.9	1.1
	Z	6.7	0.6

Table 3-3 Accuracy of HJC determination, averaged over 8 trials, 3 clusters and3 algorithms, before and after compensation

The compensation also improved precision. Standard deviation of original data was of 10 mm for X and Y, and of 5 mm for Z. Again, the standard deviation was reduced of one order of magnitude.

		NC	C
Experimental data	**X**	9.3	0.7
	Y	10.4	1.2
	Z	4.6	0.7

Table 3-4 Precision of HJC determination,averaged over 8 trials. 3 clusters and 3 algorithms, before and after compensation

3.4.4 Discussion and Conclusions

Results on HJC determination indicate that STA is the most detrimental effect for HJC among those analysed (cluster and algorithm) and that the new technique consistently reduced this effect, improving both accuracy and precision of the estimate.

CHAPTER 4. ANATOMICAL CALIBRATION

List of symbols

FRAMES

GF	GLOBAL FRAME
CF	MARKER CLUSTER FRAME
AF	ANATOMICAL FRAME
MF	MORPHOLOGY FRAME

POINTS

UP	UNLABELLED POINT
AL	ANATOMICAL LANDMARK
GT	GREATER TROCHANTER
ME, LE	MEDIAL AND LATERAL EPICONDYLES
MP, LP	ANTERO-MEDIAL AND ANTERO-LATERAL RIDGE OF THE PATELLAR SURFACE GROOVE
LASI, RASI	LEFT AND RIGHT ANTERIOR SUPERIOR ILIAC SPINES
LPSI, RPSI	LEFT AND RIGHT POSTERIOR SUPERIOR ILIAC SPINES
TT	TIBIAL TUBEROSITY
LM,MM	LATERAL AND MEDIAL MALLEOLI
HF	HEAD OF THE FIBULA
MLP, MMP	MOST LATERAL AND MEDIAL POINTS OF THE TIBIAL PLATEAU

TRANSFORMATION MATRICES

${}^{y}\mathbf{T}_{x}$	TRANSFORMATION MATRIX FROM FRAME X TO FRAME Y.

VECTORS

${}^{x}\mathbf{v}[i]$	POSITION VECTOR IN FRAME X INDEXED BY I
${}^{\bar{\hat{a}}}\boldsymbol{\theta}_{\hat{a}}$	ORIENTATION VECTOR OF EACH TRIAL AF IN THE MEAN AF

4.1 Introduction

The analysis of human movement calls for the collection of data that allows to reconstruct the movement of subject-specific bones in a three-dimensional (3D) virtual space and in each sampled instant of time. To this purpose, local frames are used which are normally constructed using the instantaneous global position of superficial markers tracked by a photogrammetric system. They are referred to as marker cluster frames (CFs) and their pose is described using 4x4 transformation matrices (${}^{g}\mathbf{T}_{c}$) (Cappozzo et al. 2005). This pose is generally arbitrary with respect to the underlying bone. Repeatability of a local frame is obtained by relying on specific morphological features of the bone. An adequate number of distinct anatomical landmarks (ALs) is selected and their position relative to the CF is determined (${}^{c}\mathbf{a}[a]$, a=1, …, A). Using the positional information and a deterministic or statistical geometric rule, a local anatomical frame (AF) is defined, and the transformation matrix ${}^{c}\mathbf{T}_{a}$ is calculated which, in turn, allows for the estimation of the global pose matrix ${}^{g}\mathbf{T}_{a}$ (Wu et al. 2002; Della Croce et al. 2003). In principle, AFs are repeatable both within and across subjects and represent a fundamental prerequisite for the quantitative analysis of movement. This approach to movement analysis is often referred to as the calibrated anatomical system technique, CAST (Cappozzo et al. 1995) (Figure 4-1).

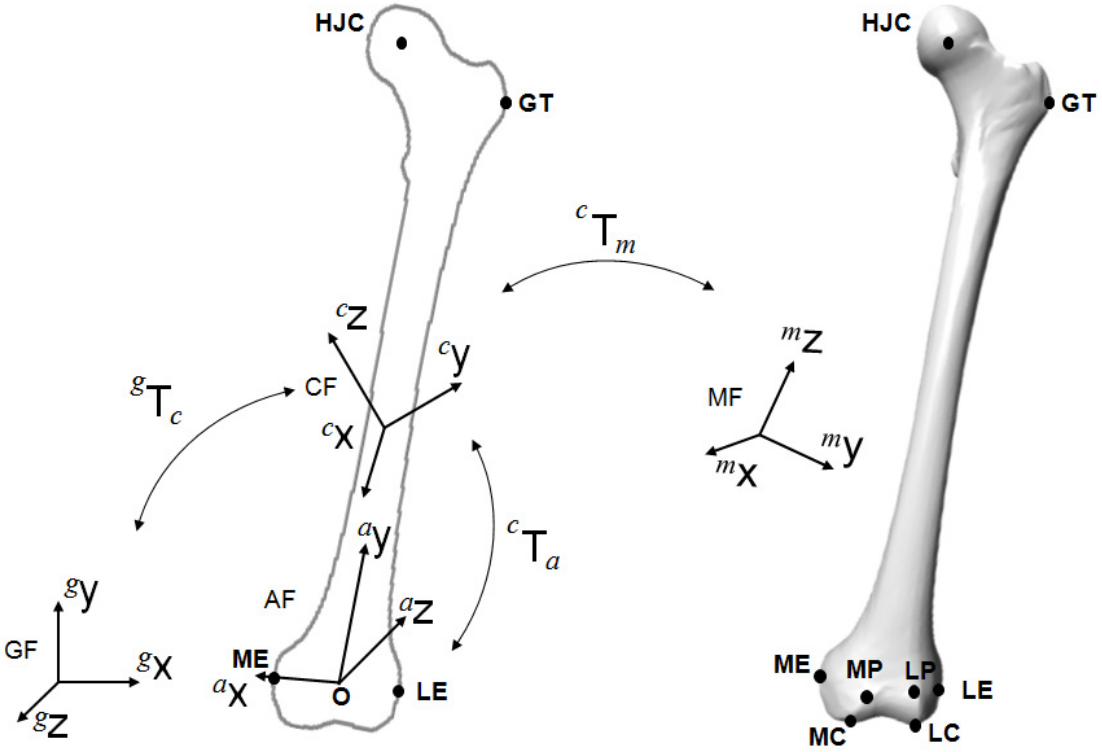

Figure 4-1 Global frame (^{g}x, ^{g}y, ^{g}z, GF), morphology frame (^{m}x, ^{m}y, ^{m}z, MF), marker cluster (^{c}x, ^{c}y, ^{c}z, CF) frame, and anatomical frame (^{a}x, ^{a}y, ^{a}z, AF). Curved arrows indicate the transformation matrices from a frame to another. For the AL definitions see acronyms in the symbol list.

In most movement analysis laboratories, external ALs that correspond to bony prominences are identified through manual palpation. Their location relative to the CF (vectors $^{c}\mathbf{a}$) is then determined through photogrammetry, either by placing temporary markers on them or pointing to the ALs with a wand fitted with two or more markers (Cappozzo et al. 1995).

Internal AL positions are normally estimated using the location of superficial ALs and predictive models (Bell et al. 1990; Davis et al. 1991; Seidel et al. 1995; Camomilla et al. 2006). In the case of the centre of the femoral head, the fact that it can be considered to coincide with the centre of rotation of the femur relative to the pelvis allows to determine its location using movement data (functional approach, (Cappozzo 1984; Leardini et al. 1999; Camomilla et al. 2006).

When, in addition to an AF and a few ALs, the analysis requires a high resolution subject-specific bone morphology, a bone digital model, obtained through imaging methods, is provided relative to a morphology frame (MF), normally different

from the CF. The model consists of the position of unlabelled bone superficial points (${}^{m}\mathbf{b}[b]$, b=1, …, B), accompanied with relevant AL locations, defined in the MF (${}^{m}\mathbf{a}[a]$, Figure 4-1). In this case, a registration transformation matrix (${}^{c}\mathbf{T}_{m}$), that allows merging movement and morphology data, must be made available. This matrix may be estimated using the position in both the MF and the CF of the same set of labelled points, either ALs or markers.

The parameters that describe bone morphology and the parameters incorporated in ${}^{c}\mathbf{T}_{m}$ are named anatomical parameters, while the procedure used to identify them is named anatomical calibration.

High resolution anatomical calibration is very rarely possible, since movement analysis laboratories normally do not have easy access to medical imaging equipments and some imaging methods are regarded as invasive. Further problems arise from the difficulty of identifying the ALs in-vivo using manual palpation due to the interposed soft tissues and to the fact that these points are arbitrarily located within the relatively large and irregular area described by anatomy manuals as being anatomical landmarks. These circumstances affect both accuracy and precision of AL location. Intra- and inter-examiner identification precision of different ALs of the pelvis and the lower limb, considered as root mean square distance from the mean position, has been found to be in the range of 6-21 mm and 13-25 mm, respectively (Della Croce et al. 1999). The propagation of these inaccuracies to the orientation of the AFs causes important distortions of the kinematics and kinetics of the joints involved, to the extent that the information relative to smaller quantities is concealed (Ramakrishnan et al. 1991; Della Croce et al. 1999; Stagni et al. 2000). Moreover, the manual identification requires expert knowledge and it is time consuming. These circumstances, together with other factors, may contribute to making movement analysis in a clinical context cumbersome and uneconomical (Simon 2004).

The problems illustrated above, with reference to the conventional anatomical calibration procedure, call for the following actions to be taken:

- to devise a subject-specific bone digital model estimation procedure;
- to improve the precision of AL identification procedures;
- to minimize the time required to perform anatomical calibration;

- to allow for the entire procedure be performed by ancillary health technicians in place of highly skilled professionals without compromising the outcome;

- to exploit redundancy of information by increasing the number of ALs used to define an AF, and to design the rule that constructs it so that AL inaccuracy propagation is minimised.

This thesis aims at contributing to the solution of the problems implicit in the first four issues. To this end, the following steps are taken into account:

In Chapter 4.1 a new method to automatically identify AL on digital bones is described.

In Chapter 4.2 the methodological factors that may affect the functional methods performance to assess hip joint centre (HJC) in vivo are taken into account, as a prerequisite to obtain an optimal estimate of the HJC location in order to improve the entire anatomical calibration protocol.

In Chapter 4.3 an alternative calibration procedure is developed, based on the estimate of a subject-specific bone or portion of bone.

In Chapter 4.4 .the propagation of the anatomical landmarks misidentification on the angular kinematics when using the above illustrated method is described.

4.2 Virtual Palpation

4.2.1 Introduction

This chapter deals with an automatic technique that allows the identification of the AL location on a digital bone.. Manual digital palpation may be carried out using a suitable graphic software and either a written description of the ALs or a 3-D representation of a labelled template bone (LTB) that carries the indication of the ALs locations. Automatic digital palpation uses a LTB and, through the mathematical procedure presented in this section, identifies the ALs. The technique was validated by comparing its performance with that of the manual digital palpation associated with a LTB as a reference.

4.2.2 Materials and methods

Four digital femurs were available (courtesy of Laboratorio di Tecnologia Medica, IOR, Bologna). The following ALs, represented as in Figure 4-1, were taken into consideration: antero-lateral and antero-medial ridges of the patellar surface groove, LP and MP, greater trochanter, GT, lateral and medial epicondyles, LE and ME.

One of the femurs was taken as template bone and its ALs were manually labelled by four expert operators using written definitions (Van Sint Jan et al. 2002). A LTB was obtained by using the average location of these ALs. Six operators, who did not include the four previous ones, carried out the manual palpation in the three remaining unlabelled bones (UB) using the LTB as a reference. The relevant standard deviation accounted for the inter-operator variability of manual palpation.

The automatic virtual palpation was performed using a five-step algorithm:

1. the LTB and the UB were represented in bone embedded frames built using the respective principal axes (a method to solve the non-unicity of principal axes was implemented).
2. The LTB was scaled to match the dimensions of the UB.
3. The LTB was deformed to match the morphology of the UB. To this aim an affine transformation was carried out by combining the Iterative Closest Point

algorithm (Besl et al. 1992), used to align the bones, and the Simulated Annealing algorithm (Kirkpatrick et al. 1983), used to avoid local minima.

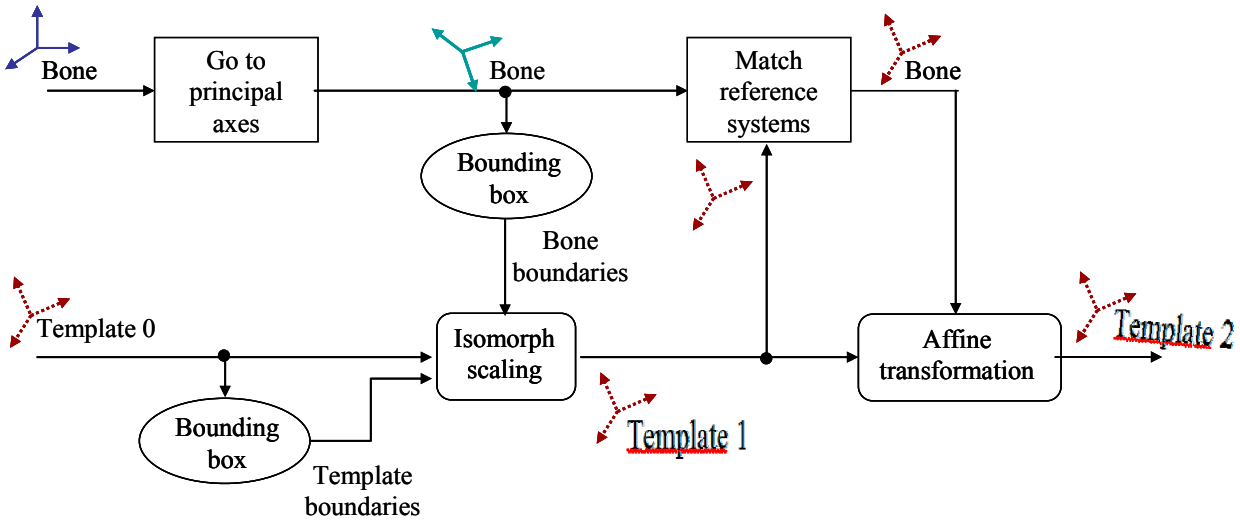

Figure 4-2 Steps 1,2 and 3 of the algorithm to align LTB and UB.

4. A spherical surface with radius equal to 10% of the maximal UB dimension and centred in the selected AL, was used to isolate a surface of the LTB around that AL. The same operation was carried out with the UB using its closest point to the AL of the LTB as centre of the spherical surface.
5. The LTB surface was deformed to match the UB surface as in the third step, and the point of the latter surface nearest to the LTB AL was labelled.

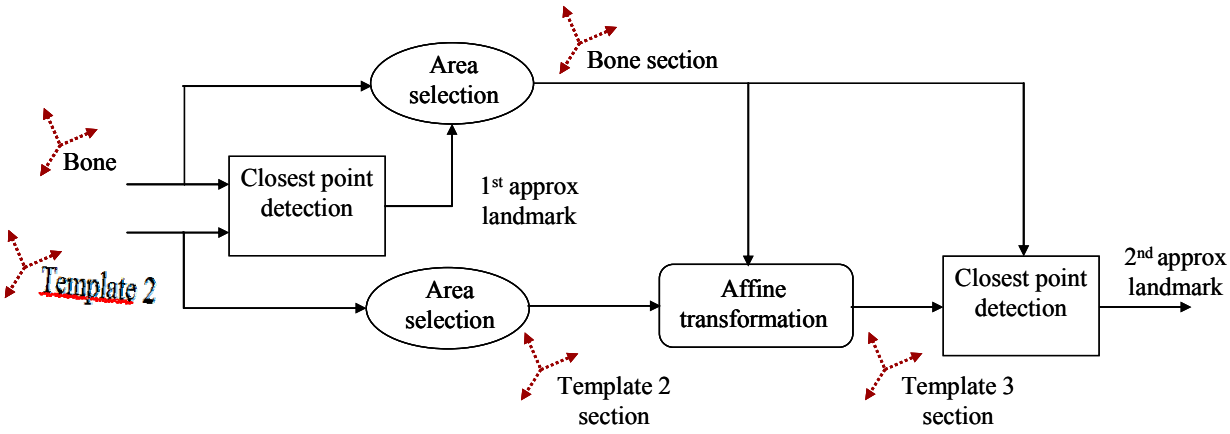

Figure 4-3 Steps 4 and 5 to align the selected areas.

The automatic digital palpation was carried out for the three bones available. The relevant inaccuracy was assessed by calculating the distance between the average

position of the ALs as obtained using the six operator manual palpations, taken as gold standard, and the relevant positions yielded by the automatic procedure.

4.2.3 Results

The inter-operator variability of manual palpation was in the range 3 - 9 mm and varied according to the specific AL dealt with. It looked as if AL identification could be more or less difficult depending on the UB analysed (Table 4-1). The inaccuracy of the automatic procedure exhibited values in the range 3 - 9 mm. The AL that exhibited, for a given bone, the larger inter-operator variability was also affected by a larger automatic palpation inaccuracy.

	LP			**MP**			**GT**			**LE**			**ME**		
	1	**2**	**3**	**1**	**2**	**3**	**1**	**2**	**3**	**1**	**2**	**3**	**1**	**2**	**3**
IOV	8,5	2,9	5.0	9,2	6,6	4.2	4,3	6,8	5.6	2,9	6,2	3.9	2,5	6,0	7.8
VPI	8,0	4,1	4.6	7,4	6,6	4.6	5,5	7,7	6.0	2,7	4,5	2.7	5,4	4,8	7.0

Table 4-1 Inter-operator variability (IOV, mm) and automatic palpation inaccuracy (VPI, mm).

4.2.4 Discussion

The automatic procedure for virtual ALs identification increases repeatability and eliminates subjectivity due to erroneous visual or conceptual interpretation of the relevant written or visual definitions. It also reduces costs in terms of expert time with no loss in accuracy.

4.3 An artefact compensated protocol for hip joint centre determination.

4.3.1 Introduction

In human movement analysis the hip joint centre is often used to define the longitudinal anatomical axis of the femur and, therefore, it affects the orientation of the relevant anatomical frame (Cappozzo et al., 1995; Wu et al., 2002).

In the generally accepted hypothesis that a normal hip joint may be modelled as a spherical hinge, the centre of rotation (CR) of the femur relative to the pelvis coincides with the geometrical centre of the acetabulum and, within a normal range of motion, with that of the femoral head. This point is referred to as hip joint centre (HJC) and is defined using its Cartesian coordinates in an anatomical set of axes associated with selected pelvic anatomical landmarks (Figure 4-4). Since joint kinematics may be described as the relative motion between the anatomical frames associated with the two bones involved, the HJC location affects both hip and knee joint kinematics.

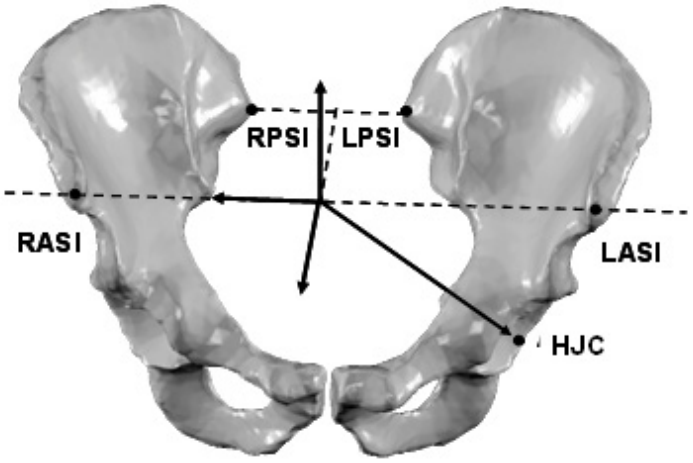

Figure 4-4 Pelvic anatomical frame defined as follows: the origin is the midpoint between the anterior superior iliac spines (ASISs); the Z axis is defined as the line passing through the ASISs with its positive direction from left to right; the X axis lies in the quasi transverse plane defined by the ASISs and the midpoint between the posterior superior iliac spines (PSISs) with its positive direction forwards; the Y axis is orthogonal to the XZ plane with its positive direction proximal. Vector c identifies AC position with respect to this reference frame. For the AL definitions see acronyms in the symbol list

For these reasons, the accuracy with which the 3-D HJC location is determined is of paramount importance and considered by human movement analysts to be a critical challenge for the future (Alderink et al., 2000; Holden and Stanhope, 1998; Kirkwood et al., 1999; Piazza et al., 2001; Stagni et al., 2000; Besier et al., 2003; Piazza et al., 2003).

Two methods are most often used to estimate the hip joint centre position: the predictive and the functional methods.

The predictive method uses regression equations that provide an estimate of the coordinates of the HJC as a function of easy to acquire anthropometric quantities. The mean error with which the position of the HJC may be predicted in able bodied adult male subjects using the available regression equations was estimated in the range 25-30 mm (Bell et al., 1990; Leardini et al., 1999).

The functional method identifies the HJC as the relevant CR (Cappozzo, 1984). According to an investigation carried out by Bell et al. (1990) using six subjects, this method allows for an accuracy in the range 14-65 mm, while Leardini et al. (1999), using 11 subjects, found errors in the range 5-15 mm. Although the discrepancy between these two results remains unjustified (Piazza et al., 2001), there exists no evidence that the latter accuracy cannot be generally attained or even improved, provided that relevant good practice guidelines are determined and applied.

In this Section the methodological factors that may affect the functional methods performance in vivo are taken into account in order to contribute to the definition of the mentioned guidelines:

- Algorithm used to estimate the CR coordinates from marker trajectory data,
- relative movement between markers and underlying bones (skin movement artefact),
- pelvic anatomical landmark identification (repeatability),
- location of the femoral marker cluster relative to the CR.

The optimization of the relevant experimental and analytical procedures is here detailed, as a prerequisite to obtain an optimal estimate of the hip joint centre

location. Precision was estimated on in-vivo data; accuracy was evaluated using the methodology explained in Chapter 3.3 generating a model of the artifact as in Chapter 3.1.

4.3.2 Materials and Methods

Twenty-four healthy young adults participated in the study (8 females and 16 males). Average age, mass and height of the subjects in each group are presented in Table 4-2. All subjects were between 20 and 36 years of age.

Marker placement and measurement system were the same as in Chapter 3.2.

CHARACTERISTIC	MALE	FEMALE
NUMBER OF SUBJECTS	16	8
AGE (YEARS)	24(4)	26(5)
BODY MASS (KG)	68(9)	56(6)
HEIGHT (CM)	178(8)	167(4)
NUMBER OF LEGS	27	13

Table 4-2 Subject group characteristics. Mean (SD)

Anthropometric parameters

Selected anthropometric parameters were measured as distances between markers in a static reference trial (Figure 4-5 and Table 4-3). In order to estimate the pelvic height without palpating awkward points, an ad hoc experiment was performed. A stick with two markers was held by the subject in contact with the lower part of his/her pelvis. The subject manually oscillated the stick about the contact point, in the lowest part of the pelvis. The distance between the XZ plane of the anatomical reference system of the pelvis and the line joining the stick markers, when parallel to the plane, was thereafter calculated.

MEASURE	ACRONYM	FROM:	TO:
SHANK LENGTH	SL	TT	LM
THIGH LENGTH	TL	GT	LE
FOOT LENGTH	FL	CA	FM
ANTERIOR PELVIC WIDTH	PAW	LASI	RASI
POSTERIOR INTER-PSIS DISTANCE	PPW	LPSI	RPSI
PELVIC DEPTH	PD	LASI	LPSI
PELVIC HEIGHT	PH	ASIS AND PSIS PLANE	STICK, WHEN PARALLEL TO THE PLANE.

Table 4-3 Anthropometric parameters, their acronym, and end-points between which the parameters were measured.

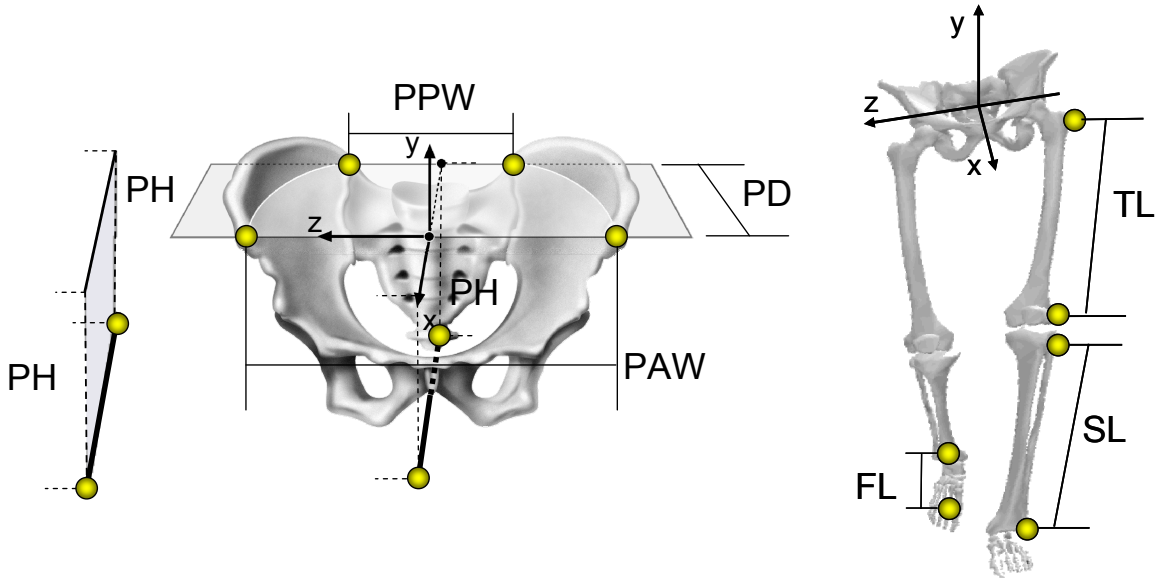

Figure 4-5 Anthropometric parameters listed in Table 4-3, and relevant marker placement.

Movements performed

Subjects were asked to perform the following movement of the femur relative to the pelvis: the foot traced a semi-star (anterior, antero-lateral, lateral, lateral-posterior, posterior movements) followed by a semi-circle, without touching the ground (Figure 4-6)

Pure flexion
Back to the reference position without touching the ground
Hip flexion combined with a slight abduction
Back to the reference position without touching the ground
Hip flexion combined with a wide abduction
Back to the reference position without touching the ground
Hip extension combined with a slight abduction
Back to the reference position without touching the ground
Hip extension combined with a wide abduction
Back to the reference position without touching the ground
Pure extension of the hip towards his back

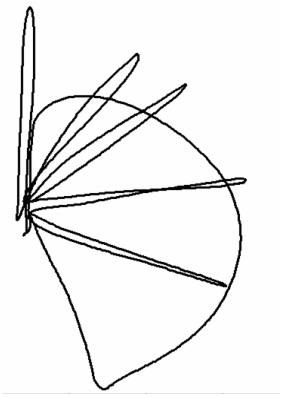

Figure 4-6 Movement performed by the subjects. The toe projection on the floor, during the movement, is depicted.

The subjects were asked to keep their foot pointed frontward to reduce rotations of the hip, and the knee locked in a full extension to avoid knee flexions, since both movements could increase the STA effects (Cappozzo et al. 1996; Leardini et al. 1999) A subset of the population (10 subjects) repeated the whole protocol without controlling the position of the foot, to evaluate the relevance of STA effects due to hip rotation on repeatability of HJC determination. Repeatability was assessed on 4 trials performed with and without controlling the foot position. Each trial was analysed using 3 different clusters and 3 algorithms. Data were compensated for STA, results before and after compensation were compared.

Trials were rejected if the peak to peak value of knee flexion was higher than 10° and/or if the standard deviation was higher than 4°. The exercise duration, 10.5±2.5s, and the acquisition frequency, 120 frames/s. In order to reduce the propagation of the error associated with the identification the pelvic landmarks and, thus, with the pelvic anatomical frame, relevant markers were repositioned, and experiments repeated thereafter, three times. For each marker placement four valid trials were performed. STA was compensated using a method similar to that proposed by Alexander and Andriacchi (Alexander et al. 2001), see Chapter 3.2. The model of the STA, incorporated in the latter method, consisted in a linear combination of the hip joint angles (Cappozzo et al. 2003) and is described in Chapter 3.2.

A comparative evaluation of accuracy and precision obtained with three different algorithms was performed in order to asses their performances on data affected by skin movement artifact. The three chosen algorithms was:

- MLD, minimal linear displacement (Holzreiter 1991);
- FS4, centre of the bias-compensated quartic best fitted sphere (Gamage et al. 2002; Halvorsen 2003);
- FHA, pivot point of weighted finite helical axes (Woltring 1990)

For each trial, the HJC pelvic coordinates were estimated using 3 different thigh clusters (distal, proximal and central), Figure 4-7, each made of 4 markers out of the 12 available, in order to evaluate the relevance of the position along the thigh of the cluster. Precision was estimated on in-vivo data. Accuracy was evaluated using the methodology explained in Chapter 3.2 generating a model of the artifact as in Chapter 3.1.

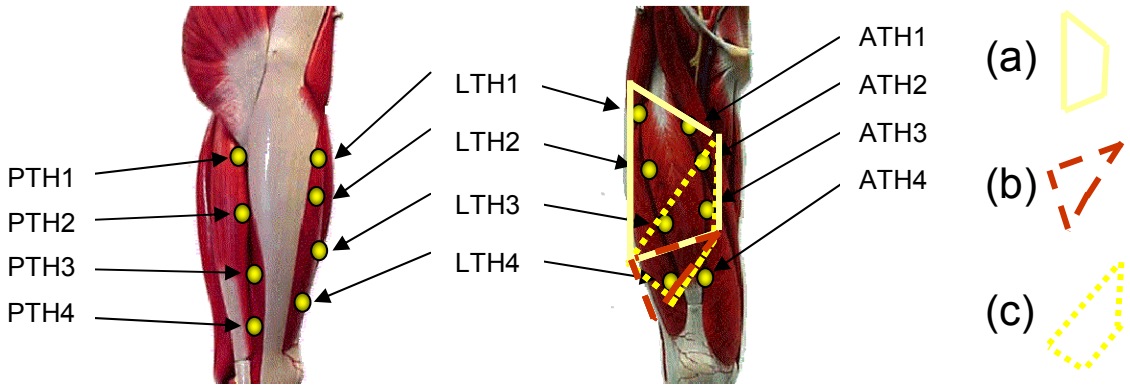

Figure 4-7 Clusters of thigh marker used for HJC determination. (a) proximal (b) distal (c) central.

4.3.3 Results

Algorithms

The highest repeatability was obtained using the FS4 method, the relevant standard deviation among clusters was of 2, 6 and 3.5mm for X, Y, and Z, respectively. For the other methods the standard deviation was of 10mm for X and around 5mm for Y and Z, Table 4-4. The highest accuracy was obtained with FS4 method as well, the rms error being lower than 5mm on all coordinates, while the error for the other methods was always higher than 7mm, going as up as 12mm for the Y coordinate, Table 4-4.

		FS4		MLD		FHA	
		rmse	**sd**	**rmse**	**sd**	**rmse**	**sd**
Simulated data	**X**	2.3	2.1	8.0	9.9	11.0	14.0
	Y	4.8	6.4	12.2	8.6	12.7	8.8
	Z	3.8	3.8	7.3	5.2	9.0	4.5
Experimental data	**X**		2.0		8.9		12.0
	Y		6.5		7.2		7.3
	Z		3.2		5.4		5.0

Table 4-4 Standard deviation, *sd*, and root mean squareerror, *rmse*, in mm, of HJC coordinates as obtained using different clusters. Only *sd* is given

Foot position effects on STA

Repeatability of HJC determination, assessed on 4 trials using for each different thigh clusters and the best algorithm available, was of 0.7 mm, 1.2 mm e 0.7 mm, for X, Y and Z respectively, if the foot position was controlled and STA compensated. STA compensation considerably reduced variability of HJC, but could not completely compensate for an external rotation of the hip, as shown in Table 4-5.

	Without control		**With control**	
	C	**NC**	**C**	**NC**
X	25	2.5	9.3	0.7
Y	13	3.5	10.4	1.2
Z	11	1.5	4.6	0.7

Table 4-5 Precision of HJC determination, averaged over 4 trials, analysed with 3 different clusters and 3 algorithms. Results are reported on data non compensated (NC) and compensated (C) with IDT-1 method, with and without controlling the foot position.

Cluster effects

The standard deviation of the HJC obtained on four trials, using the same cluster, was associated to intra-cluster variability. The standard deviation of the HJC results obtained with the three different clusters, proximal, medial, and distal, was associated to inter-cluster variability. Mean and standard deviation of intra-cluster and inter-cluster values, as obtained on 42 legs, before and after STA compensation, are reported in Table 4-6. Both intra- and inter-cluster variability were considerably reduced by STA compensation.

	Intra-cluster		Inter-cluster	
	C	**NC**	**C**	**NC**
X	2.2 ± 1.5	2.5 ± 2.5	0.6 ± 0.6	1.8 ± 1.3
Y	0.6 ± 0.6	1.9 ± 1.4	1.0 ± 0.9	3.8 ± 1.6
Z	3.2 ± 2.2	3.5 ± 2.0	0.5 ± 0.5	3.4 ± 1.5

Table 4-6 Mean error and standard deviation, e±*sd*, in mm, of intra-cluster and of inter-cluster HJC variability. Compensated (C) and non compensated (NC) data.

The highest repeatability was associated with different clusters according to the subjects. After compensation, proximal and distal cluster were the most reliable 22 and 18 times, respectively, Table 4-7. The most repeatable cluster varied for female and male subjects; the proximal cluster had the best performance for 67% of the male and only 30% of the females. The best performing cluster did not change before and after compensation in 63% of the trials; when a change did occur, it was 85% of the times towards more proximal clusters (distal to medial or proximal clusters; medial to proximal cluster).

	Female		Male	
	C	**NC**	**C**	**NC**
proximal	4	5	17	10
medial	8	5	9	12
distal	0	2	0	4

Table 4-7 Number of proximal, medial, and distal clusters that showed the highest repeatability, on compensated (C) and non compensated (NC) data.

Inter-mounting variability

HJC results obtained using the same cluster and the same pelvic mounting (4 trials) were averaged, the variability of these averages was associated to inter-mounting variability. Mean and standard deviation of the inter-mounting variability obtained over 42 legs are reported in Table 4-8. The inter-mounting variability wasn't significantly reduced by STA compensation.

	Inter-mounting	
	C	**NC**
X	3.2 ± 2.2	3.5 ± 2.0
Y	2.6 ± 1.6	3.2 ± 2.9
Z	2.3 ± 1.4	3.0 ± 2.3

Table 4-8 Mean error and standard deviation, e±*sd*, in mm, of inter-mounting HJC variability is reported for compensated (C) and non) compensated (NC) data.

For a given pelvic marker placement and thigh cluster (4 trials), the dispersion (rms distance from the mean) of the HJC position in the pelvic frame was lower than 3, 5 and 3 mm for the X (antero-posterior), Y (vertical upwards) and Z (medio-lateral) coordinate, respectively, in all subjects. This dispersion increased to 7 mm for the X and Y coordinates and 4 mm for the Z coordinate, when all trials for a given thigh cluster were considered (12 trials). The higher variability was due to change in pelvic marker placement.

4.3.4 Discussion and conclusion

The highest repeatability and accuracy of method FS4 may be due to the rigidity constraints used in determining the CR. The method imposes that each femoral marker lie, in any given instant of time during the movement, on a spherical surface, the centre of which is the CR. No assumption is made on relative distance between femoral markers, i.e. on femoral marker cluster rigidity. This constraint, imposed by the other methods considered, is hardly verified if STA is present.

The number of four trials per mounting can be considered adequate, as the reduction of intra-cluster variability after STA compensation confirmed. Inter-cluster variability was reduced as well, while differences among subjects of the best cluster does not allow for the reduction of the number of marker placed. The inter-mounting variability was not reduced by STA compensation, as was predictable, as it is due to error in marker palpation and not to soft tissue artifact.

It is thus suggested to use the FS4 method, to ask the subject to keep the foot pointing frontward as much as possible while performing the movements. If more than a trial is performed, the HJC estimated by the most repeatable cluster constitutes the best choice.

4.4 Enhanced anatomical calibration

4.4.1 Introduction

In this section an alternative anatomical calibration procedure was developed, based on the estimate of a subject-specific bone or portion of bone. This estimate is implemented by determining the position of a large number of unlabelled points (UPs) located over all prominent parts of the bone surface and matching to them a digital model of a template-bone. For this reason, the technique will be referred to as UP-CAST. The estimated subject-specific bone contains all relevant AL locations.

The validation of the procedure is limited to the femur as a paradigmatic case. Intra- and inter-examiner repeatability of AL identification was assessed both in vivo, using normal weight subjects, and on bare bones. Accuracy of the identification was assessed using AL locations directly identified on bare bones as a reference.

4.4.2 Materials and methods

The UP-CAST method

Markers placed above the diaphysis of the femur, according to the guidelines outlined in (Cappozzo et al. 1997), are used to construct a CF (Hanson et al. 1981). A further marker is placed on the greater trochanter (GT). The determination of the UP position vectors in the CF is carried out using a wand fitted with a cluster of at least three markers and a sphere on the tip that rolls over the surface to be digitized (Figure 4-8). In order to associate the digitized surface with the bone, the UP determination is performed in the body segment areas where the soft tissue layer over the bone is sufficiently thin. With reference to the femur, the relevant acquisition provides the UPs over the epiphysis (${}^{c}\mathbf{up}[n]$, n=1, …, N) as shown in Figure 4-9 a. For reasons that will become evident later, a first approximation location of three labelled points must also be made available. Two of these points are located on the medial and lateral aspects of the femoral epiphysis such that they approximate the medial and lateral epicondyles, respectively, and the third corresponds to GT.

Figure 4-8 Wand fitted with a cluster of three retroreflective markers and a sphere (radius = 5 mm) on the tip.

A template-bone is selected and its surface points are given relative to a MF ($^{m}\mathbf{b}$; Figure 4-9 b). This template may be selected from a database using the available information about the subject's bone and a similarity criterion. The template ALs are identified and labelled using a virtual palpation technique ($^{m}\mathbf{a}[a]$). The same portion, or portions, of the bone digitized in vivo are then selected (template epiphysis: $^{m}\mathbf{e}[e]$, e=1, …, E; Figure 4-9 b).

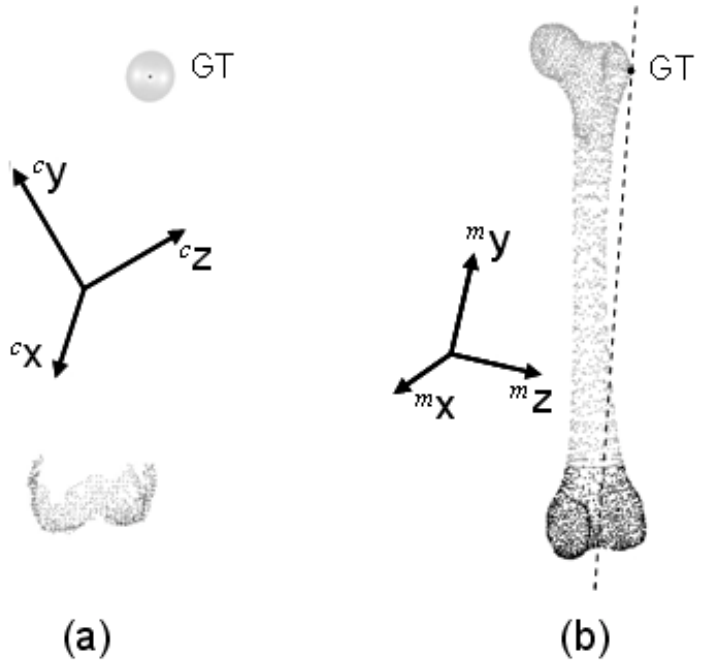

Figure 4-9 (a) Experimental UPs (^{c}up[n], n=1, …, N) and a sphere centred in the GT. (b) Digital template points before (^{m}b[b], b=1, …, B; light grey) and after (^{m}e[e], e=1, …, E; dark grey) the selection of the distal portion.

Having carried out the preliminary procedures illustrated above, the subject-specific bone model, $^{c}\hat{\mathbf{b}}$, and the AL position vector estimates, $^{c}\hat{\mathbf{a}}$, are determined as

follows. An isomorphic deformation and a re-orientation of the ${}^{m}\mathbf{e}$ vectors, aimed at matching the relevant points with the measured UPs, are carried out. The superficial points of the subject-specific epiphysis are represented as:

$${}^{c}\hat{\mathbf{e}}[\mathrm{e}] = d \cdot {}^{c}\mathbf{T}_{m} \cdot {}^{m}\mathbf{e}[\mathrm{e}], \tag{4.1}$$

where d is the isomorphic deformation scale factor and ${}^{c}\mathbf{T}_{m}$ is the transformation matrix which actuates the re-orientation. These parameters are estimated ($\hat{d}$ and ${}^{c}\hat{\mathbf{T}}_{m}$) through the minimization of the mean direct Hausdorff distance between the template epiphysis points and the UPs, and also by using the information from the respective GT locations.

The optimization problem cost function is:

$$f(\hat{d}, {}^{c}\hat{\mathbf{T}}_{m}) = \frac{1}{\mathrm{E}} \sum_{\mathrm{e}=1..\mathrm{E}} \left(\min_{\mathrm{n}=1..\mathrm{N}} \left| \hat{d} \cdot {}^{c}\hat{\mathbf{T}}_{m} \cdot {}^{m}\mathbf{e}[\mathrm{e}] - {}^{c}\mathbf{up}[\mathrm{n}] \right| \right) \Big/ flag, \tag{4.2}$$

The flag variable is designed to abruptly decrease the cost function value when the experimental GT area is close to that of the template. A line, defined by the midpoint of the epicondyles and the GT, is associated with the ${}^{m}\mathbf{e}$ vectors (Figure 4-9b). A sphere, centred in the GT of the analysed bone (Figure 4-9a), is associated with the ${}^{c}\mathbf{up}$ vectors; this sphere has a radius equal to 20 mm (identification inaccuracy as provided in (Della Croce et al. 1999). The flag switches from a low to a high value when this line intersects the sphere. Despite the fact that the in vivo identification of the GT suffers from a large uncertainty, given its relatively large distance from the epiphysis, it helps the accuracy of the re-orientation exercise in the sagittal plane. This is particularly critical in consideration of the cylindrical symmetry of the femoral condyle. Other bones may not require the identification of ALs and may rely on UPs only.

The subject-specific bone model and AL estimates in the CF are given by

$${}^{c}\hat{\mathbf{b}}[\mathrm{b}] = \hat{d} \cdot {}^{c}\hat{\mathbf{T}}_{m} \cdot {}^{m}\mathbf{b}[\mathrm{b}] \text{ and} \tag{4.3}$$

$${}^{c}\hat{\mathbf{a}}[\mathrm{a}] = \hat{d} \cdot {}^{c}\hat{\mathbf{T}}_{m} \cdot {}^{m}\mathbf{a}[\mathrm{a}]. \tag{4.4}$$

In order to minimize the computation time, both the search space and the number of sample points may be reduced. The search space is limited by performing a preliminary re-orientation of the MF. This registration may be performed through a Singular Value Decomposition procedure (Soderkvist et al. 1993) using labelled points

available in both the CF and MF. This is the case for the first approximation ME and LE, and for the GT as measured in vivo which are made to optimally match the same ALs of the template-bone. This operation provides a first approximation registration matrix ${}^{c}\tilde{\mathbf{T}}_{m}$. After this first approximation registration is carried out, a subset of points of the two clouds (E'< E and N'< N) was selected by dividing the CF space into 3mm side voxels and randomly selecting only one UP and one epiphysis template point for each voxel. The cost function in Equation (4.2) can now be substituted with:

$$f(\hat{d},\hat{\mathbf{T}}) = \frac{1}{\mathrm{E}'}\sum_{\mathrm{e}=1..\mathrm{E}'}\left(\min_{\mathrm{n}=1..\mathrm{N}'}\left|\hat{d}\cdot\hat{\mathbf{T}}\cdot{}^{c}\tilde{\mathbf{T}}_{m}\cdot{}^{m}\mathbf{e}[\mathrm{e}] - {}^{c}\mathbf{up}[\mathrm{n}]\right|\right)\Big/ flag\,, \tag{4.5}$$

where ${}^{c}\hat{\mathbf{T}}_{m} = \hat{\mathbf{T}}\cdot{}^{c}\tilde{\mathbf{T}}_{m}$, and $\hat{\mathbf{T}}$ is close to an identity matrix. For the purpose of the flag value determination, the position vector of the GT in the MF is also transformed using the matrix ${}^{c}\tilde{\mathbf{T}}_{m}$.

Data Processing

The performance of the UP-CAST method was assessed for accuracy using two bare femoral bones, and, for precision, using both the bare bones and two able-bodied, normal weight subjects (1 male, 1 female with body mass index of 19.5 and 22.7 kg m^2, respectively). An informed consent was signed by the two volunteers.

Four markers were applied onto the thigh of the volunteers and on the diaphysis of the bare bones. The position of the tip of the wand relative to the wand markers was determined through a stereophotogrammetric calibration procedure. The accuracy of this calibration was assessed by rolling the tip over a metal sphere of known radius and was found to be within 1mm. During the experiments, the tip of the wand was kept approximately orthogonal to, and always in contact with, the surface to be digitized and was kept as close as possible to the volunteers' bone by slightly compressing the soft tissues. All the accessible areas of the distal femur were explored with the wand. The exploration started from the lateral epiphysis, close to the LE, and ended at the medial epiphysis, close to the ME (Figure 4-1) so that a first approximation location of these ALs was available. During this exercise, care was taken not to cause movements of the skin markers relative to the underlying bone. The GT was also digitized. The instantaneous global position of all markers was acquired at 120 samples per second using a 9 camera Vicon® 612

stereophotogrammetric system and the data set, illustrated in Figure 4-9a, was produced.

For each of the four femora involved in the analysis, six experimental sessions were carried out. In each session a different examiner, with no specific anatomy training, performed six anatomical calibrations (repetitions) (Table 4-9).

As far as the two bare bones were concerned, the six epiphysis ALs depicted in Figure 4-1 were identified and their location in the CF digitized twice by two examiners who had a specific training in bone landmark identification (Table 4-9). The resulting position vectors were thereafter averaged and determined in the nominal AF through rigid transformation ($^{a}\mathbf{ba}$). This vector was considered as a reference for the purpose of accuracy assessment. The same ALs were identified in the selected template-bone using the automatic virtual palpation software described in Chapter 4.1 (Donati et al. 2005) based on the pictorial instructions delivered in the Vakhum EU project(Van Sint Jan et al. 2002).

The minimization of the cost function, Equation (4.5), was accomplished using the genetic algorithm described in (Michalewicz 1996) with an initial population of 2500 “individuals” (each individual is a 7 element vector: 3 rotations, 3 translations, and 1 scale factor) and 200 iterations.

BONES (N)	PALPATION	ALS	EXAMINERS (N)	TRIALS PER EXAMINER	PRECISION	ACCURACY
TEMPLATE BONE (1)	VIRTUAL AL PALPATION	MEASURED,	--	--	ACCORDING TO LITERATURE	THEORETICALLY NOT ASSESSABLE
BARE BONES (2)	MANUAL AL PALPATION	MEASURED, ^{A}BA	SKILLED (2)	2	--	THEORETICALLY NOT ASSESSABLE
BARE BONES (2)	MANUAL UPS PALPATION	ESTIMATED, $^{A}\hat{A}$	UNTRAINED (6)	6	SEE METHODS SECTION.	COMPARISON WITH ^{A}BA
SUBJECT BONES (2)	MANUAL UPS PALPATION	ESTIMATED, $^{A}\hat{A}$	UNTRAINED (6)	6	SEE METHODS SECTION.	PRACTICALLY NOT ASSESSABLE

Table 4-9 The characteristics of the bone, palpation, AL evaluation procedure and relevant vector output, examiner, and procedure for precision and accuracy assessment are given. The number of bones, examiners, and trials are also quoted.

Each experimental session provided six data sets each made of the vectors $^{c}\hat{\mathbf{a}}[a]$ (a = 1, …, 6) and a GT vector. For the purpose of result interpretation, these vectors were represented in an AF associated with the relevant bone. Trial AFs were determined and represented using both a transformation matrix and an orientation vector (Spoor et al. 1980). A mean AF was determined using the means of all the relevant $^{c}\hat{\mathbf{a}}$ vectors. Thereafter, vector transformation were applied to obtain the vectors $^{\bar{a}}\hat{\mathbf{a}}$ and the orientation vectors $^{\bar{a}}\boldsymbol{\theta}_{\hat{a}}$ of each trial AF, all relative to the mean AF.

Internal consistency of the UP-CAST method was evaluated using the Cronbach's alpha coefficient (Cronbach 1951) on the $^{\bar{a}}\hat{\mathbf{a}}$ vectors of the bare bones and of the two subjects.

To demonstrate that changing the examiner does not significantly influence the measures obtained with UP-CAST, a repeated measures analysis of variance (ANOVA) was used with a between group factor (examiner: six levels, one for each examiner), and two within group factors (trial: six levels, one for each trial performed

by the examiner and AL: six levels, one for each AL). Four separate ANOVAs were performed for each of the bones and subjects. Significance level was set at ($p<0.05$).

When no significant interaction between trials and examiner was observed, the precision of the method was evaluated in terms of standard deviation of all $^{\bar{a}}\hat{\mathbf{a}}$ and $^{\bar{a}}\boldsymbol{\theta}_{\hat{a}}$ vectors for each bone and subject. To assess the accuracy, the distance between $^{a}\mathbf{ba}$ and all the $^{\bar{a}}\hat{\mathbf{a}}$ was calculated. Mean and standard deviation of the accuracies were calculated for each landmark.

4.4.3 **Results**

UP-CAST was shown to have a very high internal consistency, with Cronbach's alpha values larger than 0.997 for both bare bones and subjects. The repeated measures ANOVA, for both the bones and the subjects, showed that, firstly, there was no difference between examiners for any of the measures and, secondly, there was no within trial differences and no within ALs differences.

As there was no between examiner effect , the precision of the method was evaluated in terms of standard deviation of all $^{\bar{a}}\hat{\mathbf{a}}$ (Table 4-10) and $^{\bar{a}}\boldsymbol{\theta}_{\hat{a}}$ (Table 4-11). The standard deviations ranged from 0.9 to 7.6 mm and from 0.4 to 7.0 deg, respectively. On all bones, the epicondylar landmarks appeared to have higher errors in the antero-posterior direction, while the patellar groove landmarks appeared, in general, to be more dispersed along the medio-lateral axis. The most distal landmarks tended to be more scattered on the transverse plane than vertically. While in general the precision range on subject bones (1.9 to 7.6 mm and 0.8 to 7.0 deg) appeared higher than on bare bones (0.9 to 4.6 mm and 0.4 to 4.9 deg), in many cases the precision values were comparable between the bones and the subjects. This indicates that the error associated with the discrepancy between the template morphology and the analysed bone morphology prevails on trial specific error sources, such as the presence of soft tissue.

	LE				ME				LP				MP				LC				MC			
	ML	**V**	**AP**	**3D**	**ML**	**V**	**AP**	**3D**	**ML**	**V**	**AP**	**3D**	**ML**	**V**	**AP**	**3D**	**ML**	**V**	**AP**	**3D**	**ML**	**V**	**AP**	**3D**
Bone 1	0.9	1.1	2.4	2.8	1.2	0.9	3	3.4	2	1.3	0.9	2.5	2.1	1	1.2	2.6	0.9	1	2.1	2.5	0.9	0.9	2	2.4
Bone 2	1.4	2.2	3.6	4.4	2	1.6	3.6	4.4	3.5	2.8	1.2	4.6	3.3	2.4	1.4	4.3	1.6	1.8	2.9	3.8	2	1.4	1.8	3
Subject 1	3.4	2.5	5	6.5	3.3	3.2	4.6	6.5	2.7	3.3	3.2	5.3	2.7	3.1	3	5.1	3.5	1.9	4.4	5.9	3.4	2.4	3.3	5.3
Subject 2	2	2.3	5.5	6.3	2.5	2.6	6.7	7.6	4.9	2.7	2.8	6.3	4.3	2.4	3.9	6.3	2.2	2	4.5	5.4	2.5	2.1	4	5.2

Table 4-10 Precision with which the local position of anatomical landmarks was determined. Standard deviation of landmark positions (see Figure 4-1 and list of symbols for acronyms) calculated over all examiners and trials along the anatomical axes (Medio-Lateral, Vertical, and Antero-Posterior) and 3D. Measures in millimetres.

	ML	V	AP
Bone 1	0.4	3.6	0.9
Bone 2	0.6	4.9	0.9
Subject 1	0.9	7.0	1.3
Subject 2	0.8	5.0	1.0

Table 4-11 Precision with which anatomical frames were determined. Standard deviation of the orientation vectors of the anatomical frames were calculated for all examiners and trials and were projected onto the anatomical axes (Medio-Lateral, Vertical, and Antero-Posterior). Measures in degrees.

The accuracy was dependent on the bone and the landmark analysed (Table 4-12). The variability of the accuracy over the trials was different between bones, but similar for landmarks of the same bone. This confirms that bone morphology is a main source of low identification precision.

	LE	ME	LP	MP	LC	MC
Bone 1	2.8 (1.0)	3.2 (1.6)	7.5 (0.8)	9.3 (1.8)	2.7 (1.1)	3.3 (1.4)
Bone 2	6.8 (1.9)	6.9 (2.2)	11.3 (3.2)	8.1 (1.4)	5.9 (1.8)	6.5 (1.5)

Table 4-12 Accuracy with which the position of the anatomical landmarks was determined. Mean (standard deviation) of the accuracy over six examiners. Measures in millimetres.

4.4.4 Discussion

The precision of the proposed anatomical calibration procedure, based on the determination of UPs, has been described and compared with those of the AL palpation approach. The absence of significant interactions both between and within factors confirmed that a change in the examiner did not influence the performance of UP-CAST, both in terms of the trials and of the AL locations. Moreover, as there was no within trial effect, this showed that there was no learning effect. Thus, the UP-CAST calibration can be carried out by ancillary health technicians in place of skilled professionals. This allows the changeover of laboratory technicians to occur without losing precision. In addition, the time required for landmark identification is drastically reduced. For the distal femur the identification of six landmarks via conventional calibration could require 5 to 10 minutes, while only 40-60 s are required to calibrate the selected area using the UP procedure.

As previously shown using a calibration based on the manual identification of landmarks (Della Croce et al. 1999), the most distal landmarks were characterized by a lower precision in the antero-posterior direction while the patellar groove landmarks were more dispersed along the medio-lateral axis. Conversely, the epicondyles had the lowest precision along the antero-posterior direction and not along the medio-lateral direction shown in the conventional calibration. The anatomical frame orientation was confirmed to have a larger variability around the vertical axis (Table 4-11). This is due to the femoral shape characterized by a predominant longitudinal dimension relative to the other two dimensions.

The UP-CAST precision along the anatomical axes (range: 1.9 – 7.6 mm) was remarkably higher than that exhibited by the conventional calibration (inter-examiner: 13.4 – 17.9 mm; intra-examiner: 1.4 – 10.8 mm) (Della Croce et al. 1999).Since AL identification is carried out on the template, and therefore does not contribute to variability, this result demonstrates that the UPs acquisition procedure and the related template registration and isomorphic deformation exercise are highly precise.

Identification precision obtained on subjects was only slightly worse than that obtained on bare bones. Moreover, results relative to the subjects were comparable despite different anthropometry and soft tissue thickness around the knees. These results, even if obtained on the low number of subjects and bones available, suggest that soft tissues do not markedly interfere with the proposed method. As the method used in the present study assumes that the thin layer of tissue typical of the areas where the digitization is performed is part of the bone morphology, it is not surprising that soft tissues can cause errors similar to those obtained when comparing different bones.

The accuracy, assessed on bare bones, was up to three times worse than precision (for the ME landmark, for example, the accuracy for the first and second bone was of 3.2 and 6.9 mm while the precision was 3.4 and 4.4 mm, respectively). This is mostly due to the differences between the template and the morphologies of the other tested bones. Moreover, virtual palpation is prone to errors itself: for the considered distal femur landmarks a 3D standard deviation was assessed within 1.8 and 2.9 mm (Van Sint Jan et al. 2005).

The principal limitation of the method resides in the morphological difference between the template and the bone under analysis. Usually, a digital bone specific of the subject is not available and any other template carries an intrinsic error associated with inter-subject variability of bone morphology. In order to reduce this error, it is highly desirable to rely on a large database of templates representative of different populations. In addition, an improvement of the subject-specific bone estimation could be attained if more accurate UPs were available. This could be accomplished using suitable imaging equipment, such as ultrasound, to be integrated in the movement analysis practice.

The validation of the procedure was limited to the femur, but, at least in principle, it can be extended to other bones, provided that a sufficient portion of their surface is covered with a thin layer of soft tissue.

4.5 A protocol for a repeatable anatomical calibration in in-vivo gait analysis

4.5.1 Introduction

In this section a movement analysis protocol that incorporates the proposed UP-CAST anatomical calibration is presented. To demonstrate the robustness of the method in gait analysis, the repeatability of the determination of pelvis and lower limb ALs and of the estimate of hip and knee kinematics, was assessed.

4.5.2 Materials and methods

Prior to the experiments, the digital models of an adult male pelvic bones, a femur bone, and a tibia and fibula complex were made available (BEL). On these bone models the ALs listed in Figure 4-10 were identified using the written and pictorial instructions delivered in the Vakhum EU project (Van Sint Jan et al. 2002).

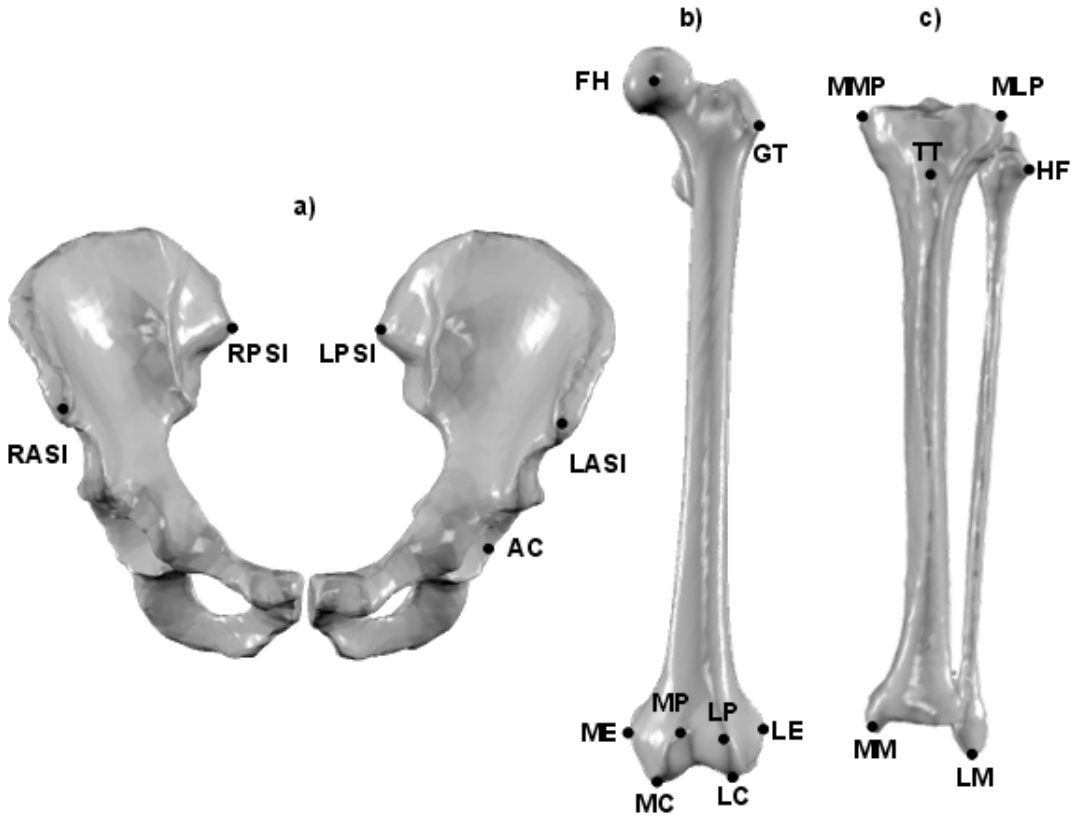

Figure 4-10. Position and acronyms of the selected landmarks. a) Pelvis: left and right anterior superior iliac spines (LASI, RASI), left and right posterior superior iliac spines (LPSI,RPSI), centre of the acetabulum (AC). b) Femur: lateral and medial epicondyles (LE, ME), antero-medial (MP) and antero-lateral (LP) ridge of the patellar grove, lateral and medial most distal point of the condyles (LC, MC), femoral head (FH). c) Tibia and Fibula: tibial tuberosity (TT), lateral and medial malleoli (LM,MM), head of the fibula (HF), most lateral and medial points of the tibial plateau (MLP, MMP).

Since only part of the bones can be digitized using UP-CAST, for each bone model, only the areas that can be digitized were selected: the distal portion plus the centre of the femoral head (FH) for the femur; the areas around the iliac spines and the iliac crest for the pelvis; the frontal and medial surface for the tibia and the lateral surface for the fibula (Figure 4-11).

Figure 4-11 Areas of the bones can be digitized using UP-CAST. a) Pelvis: the iliac spines. b) Femur: condyles and the prominent patellar grove. c) Tibia: tibial tuberosity along the anterior crest down to the medial malleolus; Fibula: areas around the head and the lateral malleolus

Five adult able-bodied volunteers were selected in order to represent both genders, body mass indexes in the normal and over-weight ranges (BMI = 18.5 – 25.0 kg/m^2). Skin fold thickness measurements were carried out at relevant sites and relevant body fat (Table 4-13) (Siri 1961; Jackson et al. 1978; Jackson et al. 1980). Although it had been shown, in the previous Chapter, that a change in the examiner does not influence the performance of this method, it seemed reasonable, while evaluating the validity of these results for the pelvis and shank bones, to assess the potentially wider error (the inter-operator precision). Therefore, the experiments were carried out by six different operators that, as in the previous chapter, had no specific competences in AL identification through palpation.

SUBJ	GENDER	BMI [kg/m²]	BFP [%]	ILIAC CREST [mm]	FRONT THIGH [mm]
1	M	23.9	11.1	11.8	11.3
2	M	21.6	7.4	5.1	11.2
3	M	19.4	11.4	14.9	8.8
4	F	20.4	21.0	13.3	25.7
5	F	21.8	16.4	5.7	23.6

Table 4-13 Subjects' gender, body mass index and skin fold thickness measurements on iliac crest and front thigh.

For anatomical calibration purposes, the pelvis, thigh, and shank of the volunteers were fitted with rigid clusters of markers, the geometry of which followed the recommendations given in Cappozzo et al. (Cappozzo et al. 1997), (Figure 4-12a). Locations were chosen to minimally interfere with the anatomical calibration procedure. Based on these clusters, cluster frames were constructed (CF-UP, Figure 4-12a).

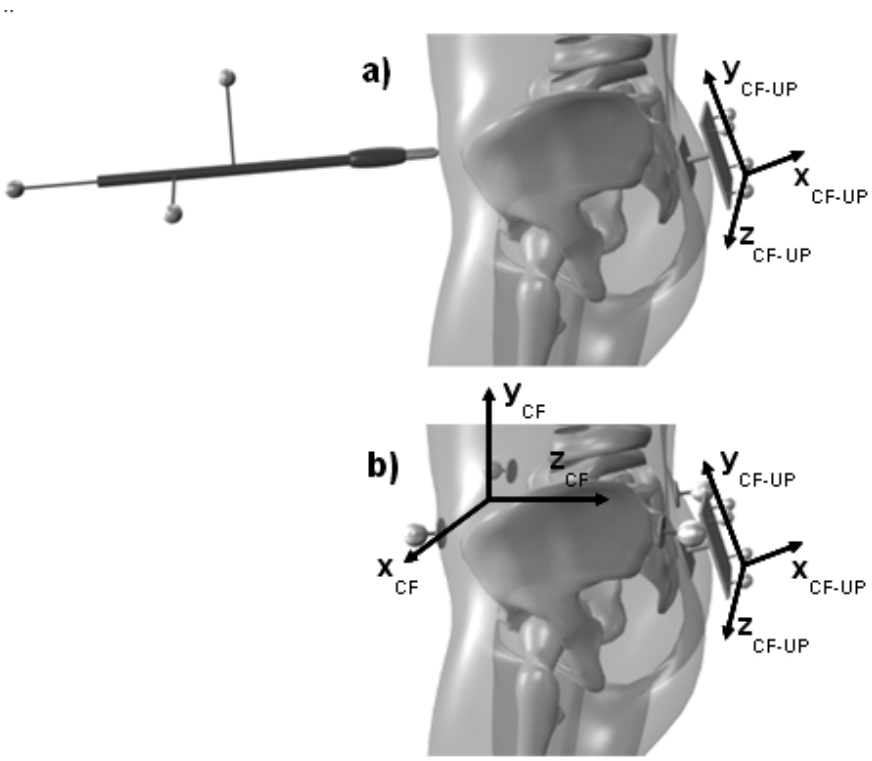

Figure 4-12. a) technical cluster and cluster frame (CF-UP) that minimally interfere with the anatomical calibration. b) technical cluster frame (CF) that, during movement, is less affected than the CF-UPs by inertial effects and soft tissue artifacts.

The positions of unlabelled points (UPs), located over all prominent parts of selected bones, were determined with respect to the relevant bone CF-UP, using a wand equipped with a cluster of three markers and a sphere on the tip that rolls over the surface to be digitized. This was done in the body segment areas where the soft tissue layer over the bone was sufficiently thin so that the digitized surface could be associated with the bone. Specifically, the areas acquired were: for the pelvis, around the iliac spines; for the femur, on the condyles and the prominent patellar grove; for the tibia, on the tibial tuberosity along the anterior crest down to the medial malleolus; for the fibula, around the head and the lateral malleolus. This procedure was carried out by each of the six operators, Figure 4-13. The subjects were asked to stand during the pelvis calibration and to keep their knee flexed at 90° degrees when calibrating femur, tibia, and fibula.

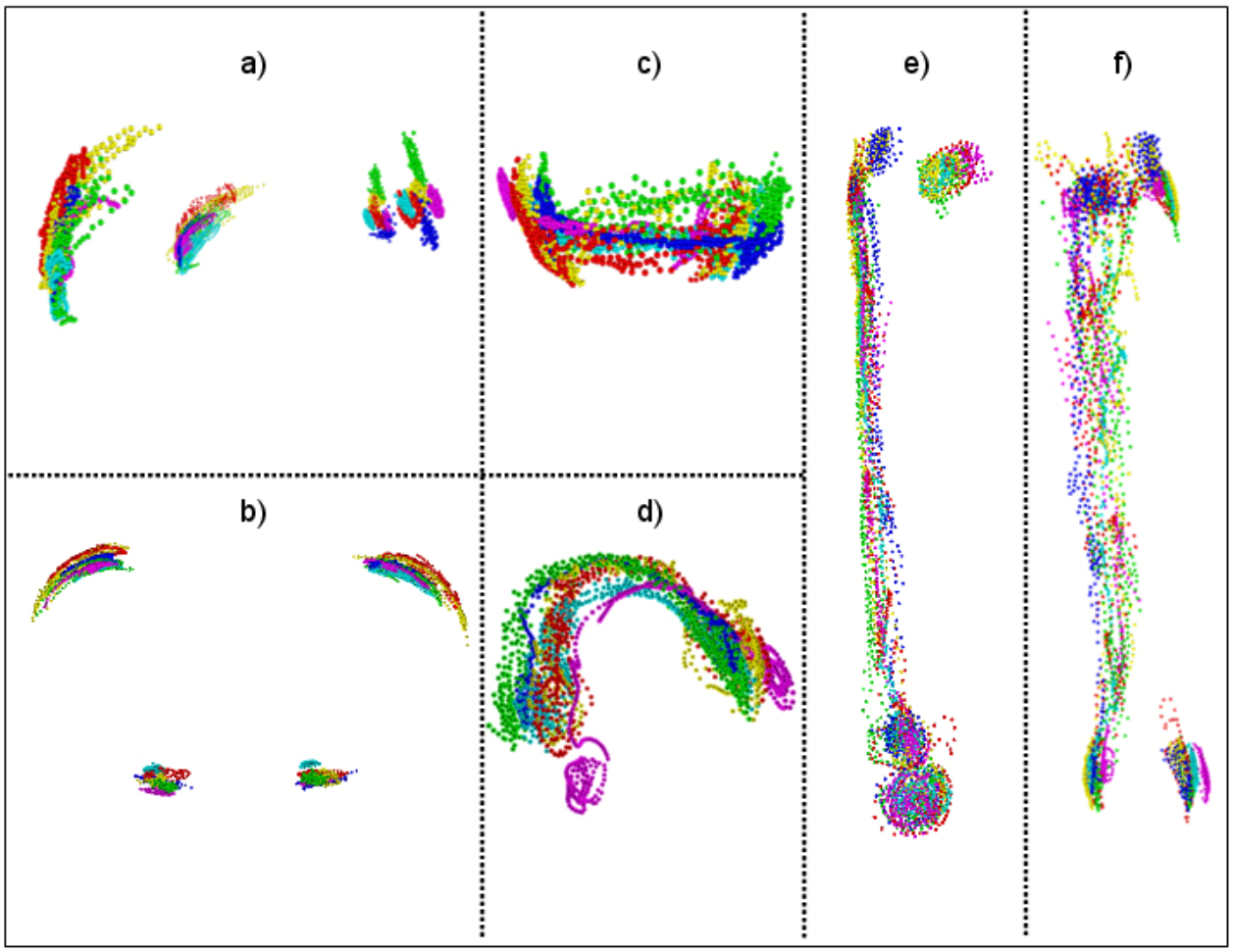

Figure 4-13 : measured UPs of six operators. a) side view of the pelvis UPs; b) top view of the pelvis UPs; c) Front view of the femoral condyle UPs; d) top view of femoral condyle UPs; e) side view of the shank UPs; f) front view of the shank UPs.

In order to improve instantaneous bone pose estimation during the acquisition of the subsequent tasks, four markers for each segment were added. Using them, CFs were built that, during movement, were less affected than the CF-UPs by inertial effects and soft tissue artifacts (Figure 4-12b). Two static acquisitions were performed, while the subjects assumed the same positions as during the calibrations, in order to determine, for each segment, the transformation matrices between CF and CF-UP.

The location of FH, assumed to coincide with the centre of the acetabulum (AC), was determined in the femur and the pelvic CFs using the functional approach described in Camomilla et al (Camomilla et al. 2006). To this purpose, volunteers were asked to move their thigh relative to their pelvis by flexing, extending and circumducting it (Figure 4-6). The volunteers were then asked to perform five level walking tasks at a self selected speed of progression. Markers were tracked by a nine cameras photogrammetric system (Vicon® MX13+) at 120 frames per second.

Data processing

CFs were constructed using a least squares approach (Hanson et al. 1981) that exploited the redundancy of the markers. The AC was determined in the pelvic CF using a bias-compensated quartic best fit algorithm (Gamage et al. 2002; Halvorsen 2003) as explained in Chapter 4.2. Rigid transformation matrices, based on the static acquisitions, were used to calculate the location of the UPs, of AC, and of FH in the relevant CF-UPs.

Using the above-mentioned experimental data, the selected bone template, and the UP-CAST method proposed in Chapter 4.3, the AL position vectors were estimated. A scaling and a re-orientation of the template points vectors, aimed at matching these points with the measured UPs, were carried out. The superficial points of a subject-specific bone were represented as:

$$^{c}\hat{\mathbf{p}} = \mathbf{d} \cdot {}^{c}\mathbf{T}_{m} \cdot {}^{m}\mathbf{tp}, \tag{4.6}$$

where $\mathbf{d}$ is a diagonal matrix of the scale factors and $^{c}\mathbf{T}_{m}$ is the transformation matrix which actuates the re-orientation. These parameters are estimated through a first approximation registration and a consequent minimization of a cost function,

based on the direct Hausdorff distance between the template points and the UP points, that is an enhanced version of that proposed in the previous Chapter:

$$f(\mathbf{d}, {}^{c}\mathbf{T}_m) = \frac{1}{\left|\mathbf{UP}\right| \cdot flag} \sum_{{}^{c}\mathbf{up} \in \mathbf{UP}} \mathrm{w}_{\mathbf{up}} \left(\min_{\hat{\mathbf{p}} \in \mathbf{TP}} \left| {}^{c}\mathbf{up} - {}^{c}\hat{\mathbf{p}} \right| \right), \qquad (4.7)$$

where the *flag* and w_{up} variables were included to increase the robustness of the method. The *flag* variable weights the cost function based on the use of a fiducial point. For the femur and pelvis, the hip joint centre was used. When this point is close to the relevant area of the template under analysis the *flag* value abruptly decreases the cost function value. The w_{up} doubles the minimal distances averaged in the Hausdorff distance only for the **up** points lying inside the template surface, TP. These points are identified by calculating their signed distance from TP (ref). Femur, tibia, fibula, left and right iliac bones were considered separately in terms of re-orientation, each was associated to an independent transformation matrix. The scaling was isomorphic for the femur, since the prominent areas available do not give satisfactory information on its tridimensionality, no independent degree of freedom can be allowed for this bone along the vertical direction. A non isomorphic scaling was performed on the other bones; the iliac bones were equally scaled, while tibia and fibula were considered independent.

Each anatomical calibration provided three data sets made of the anatomical landmarks vectors, ${}^{c}\hat{\mathbf{a}}_j$ for the j-th bone. For the purpose of result interpretation, these vectors were represented in three anatomical frames (AF) associated with the relevant bones, constructed as proposed in Cappozzo et al. (Cappozzo et al. 1995). A mean AF was determined, for each bone, using the means of all the relevant ${}^{c}\hat{\mathbf{a}}_j$ vectors. Thereafter, vector transformation were applied to obtain the anatomical landmarks relative to the mean AFs, ${}^{\bar{a}}\hat{\mathbf{a}}_j$. The precision of the method was evaluated in terms of root mean square error from the mean of all ${}^{\bar{a}}\hat{\mathbf{a}}_j$ vectors for each subject and bone. Three-dimensional AL position precisions were also calculated as the RMS of the norm of ${}^{\bar{a}}\hat{\mathbf{a}}_j - {}^{\bar{a}}\overline{\hat{\mathbf{a}}}_j$, i.e. the distances between each AL and its mean position.

For each gait trial, hip and knee joint kinematics were computed using the different anatomical calibrations, adopting the Cardan angular convention (Grood et al. 1983) Hip and knee angles are expected to be affected by the AL location errors during both upright posture and gait. To separate the two effects, the time functions of the angles during movement were aligned with respect to the relative upright posture angles. Let $\phi(t)$ denote one of the gait angles aligned with the relative upright posture, and let the indices k and m denote operator and trial. Then, $\phi_{k,m}^{subj}$ is a gait angle for one subject (subj) associated with a single trial (m) and a single operator (k). The variable $\phi_{k,m}^{subj}(t)$ is time-dependent. For each subject the following parameters, modified from those defined in Schwartz et al. (2005), were derived:

inter trial: $$\bar{\phi}_k^{subj}(t) = \frac{1}{N_{trials}} \cdot \sum_{m=1}^{N_{trials}} \phi_{k,m}^{subj}(t) , \qquad (4.8)$$

inter operator: $$\bar{\phi}^{subj}(t) = \frac{1}{N_{trials}} \cdot \frac{1}{N_{oper}} \cdot \sum_{k=1}^{N_{oper}} \sum_{m=1}^{N_{trials}} \phi_{k,m}^{subj}(t) \qquad (4.9)$$

The estimated standard errors of each ϕ are the standard deviation of the differences between ϕ and the relevant mean.

inter trial: $$\sigma_{\phi(t)}^{subj,\ trials} = \sqrt{\frac{1}{N_{trials} \cdot N_{oper} - 1} \sum_{k=1}^{N_{oper}} \sum_{m=1}^{N_{trials}} \left(\phi_{k,m}^{subj}(t) - \bar{\phi}_k^{subj}(t) \right)} \qquad (4.10)$$

inter operator: $$\sigma_{\phi(t)}^{subj,\ oper} = \sqrt{\frac{1}{N_{trials} \cdot N_{oper} - 1} \sum_{k=1}^{N_{oper}} \sum_{m=1}^{N_{trials}} \left(\phi_{k,m}^{subj}(t) - \bar{\phi}^{subj}(t) \right)}$$

(4.11)

The estimated standard error of ϕ was also computed considering each trial singularly.

$$\sigma_{\phi(t)}^{subj,\ i^{th}\ trial} = \sqrt{\frac{1}{N_{oper} - 1} \sum_{k=1}^{N_{oper}} \left(\phi_{k,i}^{subj}(t) - \frac{1}{N_{oper}} \cdot \sum_{k=1}^{N_{oper}} \phi_{k,i}^{subj}(t) \right)} \qquad (4.12)$$

Mean estimated standard errors $\bar{\sigma}_\phi$ were obtained by averaging over time the defined $\sigma_{\phi(t)}$:

$$\bar{\sigma}_{\phi}^{subj,var} = \frac{1}{N_{frames}} \sum_{t=1}^{N_{frames}} \sigma_{\phi(t)}^{subj,var} \quad ; var = trials, oper, i^{th}\ trial, \qquad (4.13)$$

The reliability of each joint angle was evaluated in terms of the ratio of the inter-operator error to the inter-trial error ($\bar{\sigma}_{\phi}^{subj,\ oper} \Big/ \bar{\sigma}_{\phi}^{subj,\ trials}$). The inter-trial error is free of methodological errors, and thereby serves as an appropriate baseline for comparisons.

4.5.3 Results

Precision of UP-CAST in locating the anatomical landmarks was evaluated for each bony segment in terms of RMS averaged for the six subjects (Table 4-14). Relevant values ranged from 2.9 to 7.3 mm for the pelvis, from 2.6 to 7.2 mm for the thigh and from 1.7 to 6.6 mm for the shank.

		AP	V	ML	3D
PELVIS	LASI	2.9	7.3	4.1	8.4
	RASI	3.0	6.1	5.3	8.2
	LPSI	3.8	5.3	2.8	6.9
	RPSI	3.0	5.1	3.3	6.4
THIGH	LE	4.4	5.1	2.9	6.8
	ME	7.2	4.8	3.2	8.5
	LP	3.5	4.1	2.6	5.7
	MP	6.1	4.0	3.1	7.4
	LC	3.3	5.1	2.6	6.1
	MC	4.9	4.8	4.1	7.4
SHANK	TT	1.7	5.2	3.3	6.2
	HF	3.9	2.6	2.1	5.1
	LM	2.9	3.7	2.1	4.8
	MM	5.5	4.8	3.9	8.1
	MLP	5.2	6.1	5.1	9.1
	MMP	6.6	5.7	6.6	10.6

Table 4-14 Inter-examiner precision of the anatomical landmark position components (antero-posterior, AP, vertical, V, medio-lateral, ML) in the relevant mean AF. The 3D precision is also reported. Measures in millimetres.

On the pelvis, errors were slightly higher in the vertical direction. Anterior ALs resulted more dispersed that the posterior ones. Femoral medial ALs (ME, MP, MC) were partly more dispersed along the antero-posterior direction. On the shank, results confirmed HF as the most precise AL, but similar performances were obtained for the malleoli and for TT. MMP and MLP confirmed to be dispersed even if presenting 3D error less than 10.6mm.

Differences were outlined between males and females. For male subjects, a better identification was carried out on both pelvis and thigh (mean percentage of the difference was 22.4%), while the shank landmarks were similarly identified on all subjects.

The repeated anatomical calibration affected the upright posture angles of all subjects in similar way (Figure 4-14). Both hip and knee internal–external rotation errors underwent the highest variations.

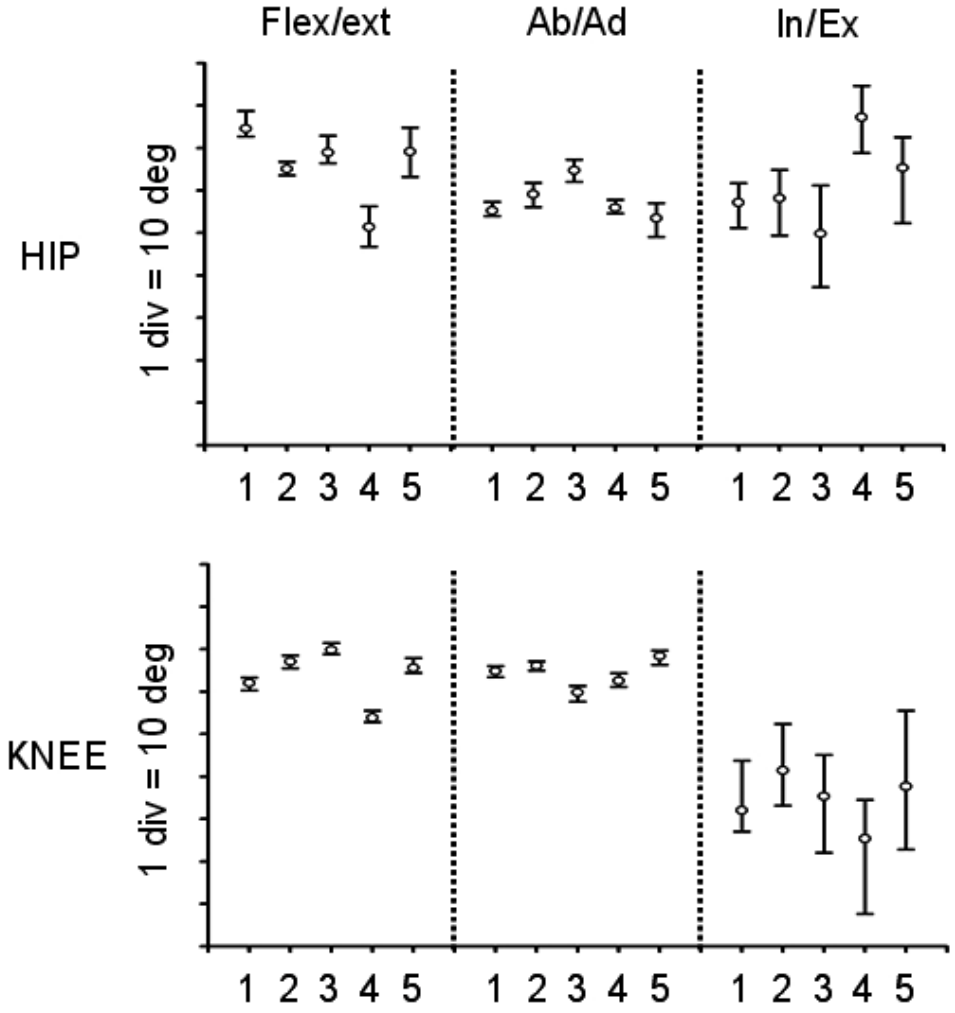

Figure 4-14 Upright posture angles for all subjects: minimum, maximum and average over all operators.

Repeatability of joint kinematics was visibly high, as reported in Figure 4-15 for all hip and knee angles.

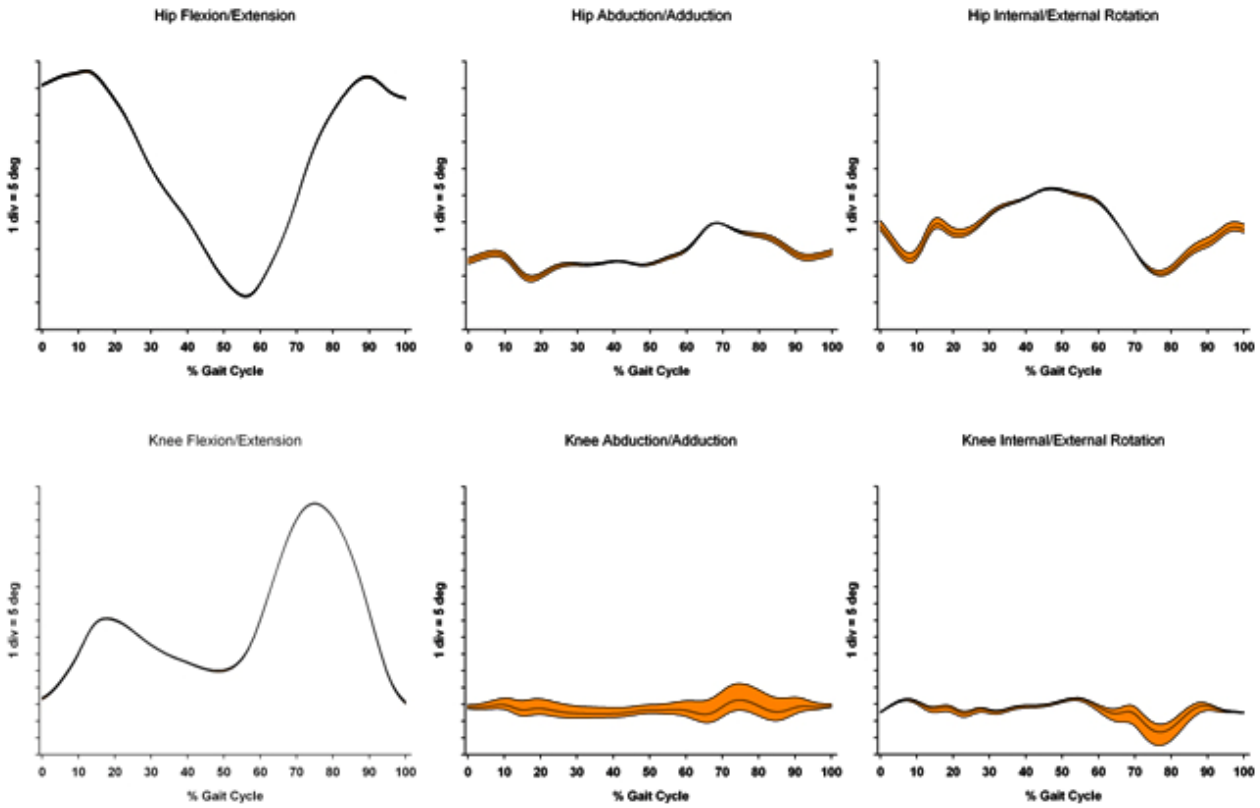

Figure 4-15 Hip and knee kinematic inter-operator variability for 1 subject and 1 gait cycle: : minimum, maximum and average over all operators.

The precision relative to all angles, reported in Table 4-16, was unaffected by the inter-operator error except for the ab-adduction and internal-external rotation errors of the knee, which were however found to be always less than 3deg. The inter-operator error was comparable to the inter-trial for all hip angles and for knee flexion-extension (Table 4-15). Knee internal-external rotation σ^{oper} were, on average, 10% greater than the relevant σ^{trials}, while knee ab-aduction σ^{oper} was from 10% to 60% greater than the relevant σ^{trials}.

	HIP			KNEE		
	fe	**aa**	**ie**	**fe**	**aa**	**ie**
subj 1	1,0	1,0	1,0	1,0	1,2	1,0
subj 2	1,0	1,0	1,0	1,0	1,6	1,1
subj 3	1,0	1,0	1,0	1,0	1,4	1,2
subj 4	1,0	1,0	1,0	1,0	1,1	1,1
subj 5	1,0	1,0	1,0	1,0	1,1	1,0

Table 4-15. Ratio between $\overline{\sigma}_{\phi}^{subj,\ oper}$ and $\overline{\sigma}_{\phi}^{subj,\ trials}$ is given for each subject and each angle under analysis (fe: flexion-extension; aa: abduction-adduction; ie: internal-external rotation).

	HIP			KNEE		
	fe	**aa**	**ie**	**fe**	**aa**	**ie**
subj 1	0,1	0,2	0,3	0,2	1,7	0,9
subj 2	0,1	0,3	0,7	0,2	1,9	1,0
subj 3	0,1	0,3	0,6	0,5	2,9	2,0
subj 4	0,2	0,4	0,4	0,4	2,2	0,9
subj 5	0,3	0,5	0,9	0,4	1,9	1,0

Table 4-16. Average of the inter-operator error $\overline{\sigma}_{\phi(t)}^{subj,\ i^{th}\ trial}$ i= 1..5; [deg] for each subject and each angle under analysis (fe: flexion-extension; aa: abduction-adduction; ie: internal-external rotation). Data in degrees.

4.5.4 Discussion

The robustness in gait analysis of the UP-CAST method, not requiring the accurate in-vivo identification of ALs through palpation, was assessed. The calibration procedure, previously validated for the femur in the Chapter 4.3, was modified and extended also to the pelvic and shank bones and its effects on the repeatability of joint kinematics were evaluated. The UP-CAST method was shown to be suitable for improving the precision in locating anatomical landmarks and, therefore, to reduce error propagation to 3D joint kinematics.

The UP-CAST precision, determined along the anatomical axes for all bones (range: 1.7 – 7.3 mm), strengthened the results previously obtained on the femur. These results, including pelvis and shank, confirm that the new calibration approach performs better than the conventional calibration (inter-examiner precision range: 1.9 – 17.9 mm) (Della Croce et al. 1999). The subjective interpretation associated to the AL determination, that was considered the main source of error by della Croce and colleagues and was overcome by the use of UP-CAST. The operators simply palpate the prominent bone areas and do not identify the ALs singularly. Consequences of possible erroneous palpation of these areas is mitigated by the a-priori information included in the digital bone model. This makes the present approach particularly valuable in identifying ALs that are broad areas instead of mere points. For example, the greatest improvements with respect to the conventional calibration (Della Croce et al. 1999) were obtained for the pelvic ALs. The dispersion of these ALs, responsible of the higher errors for the conventional calibration, became similar to that of the thigh and shank landmarks.

As expected, the upright posture angles were affected by AL misidentification and implied a systematic error in the angle time functions during gait. The error propagation to posture angles, while confirming previous results (Della Croce et al. 1999; Stagni et al. 2000; Camomilla et al. 2006), showed a reduced range (less than 2 deg) for flexion-extension and ab-adduction of both hip and knee. The highest variability of both hip and knee internal–external rotation posture angles can be attributed to the greater error in the identification of the anatomical transverse plane with respect to the other planes of both femoral and shank AFs.

During gait, errors due to the anatomical calibration exercise is generally superimposed to joint kinematics.

Table 4-15 summarizes all $\overline{\sigma}_{\phi}^{subj,\ oper} / \overline{\sigma}_{\phi}^{subj,\ trials}$ calculated for the mentioned joints using UP-CAST. Besides, for comparison purposes, the same ratios was reported also for the VCM protocol (Davis et al. 1991)as applied in two different laboratories (Charlton et al. 2004; Schwartz et al. 2004). The proposed calibration method shows an improved robustness to error propagation for all hip and knee angles. All the three hip angles and the knee flexion-extension don't show differences between inter-operator error and inter-trial error and the averages of the relevant inter-operator error ranged from 0.1 to 0.9deg (Table 4-16). The errors showed to influence only the knee ab-adduction and internal-external rotation, that showed a slightly lower repeatability, being their averaged inter-operator errors between 0.9 and 2.9 deg. These angles confirm to be the most sensitive to all experimental errors, like kinematic cross talk (Della Croce et al. 2005) and soft tissue artifact (Leardini et al. 2005). The inter-operator variability affects the AF determination and, consequently, modifies the way in which the other experimental errors are projected onto the anatomical planes and, thus, how they propagate to the knee angles.

	HIP			KNEE		
	fe	**aa**	**ie**	**fe**	**aa**	**ie**
UP-CAST	1,0	1,0	1,0	1,0	1,4	1,1
VCM (Charlton et al. 2004)	1,4	1,3	1,5	1,6	1,6	1,8
VCM (Schwartz et al. 2004)	4,2	3,8	3,0	~2	5,0	~3

Table 4-17 Ratio between inter-operator and inter-trial error for the proposed UP-CAST method and for the Vicon Clinical Manager assessed in two laboratories (Charlton et al. 2004; Schwartz et al. 2004) using different numbers of subjects and operators. Most of the numbers were extracted from graphs.

Two further strengths of UP-CAST regard both the time needed to carry out the calibration protocol and the anatomy-related knowledge required to the operator. First, the time required for landmark identification is drastically reduced. For pelvis, distal femur, tibia and fibula the identification of the mentioned 16 landmarks via conventional calibration (Wu et al. 2002) could require 10 to 15 minutes, while only 5-6 minutes are required to calibrate the selected areas using the UP-CAST procedure.

Higher number of landmarks can also be made available without lengthen the required duration. Furthermore, the application of UP-CAST is not constrained to be carry out only by health professionals, but may fruitfully be applied by non skilled operators. This represents a key point while doing movement analysis, because it is possible to widen applications without losing precision.

Attention has to be paid to the morphological difference between the template and the bone under analysis, while using the UP-CAST calibration. Since a subject-specific digital bone is not generally available, it is necessary to reduce the error associated with the inter-subject variability of bone morphology. In this respect, further efforts are required to widen the size of the bone database available in order to make it more representative of possible morphological variations

CHAPTER 5. CONCLUSION

The fundamental challenges in human movement analysis consist in minimizing the errors due to the artefact movement of soft tissues with respect to the bone, real object of the measure, and in improving the repeatability of the identification of anatomical frames, primary prerequisite for the repeatability of human movement analysis.

Several results obtained in this thesis addressed these issues and contributed to the enhancement of the repeatablility and accuracy of the reconstruction of 3-D joint kinematics.

To minimize the effects of the soft tissue artefact, an assessment specific of the task and subject involved is the essential prerequisite for its compensation. Both aspects were dealt with in the current thesis.

- An assessment method based on coherent averaging principles (non invasive coherent averaging, NICA) was developed that is non invasive, does not impose restriction to skin motion and uses only stereophotogrammetry. Its performance was evaluated by applying it on a data-set obtained using the synchronous measurements of fluoroscopy and stereophotogrammetry (ref) and by comparing the NICA estimates with those obtained from this data-set (ref). The consistency of the results obtained using the two different methods constitutes a supportive evidence of the credibility of the NICA estimates. Such assessment provides information on the artefact in different locations of the thigh and during different motor tasks; therefore, it could allow for optimal marker placement and constitutes an indispensable prerequisite for bone pose estimator design and assessment.
- A model of the artifact, useful to compensate it during different kinds of mono-articular movements, was developed as a function of both hip and knee rotation angles and of the relevant muscular contraction. The compensation method was then validated through a simulation procedure based on the described assessment.

A contribution to improve the repeatability of joint kinematics was given developing an new anatomical calibration protocol that uses the information obtainable through stereophotogrammetry and merges it with a digital model of the

bones under analysis. The following topics relative to the enhancement of the anatomical calibration were taken into account:

- First of all, an automatic procedure was developed for the identification of anatomical landmarks on virtual bones. This procedure increases the repeatability of the identification and eliminates the subjectivity due to the erroneous visual or conceptual interpretation of the written or visual definitions of the anatomical landmarks. It also reduces costs in terms of expert time with no loss in accuracy.
- Second, the methodological factors that may affect the functional methods performance to assess hip joint centre in vivo are taken into account, as a prerequisite to obtain an optimal estimate of the HJC location in order to improve the entire anatomical calibration protocol.
- Finally, an alternative anatomical calibration procedure was developed (UP-CAST), based on the determination of the position of a large number of unlabelled points (UPs) located over all prominent parts of the bone surface and on their matching to a digital model of a template-bone. The UP-CAST method was shown to be suitable for improving the precision in locating anatomical landmarks and, therefore, to reduce error propagation to 3D joint kinematics. Moreover, the time required for landmark identification is drastically reduced. For pelvis, distal femur, tibia and fibula the identification of the landmarks typical of the conventional calibration could require 10 to 15 minutes, while only 5-6 minutes are required to calibrate the selected areas using the UP-CAST procedure. A greater number of landmarks can also be made available without lengthening the required duration. Furthermore, the UP-CAST must not necessarily be carried out only by health professionals, but may fruitfully be applied by non skilled operators. This represents a key point while doing movement analysis, because it allows to widen applications without losing precision.

RINGRAZIAMENTI

Questa lavoro rappresenta l'ultimo passo di un percorso scientifico che acquisisce un valore particolare per la realtà in cui è maturato.

Sono sinceramente grato al Prof. Aurelio Cappozzo, per avermi dato l'opportunità di entrare a far parte del suo gruppo di ricerca, che guida con sapienza e cordialità. Desidero inoltre ringraziarlo per avermi trasmesso la passione per la ricerca scientifica.

Un ringraziamento particolare va a Valentina Camomilla, che con la sua dolcezza e la sua infinita pazienza, barcamenandosi tra tantissimi impegni, è riuscita a guidarmi e a supportarmi durante questo cammino, aiutandomi a raggiungere un traguardo che qualche anno fa avrei creduto impossibile.

Un grazie di cuore va a Fabrizio, mio compagno di classe 12 anni fa, ed attualmente mio compagno di stanza, con il quale ho condiviso questi anni di studio, ma soprattutto di infinita amicizia.

Desidero ringraziare, Mounir Zok, che con la bontà che lo contraddistingue ha condiviso il lato "artistico" della nostra ricerca e con il quale mi appresto ad intraprendere una nuova sfida.

Un ringraziamento di cuore va agli "inquilini" della 123, della 118 e del Vicon: Andrea Cereatti, Domenico Cherubini, Paolo de Leva, Ugo Della Croce, Marco Iosa, Claudia Mazzà, Pietro Picerno, Giorgio Sanna e Giuseppe Vannozzi, che oltre ad essere stati stimolanti dal punto di vista scientifico, hanno reso piacevole e divertente ogni singola giornata di lavoro.

Un grazie agli "Informatici", Prof. Nicola Fantini, Salvatore Motta, Massimo Muratore, Andrea Orlandini, Valentina Poggioni, più che un gruppo un vero e proprio "distributore" di allegria.

Desidero inoltre ringraziare Flaviano Pizzardi e tutta Pool Factory, Lucia Latour e AltroEquipe, che mi hanno introdotto in una realtà creativa che pensavo non mi appartenesse.

Un grazie speciale ai miei amici di sempre e soprattutto agli "Apocalittici", persone fantastiche, compagni di tante avventure, che mi sono sempre stati vicini e a cui voglio un mondo di bene.

Ovviamente un grazie affettuoso va alla mia Laura che ha condiviso con me tutti i momenti che hanno contraddistinto questo percorso e che non ha mai smesso di incoraggiarmi e sostenermi.

Infine devo dire mille volte grazie a mio Papà che pur non condividendo del tutto la mia scelta non mi ha fatto mai mancare il suo amore e mi ha permesso di raggiungere questo traguardo.

CHAPTER 6. BIBLIOGRAPHY

Abdel-Aziz, Y. I. and H. M. Karara (1971). Direct linear transformation into object space coordinates in close-range photogrammetry. In: Proc ASP Symp Close-Range Photogram, Urbana, IL.

Alexander, E. J. and T. P. Andriacchi (2001). "Correcting for deformation in skin-based marker systems." J Biomech **34**(3): 355-61.

Alexander, E. J., C. Bregler, et al. (2003). "Non-rigid modeling of body segments for improved skeletal motion estimation." Comp Mod Eng Sci **4**: 351-364.

Andriacchi, T. P. and E. J. Alexander (2000). "Studies of human locomotion: past, present and future." J Biomech **33**(10): 1217-24.

Andriacchi, T. P., E. J. Alexander, et al. (1998). "A point cluster method for in vivo motion analysis: applied to a study of knee kinematics." J Biomech Eng **120**(6): 743-9.

Andriacchi, T. P., G. B. Andersson, et al. (1980). "A study of lower-limb mechanics during stair-climbing." J Bone Joint Surg Am **62**(5): 749-57.

Angeloni, C., A. Cappozzo, et al. (1992). Quantification of relative displacement between bones and skin and plate-mounted marker. In: Proc VIII Meeting Eur, Soc Biomech, Roma.

Arun, K., T. Huang, et al. (1987). "Least-squares fitting of two 3-D point sets." IEEE Trans Patt Anal Machine Intell **9**(5): 698-700.

Banks, S. A. and W. A. Hodge (1996). "Accurate measurement of three-dimensional knee replacement kinematics using single-plane fluoroscopy." IEEE Trans Biomed Eng **43**(6): 638-49.

Basmajian, J. V. and C. J. De Luca (1985). Muscles Alive. Their Functions Revealed by Eloctromyography. Baltimore, USA, Williams & Wilkins.

BEL, r. BEL Repository.

Bell, A. L. and R. A. Brand (1989). "Roentgenographic changes in proximal femoral dimensions due to hip rotation." Clin Orthop Relat Res(240): 194-9.

Bell, A. L., D. R. Pedersen, et al. (1990). "A comparison of the accuracy of several hip center location prediction methods." J Biomech **23**(6): 617-21.

Benedetti, M. G., A. Cappozzo, et al. (1994). Anatomical Landmark Definition and Identification.

Benoit, D. L., D. K. Ramsey, et al. (2005). "Effect of skin movement artifact on knee kinematics during gait and cutting motions measured in vivo." Gait Posture.

Berme, N. (1990). Load transducers. Worthington, Ohio: Bertec Corporation, In: N. Berme and A. Cappozzo editors.

Besier, T. F., D. L. Sturnieks, et al. (2003). "Repeatability of gait data using a functional hip joint centre and a mean helical knee axis." J Biomech **36**(8): 1159-68.

Besl, P. J. and N. D. McKay (1992). "A Method for Registration of 3-D Shapes " IEEE Transaction on Pattern Analysis and Machine Intelligence **14**(2): 239-256.

Bomze, I. M., M. Budinich, et al. (1999). The Maximum Clique Problem.

Borghese, N. A., P. Cerveri, et al. (2001). "A fast method for calibrating video-based motion analysers using only a rigid bar." Med Biol Eng Comput **39**(1): 76-81.

Borghese, N. A. and G. Ferrigno (1990). "An algorithm for 3-D automatic movement detection by means of standard TV cameras." IEEE Trans Biomed Eng **37**(12): 1221-5.

Camomilla, V., A. Cereatti, et al. (2006). "An optimized protocol for hip joint centre determination using the functional method." J Biomech **39**(6): 1096-106.

Camomilla, V., A. Cereatti, et al. (in press). "An Optimized protocol for hip joint centre determination using the functional method." J Biomech.

Cappello, A., A. Cappozzo, et al. (1997). Bone position and orientation reconstruction using external markers. Three-dimensional analysis of human locomotion. C. A. In: Allard P, Lumberg A, Vaughan K, editors. New York, Wiley & Sons Ltd**:** 147-171.

Cappello, A., A. Cappozzo, et al. (1997). "Multiple anatomical landmark calibration for optimal bone pose estimation." Human Movement Sciences **16**(2-3): 259-274.

Cappello, A., P. F. La Palombara, et al. (1996). "Optimization and smoothing techniques in movement analysis." Int J Biomed Comput **41**(3): 137-51.

Cappello, A., A. Leardini, et al. (1997). "Application of stereophotogrammetry to total body three-dimensional analysis of human tremor." IEEE Trans Rehabil Eng **5**(4): 388-93.

Cappello, A., R. Stagni, et al. (2005). "Soft tissue artifact compensation in knee kinematics by double anatomical landmark calibration: performance of a novel method during selected motor tasks." IEEE Trans Biomed Eng **52**(6): 992-8.

Cappozzo, A. (1984). "Compressive loads in the lumbar vertebral column during normal level walking." J Orthop Res **1**(3): 292-301.

Cappozzo, A. (1984). "Gait analysis methodology." Human Movement Science **3**: 27-50.

Cappozzo, A. (1991). "Three-dimensional analysis of human walking: experimental methods and associated artefacts." Human Movement Science **10**: 589-602.

Cappozzo, A. (2002). "Minimum measured-input models for the assessment of motor ability." J Biomech **35**(4): 437-46.

Cappozzo, A., V. Camomilla, et al. (2003). High resolution human movement analysis. Biomechanics of the Lower Limb in Health, Disease and Rehabilitation, Salford, England.

Cappozzo, A., A. Cappello, et al. (1997). "Surface-marker cluster design criteria for 3-D bone movement reconstruction." IEEE Trans Biomed Eng **44**(12): 1165-74.

Cappozzo, A., F. Catani, et al. (1995). "Position and orientation in space of bones during movement: anatomical frame definition and determination." Clin Biomech (Bristol, Avon) **10**(4): 171-178.

Cappozzo, A., F. Catani, et al. (1996). "Position and orientation in space of bones during movement: experimental artefacts." Clin Biomech (Bristol, Avon) **11**(2): 90-100.

Cappozzo, A., U. Della Croce, et al. (1993). Stereometric system accuracy tests. In: Measurement and data processing methodology in clinical movement analysis-preliminary. CAMARC II Internal Report.

Cappozzo, A., U. Della Croce, et al. (2005). "Human movement analysis using stereophotogrammetry. Part 1: theoretical background." Gait Posture **21**(2): 186-96.

Cappozzo, A., U. Della Croce, et al. (1997). Gait data: terminology and definition. Three-dimensional analysis of human locomotion. C. A. In: Allard P, Lumberg A, Vaughan K, editors. New York, Wiley & Sons Ltd**:** 129-132.

Cappozzo, A., T. Leo, et al. (1975). "A general computing method for the analysis of human locomotion." J Biomech **8**(5): 307-20.

Carman, A. B. and P. D. Milburn (2005). "Determining rigid body transformation parameters from ill-conditioned spatial marker co-ordinates." J Biomech.

Cereatti, A., V. Camomilla, et al. (2004). "Estimation of the centre of rotation: a methodological contribution." J Biomech **37**(3): 413-6.

Cereatti, A., V. Camomilla, et al. (2006). "Propagation of the hip joint centre location error to the estimate of femur vs pelvis orientation using a constrained or an unconstrained approach." J Biomech.

Cerveri, P., N. A. Borghese, et al. (1998). "Complete calibration of a stereo photogrammetric system through control points of unknown coordinates." J Biomech **31**(10): 935-40.

Cerveri, P., A. Pedotti, et al. (2003). "Robust recovery of human motion from video using Kalman filters and virtual humans." Hum Mov Sci **22**(3): 377-404.

Cerveri, P., M. Rabuffetti, et al. (2003). "Real-time human motion estimation using biomechanical models and non-linear state-space filters." Med Biol Eng Comput **41**(2): 109-23.

Challis, J. H. (1995). "A procedure for determining rigid body transformation parameters." J Biomech **28**(6): 733-7.

Chao, E. Y. (1980). "Justification of triaxial goniometer for the measurement of joint rotation." J Biomech **13**(12): 989-1006.

Charlton, I. W., P. Tate, et al. (2004). "Repeatability of an optimised lower body model." Gait Posture **20**(2): 213-21.

Chen, J. X., H. Wechsler, et al. (2001). "Knee surgery assistance: patient model construction, motion simulation, and biomechanical visualization." IEEE Trans Biomed Eng **48**(9): 1042-52.

Cheng, P. L. and M. Pearcy (1999). "A three-dimensional definition for the flexion/extension and abduction/adduction angles." Med Biol Eng Comput **37**(4): 440-4.

Cheze, L. (2000). "Comparison of different calculations of three-dimensional joint kinematics from video-based system data." J Biomech **33**(12): 1695-9.

Chèze, L., B. J. Fregly, et al. (1995). "A solidification procedure to facilitate kinematic analyses based on video system data." J Biomech **28**(7): 879-84.

Chiari, L., U. Della Croce, et al. (2005). "Human movement analysis using stereophotogrammetry. Part 2: instrumental errors." Gait Posture **21**(2): 197-211.

Christopher, G., S. Yoon, et al. (2003). Reliability of the functional method of hip joint centre location. In: Proceeding of ISB congress Dunedin, New Zeland.

Cronbach, L. (1951). "Coefficient alpha and the internal structure of tests." Psychometrika **16**: 297-333.

Crowninshield, R. D., R. C. Johnston, et al. (1978). "A biomechanical investigation of the human hip." J Biomech **11**(1-2): 75-85.

Dapena, J., E. A. Harman, et al. (1982). "Three-dimensional cinematography with control object of unknown shape." J Biomech **15**(1): 11-9.

Davis, R. B. I., S. Ounpuu, et al. (1991). " A gait data collection and reduction technique." Human Movement Sciences **10**: 575-587.

Della Croce, U., V. Camomilla, et al. (2003). "Femoral anatomical frame: assessment of various definitions." Med Eng Phys **25**(5): 425-31.

Della Croce, U. and A. Cappozzo (2000). "A spot check for estimating stereophotogrammetric errors." Med Biol Eng Comput **38**(3): 260-6.

Della Croce, U., A. Cappozzo, et al. (1999). "Pelvis and lower limb anatomical landmark calibration precision and its propagation to bone geometry and joint angles." Med Biol Eng Comput **37**(2): 155-61.

Della Croce, U., A. Leardini, et al. (2005). "Human movement analysis using stereophotogrammetry. Part 4: assessment of anatomical landmark misplacement and its effects on joint kinematics." Gait Posture **21**(2): 226-37.

DeLuzio, K. J., U. P. Wyss, et al. (1993). "A procedure to validate three-dimensional motion assessment systems." J Biomech **26**(6): 753-9.

Donati, M., V. Camomilla, et al. (2005). Automatic virtual palpation of bone landmarks. Xth Clinical Gait Movement Analysis Society.

Ehara, Y., H. Fujimoto, et al. (1995). "Comparison of the performance of 3D camera systems." Gait Posture **3**: 166-169.

Ehrig, R. M., W. R. Taylor, et al. (2006). "A survey of formal methods for determining the centre of rotation of ball joints." J Biomech **39**(15): 2798-809.

Everaert, D. G., A. J. Spaepen, et al. (1999). "Measuring small linear displacements with a three-dimensional video motion analysis system: determining its accuracy and precision." Arch Phys Med Rehabil **80**(9): 1082-9.

Ferrigno, G., N. A. Borghese, et al. (1990). "Pattern-recognition in 3-D automatic human motion analysis." ISPRS J Photogramm **45**(4): 227-246.

Fieser, L., E. Quigley, et al. (2000). "Comparison of hip joint centers determined from surface anatomy and CT scans: two case studies." Gait & Posture **11**: 119-120.

Fioretti, S., A. Cappozzo, et al. (1997). Joint Kinematics. Three-dimensional analysis of human locomotion. C. A. In: Allard P, Lumberg A, Vaughan K editors. New York, Wiley & Sons**:** 173-189.

Fregly, B. J., H. A. Rahman, et al. (2005). "Theoretical accuracy of model-based shape matching for measuring natural knee kinematics with single-plane fluoroscopy." J Biomech Eng **127**(4): 692-9.

Frigo, C., M. Rabuffetti, et al. (1998). "Functionally oriented and clinically feasible quantitative gait analysis method." Med Biol Eng Comput **36**(2): 179-85.

Fu, K. S., R. C. Gonzalez, et al. (1988). Robotics: Control, Sensing, Vision and Intelligence. New York, McGraw-Hill.

Fuller, J., L. J. Liu, et al. (1997). "A comparison of lower-extremity skeletal kinematics measured using skin- and pin- mounted markers." Human Movement Sciences **16**: 219-242.

Furnée, E. H. and A. Jobbagy (1993). "Precision 3-D motion analysis system for real-time application " Microprocess Micosyst **17**: 223-231.

Furnée, H. (1997). Real-time motion capture systems. Three-dimensional analysis of human locomotion. C. A. In: Allard P, Lumberg A, Vaughan K editors. New York, Wiley & Sons**:** 85-108.

Gamage, S. S. and J. Lasenby (2002). "New least squares solutions for estimating the average centre of rotation and the axis of rotation." J Biomech **35**(1): 87-93.

Gazzani, F. (1993). "Comparative assessment of two algorithms for calibrating stereophotogrammetric systems." J Biomech **26**(12): 1449-54.

Glozman, D., M. Shoham, et al. (2001). "A surface-matching technique for robot-assisted registration." Comput Aided Surg **6**(5): 259-69.

Goovaerts, H. G. and O. Rompelman (1991). "Coherent average technique--a tutorial review." J Biomed Eng **13**(4): 275-80.

Greaves, J. O. (1995). Instrumentation in video-based three-dimensional systems. Three-dimensional analysis of human movement. S. I. In: Allard P, Blanchi JP, editors, Champaign: Human Kinetics**:** 41-54.

Grood, E. S. and W. J. Suntay (1983). "A joint coordinate system for the clinical description of three-dimensional motions: application to the knee." J Biomech Eng **105**(2): 136-44.

Halvorsen, K. (2003). "Bias compensated least squares estimate of the center of rotation." J Biomech **36**(7): 999-1008.

Halvorsen, K., M. Lesser, et al. (1999). "A new method for estimating the axis of rotation and the center of rotation." J Biomech **32**(11): 1221-7.

Hanson, R. and M. Norris (1981). "Analysis of measurements based on singular value decomposition." Journal on Sciences and Statistical Computing **2**: 363-373.

Hatze, H. (1981). "The use of optimally regularized Fourier series for estimating higher-order derivatives of noisy biomechanical data." J Biomech **14**(1): 13-8.

Hatze, H. (2002). "The fundamental problem of myoskeletal inverse dynamics and its implications." J Biomech **35**(1): 109-15.

Herda, L., P. Fua, et al. (2001). "Using skeleton-based tracking to increase the reliability of optical motion capture." Hum Mov Sci **20**(3): 313-41.

Holden, J. P., J. H. Orsini, et al. (1997). "Surface movement errors in shank kinematics and knee kinetics during gait." Gait & Posture **5**: 217–227.

Holden, J. P., W. S. Selbie, et al. (2003). "A proposed test to support the clinical movement analysis laboratory accreditation process." Gait Posture **17**(3): 205-13.

Holzreiter, S. (1991). "Calculation of the instantaneous centre of rotation for a rigid body." J Biomech **24**(7): 643-7.

Hoschek, J., U. Weber, et al. (1984). "Mathematical kinematics in engineering of endoprostheses. Evaluation of the results of gait analysis." Arch Orthop Trauma Surg **103**(5): 342-7.

Jackson, A. S. and M. L. Pollock (1978). "Generalized equations for predicting body density of men." British Journal of Nutrition **40**: 497-504.

Jackson, A. S., M. L. Pollock, et al. (1980). "Generalized equations for predicting body density of women." Medicine and Science in Sports and Exercise **12**: 175-182.

Jenkins, S. M. E., M. E. Harrington, et al. (2000). The customisation of a three dimensional locomotor model to children. In Proceedings of the 6th International Symphosium on 3-D Analysis of Human Movement, Cape Town, South Africa.

Ji, Q. and Y. Zhang (2001). "Camera calibration with genetic algorithms." IEEE Trans Syst Man Cybern **31**(2): 120-130.

Kadaba, M. P., H. K. Ramakrishnan, et al. (1990). "Measurement of lower extremity kinematics during level walking." J Orthop Res **8**(3): 383-92.

Kane, T. R., P. W. Likins, et al. (1983). Spacecraft Dynamics. New York, McGraw-Hill.

Karlsson, D. and A. Lundberg (1994). Accuracy estimation of kinematic data derived from bone anchored external markers. In: Proc 3rd Int Symp on 3-D Anal Hum Mov, Stockholm.

Kirkpatrick, S., C. D. Gelatt Jr., et al. (1983). "Optimization by Simulating Annealing." Science **220**(4598): 671-680.

Lafortune, M. A. (1984). The use of intra-cortical pins to measure the motion of the knee joint during walking, The Pennsylvania State University.

Lafortune, M. A., P. R. Cavanagh, et al. (1992). "Three-dimensional kinematics of the human knee during walking." J Biomech **25**(4): 347-57.

Lafortune, M. A. and M. J. Lake (1991). Errors in 3-D analysis of human movement. In: Proc. 1st Int. Symp. on 3-D Anal Hum Mov, Montreal.

Leardini, A., M. G. Benedetti, et al. (1999). "An anatomically based protocol for the description of foot segment kinematics during gait." Clin Biomech (Bristol, Avon) **14**(8): 528-36.

Leardini, A., A. Cappozzo, et al. (1999). "Validation of a functional method for the estimation of hip joint centre location." J Biomech **32**(1): 99-103.

Leardini, A., L. Chiari, et al. (2005). "Human movement analysis using stereophotogrammetry. Part 3. Soft tissue artifact assessment and compensation." Gait Posture **21**(2): 212-25.

Levens, A. S., V. T. Inman, et al. (1948). "Transverse rotation of the segments of the lower extremity in locomotion." J Bone Joint Surg Am **30A**: 859-872.

Lu, T. W. and J. J. O'Connor (1999). "Bone position estimation from skin marker co-ordinates using global optimisation with joint constraints." J Biomech **32**(2): 129-34.

Lucchetti, L., A. Cappozzo, et al. (1998). "Skin movement artefact assessment and compensation in the estimation of knee-joint kinematics." J Biomech **31**(11): 977-84.

Manal, K., I. McClay, et al. (2002). "Knee moment profiles during walking: errors due to soft tissue movement of the shank and the influence of the reference coordinate system." Gait Posture **15**(1): 10-7.

Manal, K., I. McClay, et al. (2000). "Comparison of surface mounted markers and attachment methods in estimating tibial rotations during walking: an in vivo study." Gait Posture **11**(1): 38-45.

Maslen, B. A. and T. R. Ackland (1994). "Radiographic study of skin displacement errors in the foot and ankle during standing." Clin Biomech (Bristol, Avon) **9**: 291-296.

McGibbon, C. A., P. O. Riley, et al. (1997). "Comparison of hip center estimation using in-vivo and ex-vivo measurements from the same subject." Clin Biomech (Bristol, Avon) **12**(7-8): 491-495.

Medved, V. (2001). Measurement of Human Locomotion. Boca Raton, USA, CRC Press LLC.

Meglan, D. A., J. Pisciotta, et al. (1990). Effective use of non-sagittal plane joint angles in clinical gait analysis. 36th Annual Meeting, Orthop Res Soc., New Orleans, Louisiana,.

Michalewicz, Z. (1996). Genetic Algorithm + Data Structures = Evolution Programs. New York.

Morris, J. R. W. and A. MacLeod (1990). An investigation of the sources and characteristics of noise in a video-based kinematic measurement system. CAMARC II Internal Report. Models, connections with experimental apparatus and relevant DSP techniques for functional movement analysis.

Muijtjens, A. M., J. M. Roos, et al. (1997). "Tracking markers with missing data by lower rank approximation." J Biomech **30**(1): 95-8.

Paul, J. P. (1992). Terminology and Units. Deliverable n. 4, C.E.C. Program AIM, Project A-2002: CAMARC-II.

Piazza, S. J. and P. R. Cavanagh (2000). "Measurement of the screw-home motion of the knee is sensitive to errors in axis alignment." J Biomech **33**(8): 1029-34.

Piazza, S. J., A. Erdemir, et al. (2004). "Assessment of the functional method of hip joint center location subject to reduced range of hip motion." J Biomech **37**(3): 349-56.

Piazza, S. J., N. Okita, et al. (2001). "Accuracy of the functional method of hip joint center location: effects of limited motion and varied implementation." J Biomech **34**(7): 967-73.

Rabuffetti, M., G. Baroni, et al. (2002). "Self-marking of anatomical landmarks for on-orbit experimental motion analysis compared to expert direct-marking." Hum Mov Sci **21**(4): 439-55.

Rabuffetti, M., M. Ferrarin, et al. (2003). "Optimised procedure for the calibration of the force platform location." Gait Posture **17**(1): 75-80.

Ramakrishnan, H. K. and M. P. Kadaba (1991). "On the estimation of joint kinematics during gait." J Biomech **24**(10): 969-77.

Ramsey, D. K. and P. F. Wretenberg (1999). "Biomechanics of the knee: methodological considerations in the in vivo kinematic analysis of the tibiofemoral and patellofemoral joint." Clin Biomech (Bristol, Avon) **14**(9): 595-611.

Reinschmidt, C., A. J. van Den Bogert, et al. (1997). "Tibiocalcaneal motion during running, measured with external and bone markers." Clin Biomech (Bristol, Avon) **12**(1): 8-16.

Reinschmidt, C., A. J. van den Bogert, et al. (1997). "Effect of skin movement on the analysis of skeletal knee joint motion during running." J Biomech **30**(7): 729-32.

Richards, J. G. (1999). "The measurement of human motion: A comparison of commercially available systems." Human Movement Science **18**: 589-602.

Riley, P. O., R. W. Mann, et al. (1990). "Modelling of the biomechanics of posture and balance." J Biomech **23**(5): 503-6.

Sabel, J. C. (1994). Camera calibration with a single marker. Proceeding of the 3rd Conference on 3-D Analysis of Human Movement Stockholm.

Sangeux, M., F. Marin, et al. (2006). "Quantification of the 3D relative movement of external marker sets vs. bones based on magnetic resonance imaging." Clin Biomech (Bristol, Avon) **21**(9): 984-91.

Sati, M., J. A. de Guise, et al. (1996). "Quantitative assessment of skin-bone movement at the knee." The Knee **3**(3): 121-138.

Schwartz, M. H., J. P. Trost, et al. (2004). "Measurement and management of errors in quantitative gait data." Gait and Posture **20**: 196-203.

Seidel, G. K., D. M. Marchinda, et al. (1995). "Hip joint center location from palpable bony landmarks--a cadaver study." J Biomech **28**(8): 995-8.

Selvik, G., P. Alberius, et al. (1983). "A roentgen stereophotogrammetric system. Construction, calibration and technical accuracy." Acta Radiol Diagn (Stockh) **24**(4): 343-52.

Shea, K. M., M. W. Lenhoff, et al. (1997). "Validation of a method for location of the hip joint center." Gait & Posture **5**: 157-158.

Simon, S. R. (2004). "Quantification of human motion: gait analysis-benefits and limitations to its application to clinical problems." J Biomech **37**(12): 1869-80.

Siri, I. (1961). Body composition from fluid spaces and density: analysis and methods. Washington, DC.

Soderkvist, I. and P. A. Wedin (1993). "Determining the movements of the skeleton using well-configured markers." J Biomech **26**(12): 1473-7.

Spoor, C. W. and F. E. Veldpaus (1980). "Rigid body motion calculated from spatial co-ordinates of markers." J Biomech **13**(4): 391-3.

Stagni, R., S. Fantozzi, et al. (2003). "Experimental evaluation of the performance of the Interval Deformation

Technique for modeling and compensating Soft Tissue Artifact in Human Motion Analysis." Springer Verlag Lectures Note in Computer Science: 293-301.

Stagni, R., S. Fantozzi, et al. (2005). "Quantification of soft tissue artefact in motion analysis by combining 3D fluoroscopy and stereophotogrammetry: a study on two subjects." Clin Biomech (Bristol, Avon) **20**(3): 320-9.

Stagni, R., A. Leardini, et al. (2000). "Effects of hip joint centre mislocation on gait analysis results." J Biomech **33**(11): 1479-87.

Stevens, W. P. (1997). "Reconstruction of three-dimensional anatomical landmark coordinates using video-based stereophotogrammetry." J Anat **191 (Pt 2)**: 277-84.

Stindel, E., J. L. Briard, et al. (2002). "Bone morphing: 3D morphological data for total knee arthroplasty." Comput Aided Surg **7**(3): 156-68.

Taylor, K. D., F. M. Mottier, et al. (1982). "An automated motion measurement system for clinical gait analysis." J Biomech **15**(7): 505-16.

Tranberg, R. and D. Karlsson (1998). "The relative skin movement of the foot: a 2-D roentgen photogrammetry study." Clin Biomech (Bristol, Avon) **13**(1): 71-76.

Tylkowski, C. M., S. R. Simon, et al. (1982). Gait in Spastic Cerebral Palsy. Tenth Open Meeting of the Hip Society 10.

Van Sint Jan, S. and U. Della Croce (2005). "Identifying the location of human skeletal landmarks: why standardized definitions are necessary--a proposal." Clin Biomech (Bristol, Avon) **20**(6): 659-60.

Van Sint Jan, S., V. Feipel, et al. (2002). Lower limb anatomical landmark definition and identification within different experimental contexts.

Van Sint Jan, S., I. Hilal, et al. (2003). "Data representation for joint kinematics simulation of the lower limb within an educational context." Med Eng Phys **25**(3): 213-20.

Veldpaus, F. E., H. J. Woltring, et al. (1988). "A least-squares algorithm for the equiform transformation from spatial marker co-ordinates." J Biomech **21**(1): 45-54.

Wakeling, J. M., A. Liphardt, et al. (2003). "Muscle activity reduces soft-tissue resonance at heel-strike during walking." Journal of Biomechanics **36**: 1761-1769.

Westblad, P., K. Halvorsen, et al. (2000). Ankle-joint complex motion during stance phase of walking as measured by skin or bone anchored markers. In: 6th Int Symp on 3-D Anal Hum Mov, Cape Town, South Africa.

White, S. C., H. J. Yack, et al. (1989). "A three-dimensional musculoskeletal model for gait analysis. Anatomical variability estimates." J Biomech **22**(8-9): 885-93.

Woltring, H. J. (1990). "Estimation of the trajectory of the instantaneous centre of rotation in planar biokinematics." J Biomech **23**(12): 1273-4.

Woltring, H. J. (1994). "3-D attitude representation of human joints: a standardization proposal." J Biomech **27**(12): 1399-414.

Woltring, H. J., R. Huiskes, et al. (1985). "Finite centroid and helical axis estimation from noisy landmark measurements in the study of human joint kinematics." J Biomech **18**(5): 379-89.

Wood, G. A. (1982). "Data smoothing and differentiation procedures in biomechanics." Exerc Sport Sci Rev **10**: 308-62.

Wu, G. and P. R. Cavanagh (1995). "ISB recommendations for standardization in the reporting of kinematic data." J Biomech **28**(10): 1257-61.

Wu, G., S. Siegler, et al. (2002). "ISB recommendation on definitions of joint coordinate system of various joints for the reporting of human joint motion--part I: ankle, hip, and spine. International Society of Biomechanics." J Biomech **35**(4): 543-8.

Zihlmann, M. S., H. Gerber, et al. (2006). "Three-dimensional kinematics and kinetics of total knee arthroplasty during level walking using single plane video-fluoroscopy and force plates: a pilot study." Gait Posture **24**(4): 475-81.